THE DEVELOPMENT OF A REACTOR FOR THE MANUFACTURE OF ZINC ELECTRODES FOR A SILVER OXIDE-ZINC BATTERY

by

DAVID JACOBUS HOLTZHAUSEN
Hons BSc
MSc (Physics)

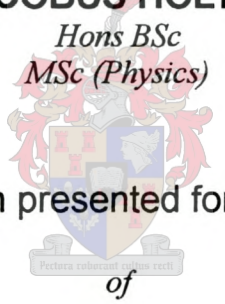

Dissertation presented for the Degree

of

DOCTOR OF PHILOSOPHY IN ENGINEERING SCIENCE
(Metallurgical Engineering)

in the Department of Chemical Engineering
at the University of Stellenbosch

Promoter:
PROF. L. LORENZEN

STELLENBOSCH
September 2000

DECLARATION

I hereby certify that this dissertation is my own original work, except where specifically acknowledged in the text. Neither the present dissertation, nor any part thereof, has previously been submitted for a degree at any University.

D.J. HOLTZHAUSEN
September 2000

SYNOPSIS

Silver/Zinc batteries are extensively used for applications where a power source with a high energy density is needed. A reactor was developed to manufacture the zinc electrodes for these batteries. The parameters for the control of this reactor were identified. The interaction and relationships between the set of parameters were established and quantified. The novel design of the reactor includes features such as continuous replenishment of the constituting chemicals, parallel flow of the plating fluid, inert anodes and a serial electrical layout. The controlling parameters consist of both chemical and physical parameters. They are – zincate concentration, hydroxyl concentration, density, temperature, flow rate of the plating fluid, and current density. The unique solubility characteristics of zinc oxide in potassium hydroxide lend themselves to a novel approach for the determination of the zincate concentration in the plating solution. A set of conditions for the manufacturing of electrodes, with the required characteristics, was identified. The requirements are densely packed zinc dendrite morphology with high porosity and mechanical stability. The designed reactor complies with the industries safety requirements. The batteries were successfully applied in their operational domain (torpedoes) after this extensive research project was completed.

OPSOMMING

Silwer/Sink batterye word intensief aangewend in gebruike waar 'n kragbron met hoë energie digtheid benodig word. 'n Reaktor is ontwikkel wat die sink elektrodes van die tipes batterye vervaardig. Die veranderlikes vir die beheer van die reaktor is bepaal. Die interaksie en verwantskap tussen die stel veranderlikes is verkry en gekwantifiseer. Die unieke ontwerp van die reaktor het die volgende karakteristieke, nl. aaneenlopende vervanging van die chemikalië verbruik, parallelle vloei van die plateringsvloeistof, inerte anodes en elektriese uitleg in serie. Die chemiese en fisiese veranderlikes is beide beherende veranderlikes. Hierdie fisiese en chemiese veranderlikes wat die proses beheer is die sinkaat konsentrasie, hidroksiel konsentrasie, digtheid, temperatuur, vloeitempo van die plateringsvloeistof en die stroomdigtheid. Die unieke oplossingskarakteristieke van sinkoksied in kalsium hidroksied leen hom tot die unieke proses om die sinkaat konsentrasie in die plateringsvloeistof te bepaal.

'n Stel operasionele kondisies vir die vervaardiging van die elektrodes met die spesifieke spesifikasies soos verlang, is geïdentifiseer. Hierdie kondisies is die diggepakte sinkdendriet morfologie met 'n hoë porositeit en meganiese stabiliteit. Die ontwerpte reaktor voldoen aan die industriële veiligheidsvereistes en die ergonomiese maatstawwe. Die batterye is suksesvol gebruik in hulle industriële aanwending as gevolg van die suksesvolle afhandeling van die stuk navorsing.

ACKNOWLEDGEMENTS

Gratitude is expressed to Silvetech (Pty) Ltd. who initiated the project and provided all the necessary infrastructure and materials. A special word of gratitude is expressed towards Professor L. Lorenzen for his guidance and support during the project as my promoter.

The technical assistance provided by Miss E. Rossouw, Mr J. Berg and Mr S. Brown and the typing done by Mrs E. Thom is gratefully appreciated. To all colleagues, academics and friends, without whose contributions the successful completion of this technology development would not have been possible, thank you.

DEDICATION

This thesis is dedicated to Marthie, our children and our family.

TABLE OF CONTENTS

LIST OF TABLES

LIST OF FIGURES

LIST OF SYMBOLS

E_{eq} = Equilibrium Potential [V]

E_0 = Standard Reduction Potential [V]

F = Faraday Constant [Coulomb/g.ekw)

k = Boltzmann Constant [mho/m]

K_{ab} = Mass Transfer Coefficient [m/s]

K^{-1} = Debye Length [m]

λ = Equivalent Conductivity [mho/m]

K_c = Specific Conductivity [mho/m]

h = Planck Constant

R = Gas Constant [Pa m^3 k^{-1} mol^{-1}]

T = Temperature [K]

t = Time [sec]

B = Symmetry Factor [dimensionless]

G = Gibbs Free Energy [kJ/mol]

η = Over Potential [V]

A = Ampere [A]

A = Active Electrode Area [m^2]

C_b = Bulk Reactant Concentration [$mol.m^{-3}$]

ΔC = Change in bulk reactant Concentration [$mol.m^{-3}$]

D = Diffusion coefficient [$m^2.s^{-1}$]

E = Measured or applied electrode potential [V]

E_{CELL} = Cell potential (Cathode potential – Anode potential) [V]

i = Current density [$A.m^{-2}$]

I_L = Mass transport controlled limiting current [A]

k_L = Average mass transport coefficient [$m.s^{-1}$]

M = Molar Mass [$kg.mol^{-1}$]

n = Number of electrons [dimensionless]

N = Volumetric flow rate [m^3/s]

Q = Volumetric flow rate [$m.s^{-1}$]

q = Electrical Charge [C]

V_R = Reactor Volume [m^3]

v = Average, linear electrolyte velocity [$m.s^{-1}$]

Φ = Current Efficiency [dimensionless]

Sh = Sherwood number [$K_L d_e/D$] [dimensionless]

Re = Reynold number [$v\ d_e/v$] [dimensionless]

Sc = Schmidt number [v/D] [dimensionless]

p = Density [g/cm^3]

μ = Viscosity [centipoises]

μ_e = Electro-chemical potential per gram equivalent

g = Gravity Constant

Ø = Electrode Potential [V]

Chapter 1

INTRODUCTION

Silver oxide/Zinc batteries are the best batteries for the deliverance of high currents at low voltages. Depending on the design, currents of 600 A at 1.5 V is not uncommon. These characteristics make it suitable for military application where high-energy sources with low weight are needed. They are extensively used as a cheap, reliable power source in missile technology, torpedo power sources, and as emergency batteries. Depending on the application, the batteries are available in both primary (once-off use) and secondary (rechargeable) versions.

To develop such a battery, intensive research work has to be conducted on the reactor to develop the negative electrode of such a AgO/Zn battery. The quality of the zinc deposits on the negative electrodes of such a AgO/Zn battery are of utmost importance for the effective operation of this battery. Due to the military strategic sensitivity of the technology of these batteries, no real data on manufacturing such electrodes has been published. Most of the research conducted was done on military projects and is, therefore, classified and unavailable.

The use of zinc as the anode in these batteries is based on its stability, its energy and power density characteristics and its low cost per watt-hour. It is also necessary to operate with a concentrated alkaline electrolyte so that the anodic oxide film formed on zinc during discharge can be rapidly dissolved to form the zincate ion during discharge, thus preventing the electrode passivation. On deposition from an alkaline zinc solution, the zinc is either mossy or dendritic, depending on the plating conditions. The physical form of deposits obtained by plating at a constant current will depend on the value of the current. At a current less than a critical current, only moss will grow. At a current greater than this current, dendrites will first be formed and then, due to a decrease in over-potential corresponding to the increase in real surface area, there is a transition in morphology leading to the deposition of moss. During zinc deposition at constant, high current densities, the surface concentration of the zincate ion changes and the electrode over-potential becomes adequate for hydrogen evolution. The electrolyte is stirred when the hydrogen bubbles are formed

and the surface concentration of the zincate ion is changed. The numeric value of the critical current density corresponds to a limiting current potential that depends on the particular design of the electro-chemical cell used. Thus, equations developed empirically are not general, but applicable only to the system where developed.

This dissertation covers the theoretical fundamental principles, necessary for the development of a reactor like the Zn plating bath. To be able to apply the theory, measurements were conducted to determine the variables to describe, understand and optimise the system. Due to the harsh plating environment, the measurable variables were limited. These variables must serve a dual purpose, i.e. to enable the mathematical modelling of the system, and secondly to supply a handle to control the system. As reproducibility is very important in the plating process, the economics of the system are not considered in detail. To ensure this reproducibility, a parallel batch flow reactor with short electrodes combined with a serial electrical distribution system was selected after extensive empirical work. This system has, however, certain advantages and disadvantages. The advantages are:

- Homogenous electric field distribution in each sub-reactor to ensure the uniform deposits of the Zn.
- The unit can be operated in a batch mode as well as a semi-continuous process.
- Maximum versatility in batch sizes, from small batches to large batches can be handled.
- Ease of operation.
- Easy quality control.
- Small capital layout.
- Versatility in product range.
- Low maintenance.
- Inexpensive maintenance.
- Low skilled staff requirements.

The major disadvantage is the low production volumes relative to a continuous process. The advantages, however, outweigh the disadvantages by far for small-scale production units, as will always be the case for Zn electrodes. Mass production, at this stage, is not viable in our case. Contrary to the plating for surface-passivation where a homogenous non-porous structure is needed, the electrochemical application of Zn plating, for electrodes, requires a porous Zn structure with a porosity of approximately 50%.

Due to the urgency of workable control parameters for the system, the initial emphasis was on the control parameters and not on the theoretical modelling. This will ensure that the knowledge gathered can be applied directly to improve the production process. The following goals were set for the project, i.e.

GOALS

- Develop and design a cell to ensure that each foil has the same mass of plated zinc.
- Determine the influence of solution flow-speed on the voltage behaviour for this application.
- Determine a relationship between density, concentration and temperature.
- Determine a relationship between plated mass and the Ampere hours used.
- Determine if the limiting current density is reached and, if so, is it applicable in this application?
- Determine the factors that determine the crystal structure of the plated zinc.
- Determine the relationship between plating current and crystal structure.
- Develop a method to describe/quantify the crystal structure.

If all the above-mentioned goals can be achieved, it will enable one to effectively control and operate a reactor for the development of negative electrodes for a AgO/Zn battery.

Chapter 2

AN INTRODUCTION TO THE BASIC CONCEPTS OF ELECTROCHEMISTRY

2.1 INTRODUCTION

To understand the processes involved in Zn plating, a study of the fundamental principles involved in such a reactor is unavoidable. This chapter will cover the fundamental parameters describing the reactor performance. Its aim is to establish a relationship between the reactor performance and that of the manufactured Zn electrodes. With such a relationship, the criteria for electrode manufacturing can be optimised for each application.

2.2 ELECTRODE PROCESSES (Nicol, 1979a)

Electrode processes are heterogeneous chemical reactions occurring at the interface of a solid and an electrolyte, accompanied by the transfer of an electric charge through this interface. This charge transfer can involve electrons or ions, as can be seen below:

$$Zn \Leftrightarrow Zn^{2+} + 2e \qquad (2.1)$$

and

$$Zn(OH) \Leftrightarrow Zn^{2+} + (OH)^{2-} \qquad (2.2).$$

In (2.1), the reaction can be forced to proceed to the right by providing a sink for the electrons such as an external power supply or an electron-acceptor such as oxygen in solution. In (2.2) the reaction can proceed to the right by providing a zinc electron for one of the ions, such as protons. It should be taken into account that much of what is said about the transfer of electrons at interfaces applies equally well to the transfer of ions.

In general terms, an electrode process is a redox reaction, which can be represented by the following equation:

$$O + ne \Leftrightarrow R \qquad (2.3)$$

where n is the number of electrons required to reduce the oxidized form, O, to the reduced form, R. O and R can be either ionic or neutral species, and depending on the conditions, the oxidized and reduced species may be present in the solid or

solution phase. The conduction of an electrical charge is generally by the transfer of ions in the liquid phase and the transfer of electrons in the solid phase. The electrode interface is the region in which the transition from one type of conduction to another occurs.

Similar to other heterogeneous processes, electrode reactions are generally not simple but involve a number of steps, which can occur either consecutively or simultaneously. These steps include mass transport of the electro-active reactants to and products from the interface; adsorption in the so-called double-layer adjacent to the electrode surface and the actual charge-transfer reaction. However, there are two distinct and most important characteristic features of electro-chemical reactions, which are not possessed by heterogeneous processes in general. These are -

- the rate of a charge-transfer step is dependent on the electrical potential difference between the solid and the solution, and
- the rate of electrode processes is influenced by the nature of the electrochemical double-layer at the interface.

2.2.1 The Dependence of Electrode Reactions on Potential

Consider a solution containing the redox system -

$$O + ne \Leftrightarrow R \qquad (2.4)$$

in which both O and R are solution species. If an inert conductor, such as a platinum wire, is dipped into a solution containing both O and R, a continual exchange of electrons takes place between the wire and the species O and R, which come into contact with the electrode. An equilibrium is established in which the rate of the forward reaction matches that of the reverse reaction and the wire has an equilibrium potential, E_{eq}, given by the familiar Nernst equation -

$$E_{eq} = E_o - \frac{RT}{nF} Ln \frac{a_r}{a_o} \qquad (2.5)$$

where E_0 is a constant characteristic of the redox system, and a_0 and a_R are the activities of the species, respectively. Because it is not possible to measure a single electrode potential, E_{eq} must be measured with respect to another (reference) electrode in the solution. If this reference electrode is a normal hydrogen electrode which is arbitrarily assigned a value of zero, and the activities of O and R are

adjusted to unity, the $E_{eq} = E_0$ is called the Standard Reduction Potential of the redox couple.

If the potential of the electrode is changed such that $E > E_{eq}$, the electrode is no longer in equilibrium with the solution and electrons are exchanged until the potential of the solution reaches the same value as that of the electrode. In this particular case, it can be easily seen that the ratio a_R/a_0 must decrease, i.e. a net conversion of some of R to O must occur. The opposite is true for potentials $E_0 < E_{eq}$. If the current is plotted as a function of the potential, one will obtain a current - potential curve, as shown in Figure 5.4.

The rates of heterogeneous reactions are dependent on the area of the reaction interface, and are therefore expressed as a rate constant per unit area. Thus, if the rate of oxidation of R + O at a particular potential is k mole cm^{-2} sec^{-1}, then according to Faraday's law, the current density which flows at the electrode due to this reaction is -

$$i = nFk \quad (A\ cm^{-2}) \qquad (2.6)$$

The equilibrium potential is that potential at which the site of oxidation of R equals that of the reduction of O.

The terms over-potential (commonly called the over-voltage) and polarization is used to describe the deviation of the potential from the equilibrium value, E_{eq}, which is required to sustain reaction at a given rate.

For a given species R or O, the form of the current-potential curve depends on a number of chemical properties (concentration, pH, presence of complexing species), as well as surface properties (chemical and physical nature of the electrode, presence of adsorbing species).

2.2.2 Factors contributing to the Over-potential

The over-potential associated with a particular process can be due to various factors, some of the more important of which are discussed below. The total over-potential is the sum of the over-potentials for the various steps constituting the overall electrode reaction and is often governed by one (rate-determining) step. The various over-potentials are listed below:

- Transfer over-potential is due to slow electron transfer from the electrode to solution species. Generally, reactions involving the breaking of strong chemical bonds, such as those required in the reduction or oxidation of water will have a large transfer component to the over-potential.

- Diffusion over-potential is the result of decreasing reactant concentration and/or the accumulation of the reaction product in the vicinity of the electrode surface due to the limited rate of mass transport by diffusion. The effect of diffusion on the current-potential curve is to produce a potential-independent current plateau.

  At low over-potentials the rate is controlled by the rate of electron-transfer (transfer polarization). As the over-potential increases, the rate of electron-transfer increases until the rate of supply of R to the electrode surface, limits the rate of reaction (diffusion polarization).

- Reaction over-potential is observed when the transfer step is preceded or followed by a slow chemical reaction, which influences the concentrations of the reactants or products in the vicinity of the electrode. The chemical process can be a homogeneous reaction in solution or a heterogeneous one on the electrode surface such as the dissolution of an oxide film produced by anodic oxidation

- Crystallization over-potential is observed if the incorporation of the product into or release of the reactant from the metal lattice is retarded. The relative contribution of crystallization and transfer over-potential to the overall rate has important consequences in determining the morphology of electro-deposited metals.

- Nucleation over-potential is the result of the energy required to nucleate a new phase (such as a metallic crystal or a gas bubble) on an inert surface. This is often detectable as a marked hysteresis in the current-potential curve. In some instances, however, the resistance of a film on an electrode surface can also contribute significantly to the over-potential.

2.2.3 Polarisable and Non-Polarisable Electrodes - The Double-Layer

Polarization effects are dependent on the potential. If a voltage is applied across an electrochemical cell and the current quickly decays exponentially to zero after a time period, i.e. a non-continuous current is maintained, then the electrode is said to be completely polarisable in that potential region. If a similar transient is obtained which decays to the steady-state current but not to zero, the electrode is non-polarisable in

that region. These transients are similar to those obtained during the charging and discharging of a capacitor and are, in fact, due to the charging of the electrical double layer at the electrode/electrolyte interface. Several models have been proposed to describe the distribution of charge (and therefore potential) near the electrode.

2.2.3.1 Helmholtz Model

In this simple model, the excess ions attracted to the electrode are held at a fixed distance from the electrode and their charge is balanced by an equal number of electrons in the metal. This separation of charge is like a parallel-plate capacitor and is the reason for the choice of the name Double-Layer.

The hydration spheres of the ions, which remain hydrated, govern the distance x_H, and the plane at a distance x_H from the electrode is known as the outer Helmholtz plane. This distance is of the order of 10^{-7} cm and for a potential difference of say 0,1V, gives rise to an electrical field in the double-layer of 10^6 V/cm. It is this high field which is responsible for the ability of electrochemical reactions to induce significant chemical effects. The other important effect is the orientation of water

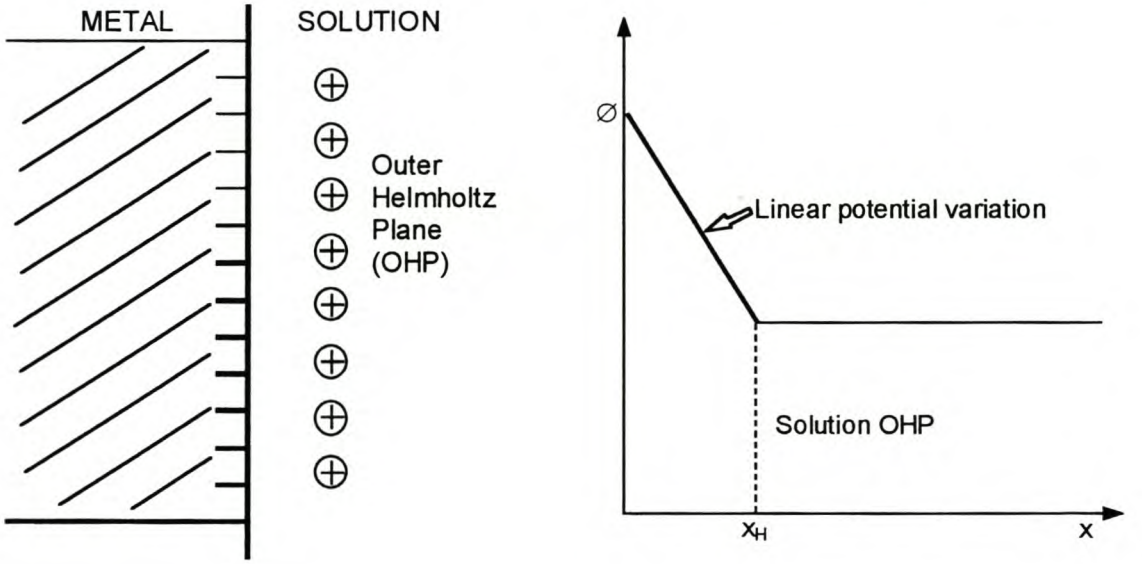

Figure 2.1: Graphical illustration of the Helmholtz Model

molecules in the field which significantly reduces the dielectric constant of the solvent in the double-layer. This reduces the capacitance of the double-layer to values of the order of 10μF cm $^{-2}$.

2.3.2.2 Gouy-Chapman Model

This model takes into account the thermal motion of the ions, which tend to reduce the ordering forces of the electric field. This model is, in fact, analogous to the well-known Debye-Huckel (D-H) theory, which describes the ionic and potential distribution around a spherical ion. As a result of thermal motion, the double-layer is more diffusive than suggested by the Helmholtz model and both the potential and charge vary exponentially with distance from the electrode surface (see Figure 2.2), i.e.

$$\phi_x = \phi_0 \exp(-Kx)$$

$$C_x = C_s \exp(-e\phi_x / kT)$$

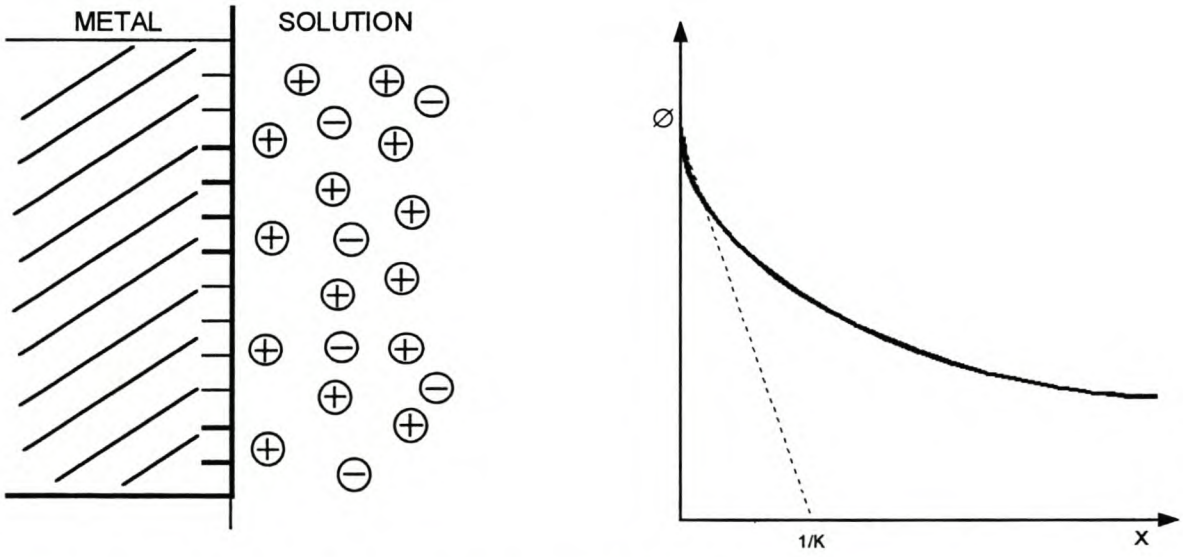

Figure 2.2: Graphical illustration of the Gouy-Chapman Model.

where K^{-1} is known as the Debye length which, as in the case of the D - H theory, varies inversely with the square root of the ionic strength -

($K^{-1} \sim 10^{-7}$cm at C_s = 0,1 mol $^{-1}$).

2.3.2.3 Stern Model

A third and better model is that of Stern who combined the ideas of Helmholtz and Gouy-Chapman. According to Stern, some of the charge in the solution lies in a plane of closest approach (Helmholtz) and the remainder is spread out in the solution (Gouy-Chapman). Each of these two regions can be simulated by a parallel-plate capacitor and therefore the double-layer is equivalent to two capacitors in series.

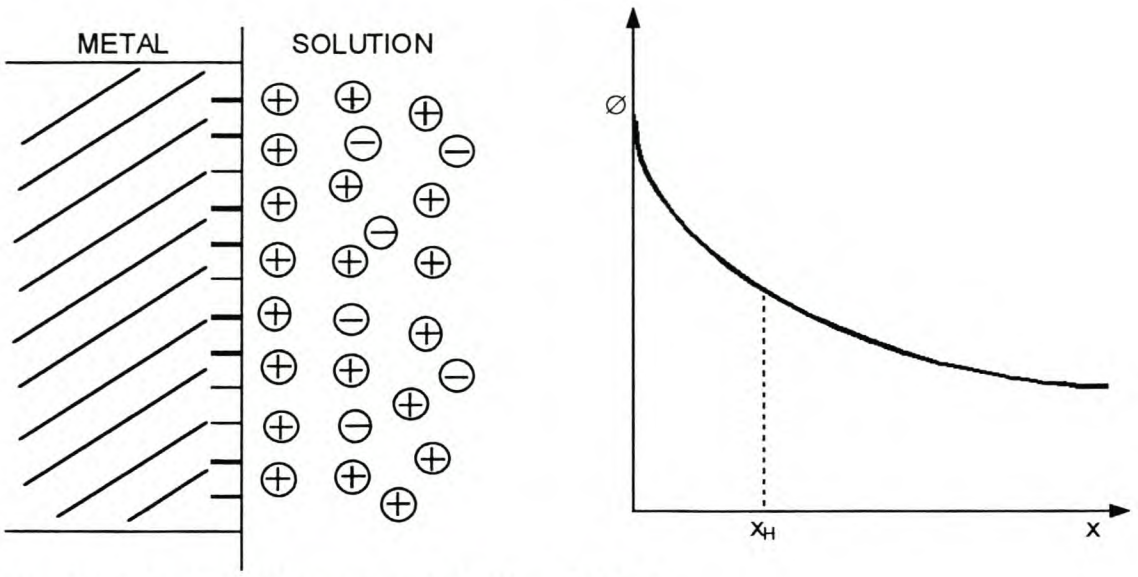

Figure 2.3: Graphical illustration of the Stern Model.

The variation of potential with distance is linear in the first region and exponential in the second (see Figure 2.3). Modern terminology often combines both of these regions into a common diffuse layer.

2.2.3.4 Specific Adsorption

The models of the double-layer described above are based upon the premise that only electrostatic forces determine the distribution of charge and potential in the double layer. Thus, even in the simplest model, it is assumed that the ions in the Helmholtz layer are separated from the electrode surface by the water molecules in the hydration spheres of the ions. To some extent, this model is similar to that of the physical adsorption of say, inert gases, on solid surfaces in which weak forces of an electrostatic nature are involved in the bonding. However, if the interaction with the surface is strong enough, the ions can lose at least part of their hydration sphere, thereby coming into direct contact with the surface. This so-called specific adsorption is most common with anions for which the hydration energies are lower than for cations. The plane passing through the centers of these specifically adsorbed ions is known as the Inner Helmholtz Plane (IHP). Often, at least partial charge transfer accompanies this type of adsorption across the interface.

2.2.4 Potential of Zero Charge (E_{zc})

It is apparent that the charge on the electrode (and therefore that on the solution side of the double-layer) can be varied in size and magnitude by altering the potential applied to the electrode. It follows therefore that there could exist a characteristic

potential at which the excess charge at the electrode surface is zero. At this potential, the double-layer capacitance will be at its minimum in dilute solutions of non-specifically adsorbed ions where the charge in the diffuse layer is zero. In the presence of specifically adsorbed ions, the diffuse-layer charge is equal and opposite of the inner-layer charge at E_{zc}. As could be expected, E_{zc} is directly related to the electronic work function of the metal, but it also depends on adsorption of specifically adsorbed ions and is therefore characteristic not only of the metal but also of the temperature and composition of the solution. Some typical E_{zc} values are given in Table 2.1 below:

TABLE 2.1: Potentials of zero charge for some metals.

Metal	*Electrolyte*	*Concentration*	E_{zc}
		Mol l^{-1}	*V vs NHE*
Cd	KCl	0,01	-0,92
Pb	KCl	0,01	-0,69
Zn	Na_2S0_4	1,0	-0,61

2.2.5 Transport of Matter and Charge in Solution

Electrochemical processes require the presence of two electrodes between which a charge is transported by electrons in the external half of the circuit and generally by ions in the medium (aqueous, non-aqueous or solid electrolyte molten salt) separating the electrodes. Sustained electrode reactions require the continual supply of both material and charge to the electrode surface. This supply can be provided via three main modes of transport.

i. Migration involves the movement of charged species under the influence of an electric field, i.e. cations migrate to the anode and anions to the cathode. The fraction of the total migration current (I) carried by a particular ion is given by t.I where t is the transport number of the ion which is related to the equivalent conductivity of the ion and all the other ions in the solution through the relationship

$$t = \lambda zC/\sum_i \lambda_i C_i \qquad (2.7)$$

where λ is the equivalent conductivity, z the ionic charge and C the concentration (in equivalents/liter) of the ion. The equivalent conductivity (Λ) of an electrolyte is a normalized (on an equivalent basis) specific conductivity, i.e.

$$\Lambda = \lambda_+ + \lambda_- = 1000K_c/C \qquad (2.8)$$

where λ_+ and λ_- are the equivalent conductivities of the individual ions and K is the specific conductivity at a concentration C.

ii. Diffusion is the transport of matter by virtue of a concentration gradient. In electrochemical cells, such gradients are set up close to electrode surfaces and this generally provides the major route for the transport of the electro-active species close to the electrode.

iii. Convection is the transport of matter by movement of the solution itself by way of differences in density, or temperature, or by way of vibration or mechanical agitation of various types.

The simplest working model of transport by convective-diffusion is that of Nernst, in which, under conditions of steady current, a diffusion layer is set up close to the surface and the reactants and products are transported to and from this layer by convection. While steady-state conditions last, the diffusion layer will have a constant thickness. This hypothesis is only an approximation to the facts, but it simplifies calculations and can often be used with acceptable results.

2.3 QUANTITATIVE ELECTRODE KINETICS (Orchard, 1979)

2.3.1 Electrode kinetics under activation control: The Butler-Volmer Equation

It should help, at the outset, to note that the equations and the methods of electrode kinetics are, in a general sense, the same as in any other branch of kinetics. Thus the form of the rate equation (rate = rate constant x f (concentration)) is no different; the only differences lie in the details. The rate of an electrode reaction is dependent on the electrode potential, and the variation of potential near the surface of an electrode depends in turn on the structure of the double layer. The simple Helmholtz model of the double layer will be adopted. Consider it to consist of two parallel sheets of charge - one at the surface of the electrode, and another at the Outer Helmholtz Plane (OHP) through the centers of solvated ions closest to the electrode surface, as shown in Fig. 2.4.

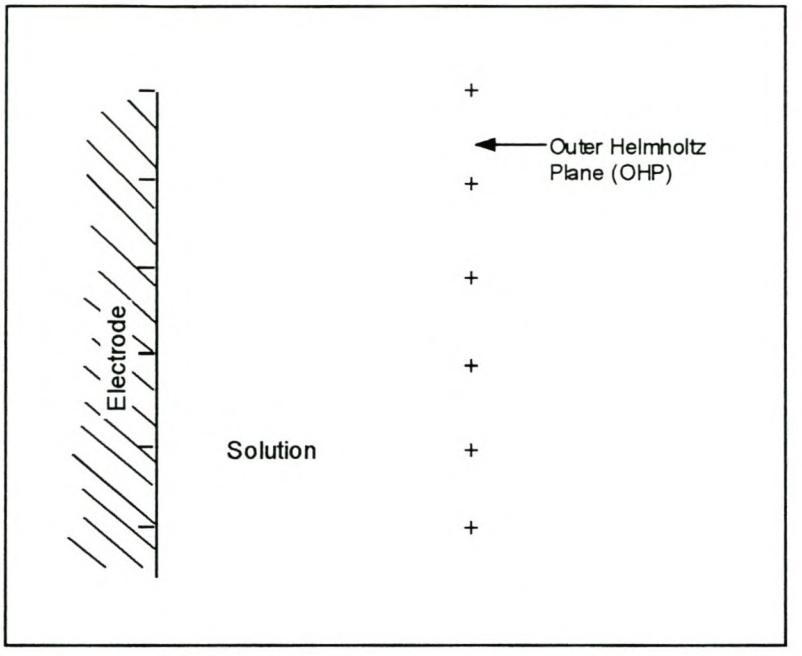

Figure 2.4: Simple electronic double layer, with all excess charge located in two parallel sheets of charge.

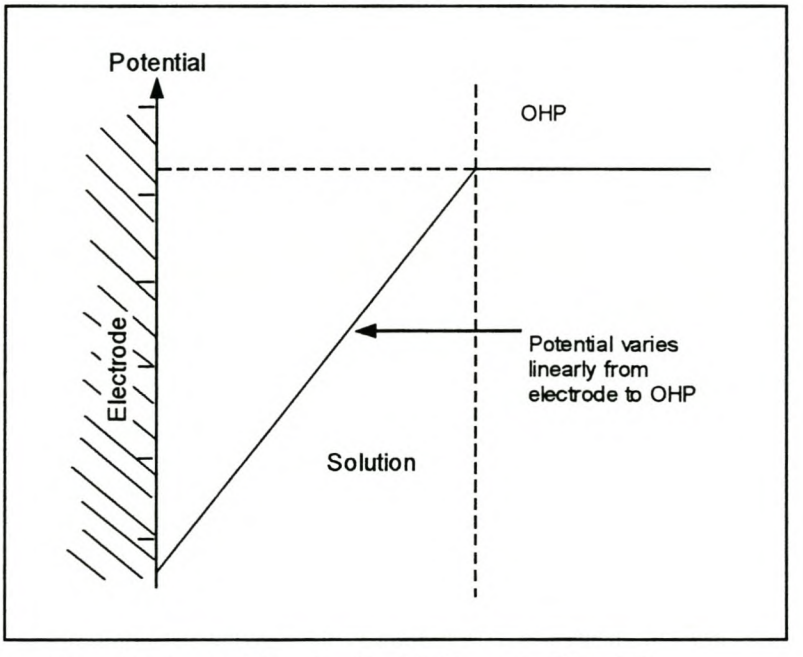

Figure 2.5: Variation of potential for the double layer in Fig. 2.8.

For this model of the double layer, the potential varies linearly between the two sheets of charge, as in Fig. 2.5. (It should noted that the Helmholtz model has shown to be oversimplified - the region of ionic charge is not planar but diffuse, as in the Gouy-Chapman and Stern models of the double layer.)

The transition-state theory of reaction rates relates the rate constant K_r of an elementary reaction to the standard free energy of activation, i.e.

$$K_r = kT/h \quad \exp(-\Delta G^0/RT) \qquad (2.9)$$

Where k is the Boltzmann constant, h is the Planck constant, and R the gas constant. (In practice eqn. (2.9) is usually indistinguishable from the better known Arrhenius equation, $K_r = A.\exp(-E_a/RT)$.) For the sake of simplicity, we will consider a one-step, one-electron reaction at a metal electrode in which an electron acceptor A is transformed into a new substance D:

$$A^+ + e^- \Rightarrow D \qquad (2.10)$$

An A^+ ion, in the process of being reduced, moves from the solution side of the double layer towards the electrode surface, experiencing activation energy barrier which controls the rate of the electronation reaction according to eqn. 2.9. When the electrode is first placed in solution, the reaction is entirely chemical in nature - no electric field has yet developed to influence the energy of ions in the interfacial region. Within microseconds, the occurrence of the electron transfer reaction causes the interface to become charged, and the rate at which ions now cross the double layer is controlled by both a chemical barrier and the electric field which has developed. It is not the total potential difference across the double layer which affects the rate of electronation of A^+ ions, but only the potential change they experience in their climb to the transition state. We, therefore, define the symmetry factor presented by the symbol β (see Figure 2.6), as:

β = (Distance across double layer to summit/distance across whole double layer)

The electrical field therefore increases the standard free energy of activation for a singly charged cation by $\beta\Delta\phi e$, and for a mole of cations by $\beta\Delta\phi F$. The standard free energy of activation can therefore be separated into a chemical and an electrical term, i.e. -

$$\Delta G^{\Rightarrow o\#} = \Delta G_c^{\Rightarrow o\#} + \beta\Delta\phi F \qquad (2.12)$$

(The $\Rightarrow$ indicates the movement of an electron from the electrode on the left to the solution on the right; in other words $\Rightarrow$ indicates electronation, $\Leftarrow$ indicates de-electronation. The subscript c identifies the chemical free energy of activation.)

Substituting $\Delta G^{\Rightarrow o\#}$ in eqn. (2.9), gives -

$$k_e^{\Rightarrow} = k_1 T/h \exp(\Delta G c^{\Rightarrow o\#}/RT)\exp(-\beta\Delta\phi F/RT)$$

$$= k_c^{\Rightarrow} \exp(-\beta\Delta\phi F/RT) \qquad (2.13)$$

($k_e^{\Rightarrow}$ and $k_c^{\Rightarrow}$ are electrochemical and chemical rate constants, respectively.) For the reverse reaction, $D \Rightarrow A^+ + e^-$, a similar expression can be obtained. Here, however, there is a different chemical activation energy $\Delta G^{\Leftarrow o\#}$, and the electric field lowers the activation barrier to de-electronation by $(1-\beta)\Delta\phi F$.

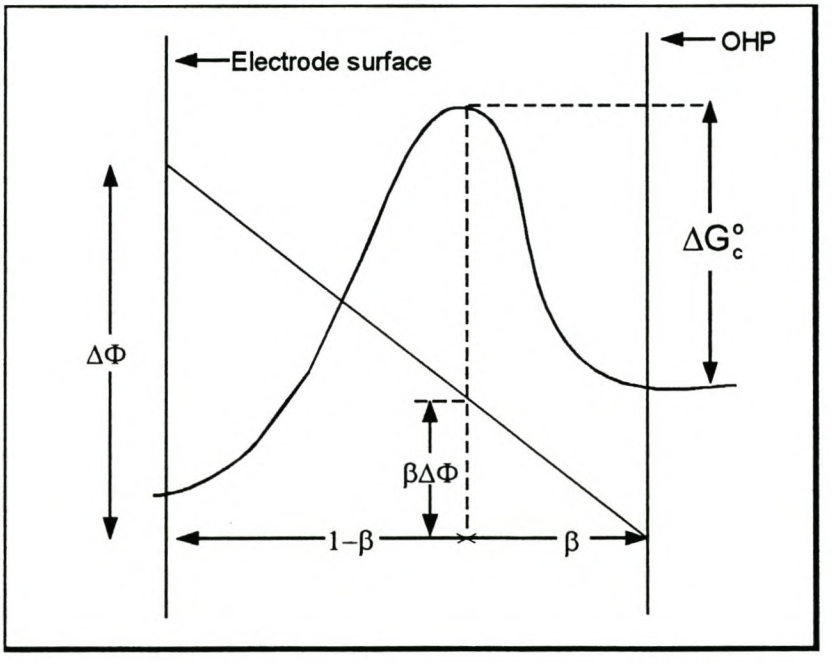

Figure 2.6: Superimposition of chemical and electrical contributions to free energy of activation for the electronation of a singly charged cation.

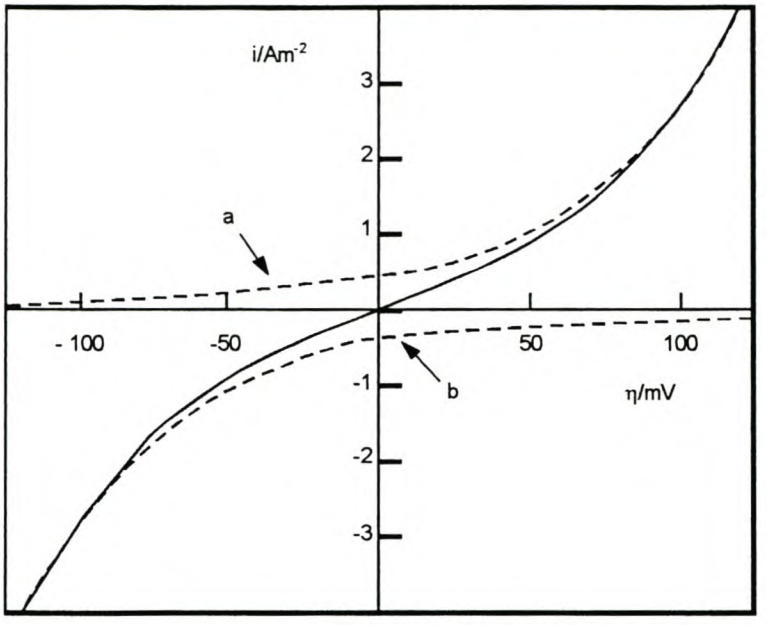

Figure 2.7: Plot of the Butler-Volmer equation and the separate anodic term (a) and cathodic term (b). (T=298K, β=0,50, i_o=0,40Am^{-2})

$$\Delta G^{\Leftarrow o\#} = \Delta G_c^{\Leftarrow o\#} - (1 - \beta)\Delta\phi F \qquad (2.12a)$$

$$k_e^{\Leftarrow} = k_c^{\Leftarrow} \exp((1-\beta\Delta)\phi F/RT) \qquad (2.14)$$

The rates of the electronation and de-electronation reactions are as follows:

$$v^{\Rightarrow}_e = k^{\Rightarrow}_e[A^+] \qquad (2.15)$$

and $$v^{\Leftarrow}_e = k^{\Leftarrow}_e[D] \qquad (2.16)$$

For the transfer of one electron, the current density and the rate are related by i = Fv.

Thus, $$i^{\Rightarrow} = F\, v^{\Rightarrow}_e \qquad (2.17)$$

and $$i^{\Rightarrow} = F\, k^{\Rightarrow}_c[A^+] \exp(-\beta\Delta\phi F/RT) \qquad (2.18)$$

Similarly, $$i^{\Leftarrow} = F\, k^{\Leftarrow}_c[D] \exp((1-\beta)\Delta\phi F/RT) \qquad (2.19)$$

The net current density is just the difference between the forward and the reverse current densities. Here $i^{\Rightarrow}$ and $i^{\Leftarrow}$ are both considered to be positive quantities, and for the net current density to comply with the sign convention mentioned earlier -

$$i = i^{\Rightarrow} - i^{\Leftarrow} \qquad (2.20)$$

and $$i = Fk^{\Rightarrow}_c[A^+] \exp(-\beta\Delta\phi F/RT) - Fk^{\Leftarrow}_c[D]\exp((1-\beta)\Delta\phi F/RT) \qquad (2.21)$$

For the special case of equilibrium, the electrode potential is just the reversible potential, $\Delta\phi_e$, and i = 0. This implies that the electronation and de-electronation currents are equal:

$$i^{\Rightarrow}{}_e = i^{\Leftarrow}{}_e = i_0 = F\, k^{\Leftarrow}{}_c[D] \exp((1-\beta)\Delta\phi_e F/RT)$$

$$= F\, k^{\Rightarrow}{}_c[A^+] \exp(-\beta\Delta\phi_e F/RT) \qquad (2.22)$$

The exchange current density, i_0, is a function of temperature and reagent concentration. Recalling our definition of η, we can substitute –

$$\Delta\phi = \Delta\phi_e + \eta \text{ in eqn.} \qquad (2.21)$$

When eqn (2.22) is also substituted in eqn. (2.21), we get the following equation -

$$i = i_0 [\exp((1-\beta) F\eta/RT) - \exp(-\beta F\eta/RT)] \qquad (2.23)$$

This relationship between current density and over-potential, often called the Butler-Volmer equation, lies at the heart of electrode kinetics. The over-potential is a readily measurable quantity; the potential at the electrode under study (the working electrode) can be measured relative to a reference electrode both when the working electrode is open circuited and when it carries a current. The difference between these two relative potentials is the over-potential; $\eta = E - E_e$ where E is the potential of a cell comprising of the working electrode and reference electrode. Experimental measurements of current density over-potential curves (polarization curves) require a three-electrode system - the working electrode and an auxiliary (counter) electrode, which carry the current, and a reference electrode for determining the over-potential at the working electrode.

We see that according to eqn, (2.23) the rate of an electrode reaction is determined by two parameters - the exchange current density, i_0 and the symmetry factor, β. Since many reactions have similar β values of about 0.50, it turns out that the exchange current density is generally the more important parameter in distinguishing one electrode reaction from another.

For positive values of η, the first exponential term in eqn. (2.23) is greater than unity, while the second is less than unity - the net current density is positive, in other words

anodic. For $\eta < 0$, the net current density is of negative sign, or cathodic. The situation at equilibrium ($\eta = 0$) is a dynamic one; though no macroscopic changes are observable, the electronation of A^+ and de-electronation of D, are still occurring at equal rates given by the value of i_0. A plot of eqn. (2.23) is shown in Figure 2.7, together with broken line plots of the separate anodic and cathodic terms. It can be seen that there is an approximately linear region for $\eta < 20$ mV, while for $\eta > 100$ mV, eqn. (2.23) is satisfactorily represented by one of its terms alone. This can be seen algebraically:

"Low field" region

By using expansion $e^x = 1 + x$ $(x \ll 1)$

Eqn. (2.23) can be changed to:

$$i = i_0 \ [1 + ((1-\beta) F\eta/RT) - 1 - (-\beta F\eta/RT)]$$

$$i = i_0 F\eta/RT \ (|\eta| < 20 \text{ mV}) \qquad (2.24)$$

'High field" region

By using $e^x \gg e^x$ $(x > 2)$, equation (2.23) can be written as follows:

$$i = i_o \exp((1-\beta) F\eta/RT) \quad \text{(anodic, p>l00 mV)} \qquad (2.25)$$

or $$1 = -i_o \exp(-\beta F\eta/RT) \quad \text{(cathodic, ~>-l00 mV)} \qquad (2.26)$$

Eqns. (2.25) and (2.26) can also be written as -

$$\ln i = \ln i_o + (1-\beta) F\eta/RT \qquad (2.27)$$

and $$\ln|i| = \ln i_o - \beta F\eta/RT \qquad (2.28)$$

These are forms of the empirical Tafel equation, i.e. $\eta = a + b \log i$. The cathodic Tafel slope, b, is represented by -

$$b = -2.3RT/\beta F \qquad (2.29)$$

whereas a plot of eqn. (2.26) could in principle be used to determine the value of the exchange current density i_0, it is in practice easier to obtain data in the high field region and use a Tafel plot, eqn. (2.23) or (2.28). Such plots, shown schematically in Figure 2.8, can yield both i_0 and β.

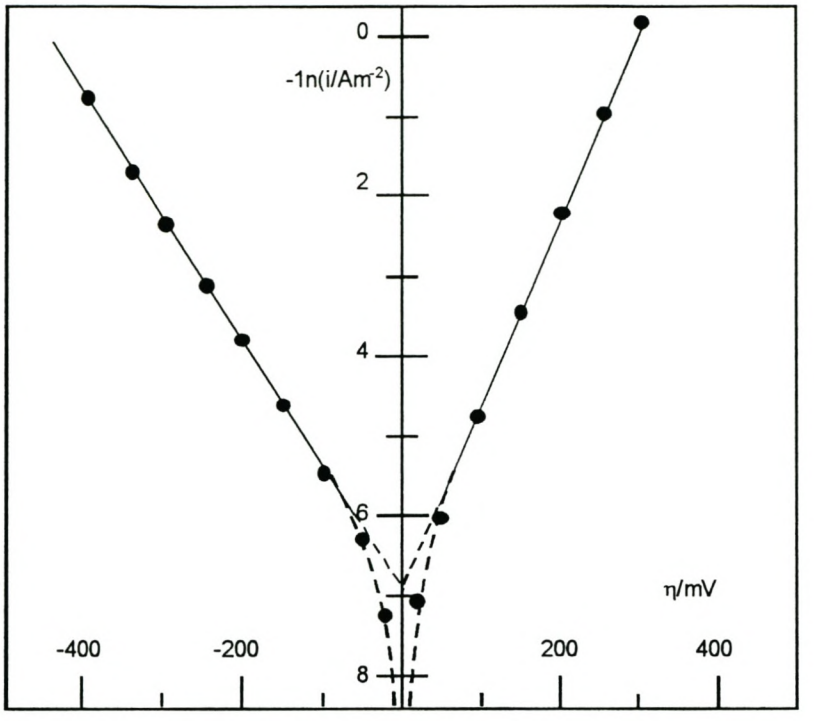

Figure 2.8: Schematic anodic and cathodic Tafel plots. (T=298K, β=0,40, $i_o=10^{-3}$ Am^{-2}) *Note common intercept on Ini axis of anodic and cathodic extrapolations.*

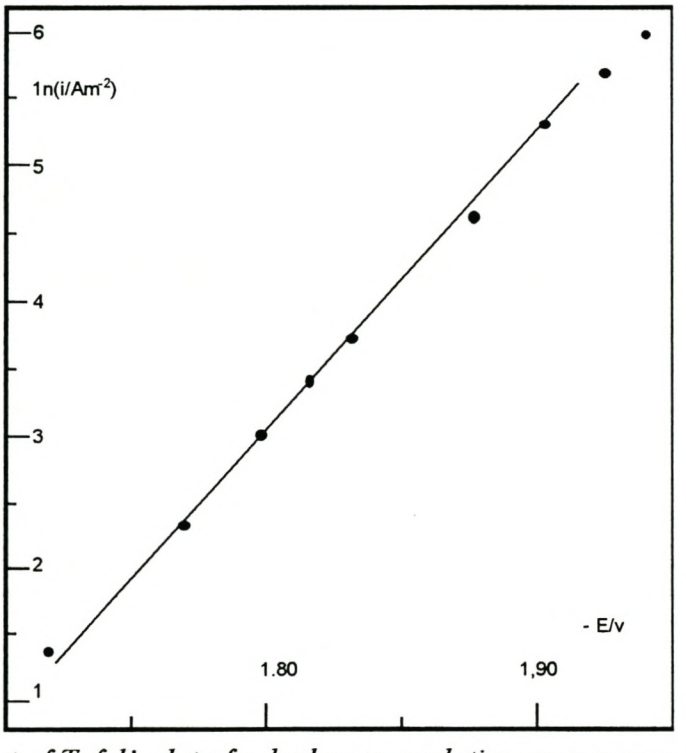

Figure 2.9: Tafel plot of Tafel's data for hydrogen evolution on mercury.

The Tafel plot of real experimental data is shown in Figure 2.9. Deviations from linearity at high current densities are due to mass transfer effects. From the linear region, the following is obtained:

- A slope of $-22{,}9\,V^{-1}$, and
- the value of $\ln(i/Am^{-2})$ extrapolated to E = -0,656 V (i.e. $\eta = 0$) is -22,5 units.

Using eqn. (2.27) (since the slope is unchanged when E is substituted for η) -

$$\text{Slope} = -\frac{BF\eta}{RT} = -22{,}9\,V^{-1}$$

$$\therefore B = 0{,}656$$

$$\ln i_0 = -22{,}5\ (A/m^2)$$

$$\therefore i_0 = 1{,}7 \times 10^{-10} A\ m^{-2}$$

It is instructive to examine the effect of variations in the values of i_0 and B on plots of the Butler-Volmer equation. In Figure 2.10, where B = 1 - B = 0,5, the curves are symmetrical about the origin.

When the exchange current density is low, as in Figure 2.10 curve (a), a large over-potential is required to ensure an appreciable reaction rate, and the electrode is said to be highly polarisable. Practical examples of this situation are the evolution of hydrogen on cathodes of mercury, lead or, to a lesser extent, zinc. These metals have high "hydrogen overvoltages". The opposite extreme (Figure 2.10 curve (c)), of a relatively non-polarisable electrode, occurs when the exchange current density is high. (Reference electrodes, which must unavoidably carry some current, however small, without appreciable changes in their potential, should be non-polarisable). Exchange current densities can vary by orders of magnitude, for different elements.

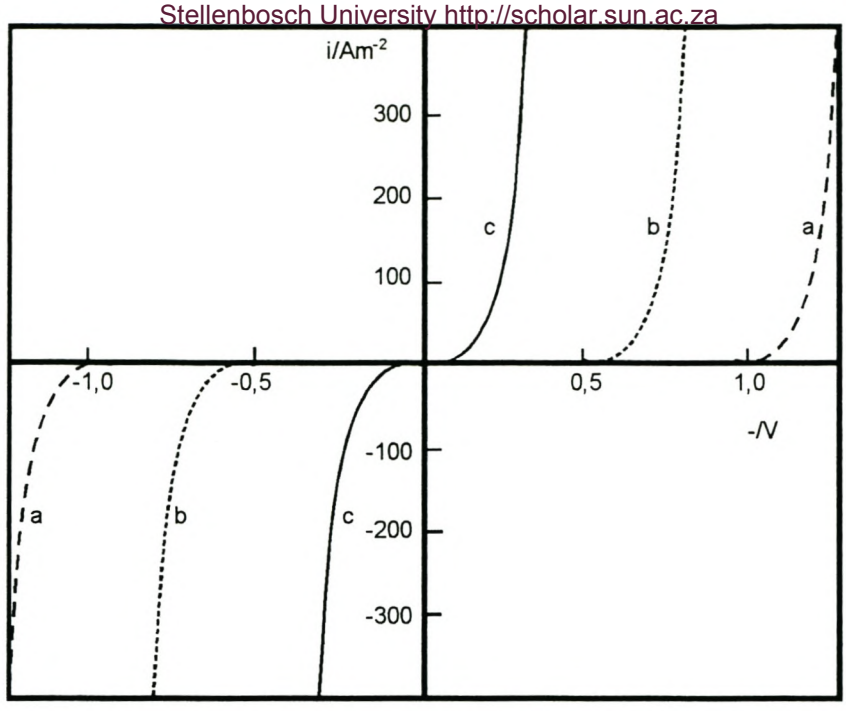

Figure 2.10: Plots of the Butler-Volmer equation showing effect of varying i_0. T=298K, B = 0,50, i /Am $^{-2}$ =10 $^{-8}$ (a), 10 $^{-4}$ (b) and 10^{-0} (c)

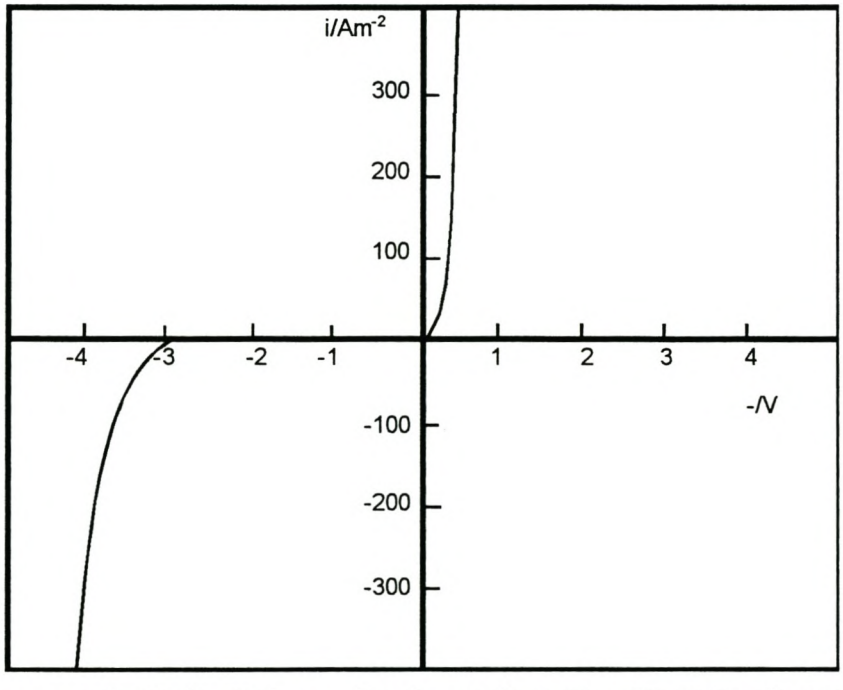

Fig 2.11: Asymmetric Butler-Volmer plot due to β≠O,50. (T-298K, β=0,10, i_o=10^{-4}Am^{-2})

The symmetry factor B, according to our definition, is a positive number less than one. Experimental values are in fact often close to 0 5.

Before finishing with the Butler-Volmer equation, consider the point where -

$$i = 0 \text{ and } \eta = 0 \qquad \text{Recalling eqn. (2.16)}$$

$$F\, k^{\Leftarrow}_c[D] \exp((1-\beta)\Delta\phi_e F/RT) = F\, k^{\Rightarrow}_c[A^+] \exp(-\beta\Delta\phi_e F/RT)$$

Re-arranging -

$$\exp(\Delta\phi_e F/RT) = k^{\Rightarrow}_c[A^+]/\, k^{\Leftarrow}_c[D]$$

or

$$\Delta\phi_e = RT/F.\ln k^{\Rightarrow}_c[A^+]/\, k^{\Leftarrow}_c[D]$$

$$= \Delta\phi_e^{\,0} + RT/F.\ln [A^+]/\,[D] \qquad (2.30)$$

where $\Delta\phi_e^{\,0} = RT/F \ln k^{\Rightarrow}_c/\, k^{\Leftarrow}_c$

Eqn. (2.22) is simply a form of the Nernst equation written here in terms of absolute electrode potentials rather than the more familiar relative electrode potentials. It should he noted that eqn. (2.30) is non-rigorous in that concentrations, rather than activities, have been employed.

2.3.2 The limitation of reaction rates by diffusion

An implicit assumption in the foregoing derivation of the Butler-Volmer equation was that the concentrations of the reagents A^+ and D were constant, and unaffected by the rate of the electrode reaction. When these conditions exist, the over-potential is associated solely with the activation of reagent ions in the electrode reaction. At high current densities the reagents may be so rapidly consumed (or products so rapidly formed) that diffusion from the electrolyte bulk to the electrode surface is not rapid enough to equalize the bulk and surface concentrations. This results in deviations from the Butler-Volmer equation, the current being smaller than that given by eqn. (2.17). Some of the over-potential, the concentration over-potential, at the electrode is now associated with the concentration gradient near the electrode surface.

In the absence of convection, an electrode reaction would give rise to changes in reagent concentrations, which with time extend progressively further from the electrode surface. These concentration changes are, however, associated with density variations, which ensure that convection is taking place, and the

concentration changes are therefore limited to a region very close to the electrode surface.

A widely used model of this diffusion layer is derived from the Nernst equation, in which the concentration of the reagent varies linearly over a distance .δ, from its surface value C_{As}^{+} to its bulk value C_{Ab}^{+}. This is an approximation to the more realistic model of a region of linear variation of C_A^{+} close to the surface, merging with a region of asymptotic approach to C_{Ab}^{+}. Figure 2.12 illustrates how the Nernst model relates to the actual concentration profile of A^+ in the situation where A^+ is being consumed at the electrode, thereby lowering the local value of C_{A+}.

The current can be related to the concentration gradient of A^+ at the electrode surface by Fick's law of diffusion, i.e. -

$$v_{Diff} = -D(C_{A+}/dx)_s$$

$$\therefore i/nF = -D(C_{A+}/dx)_s \text{ (for an n-electron transfer)} \qquad (2.31)$$

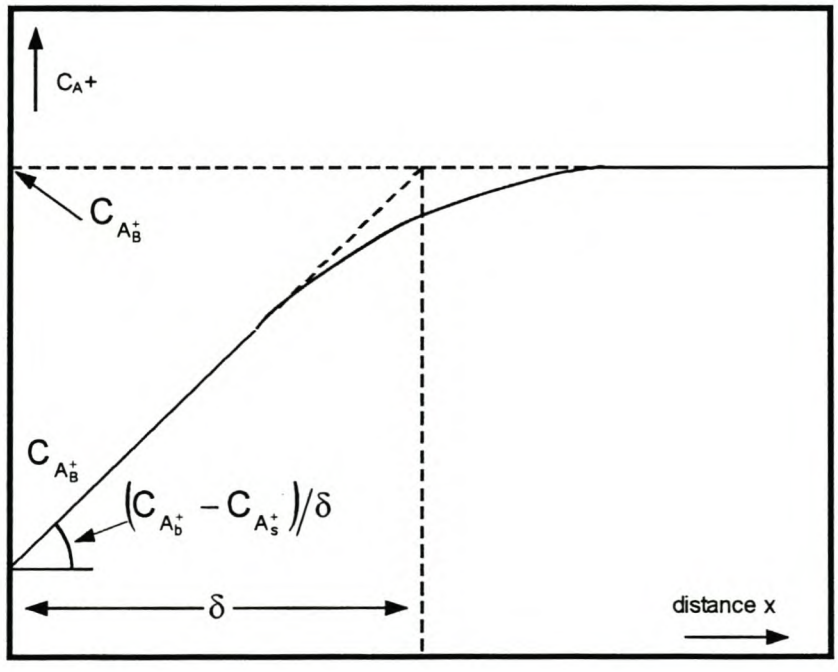

Figure 2.12: Nernst model of the diffusion layer.

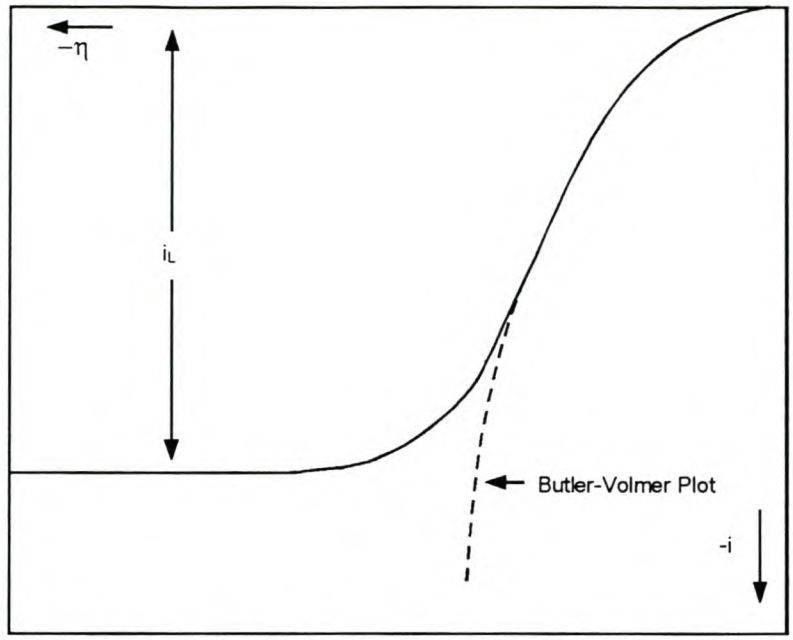

Figure 2.13: Schematic cathodic polarization curve illustrating limiting current due to slow diffusion.

The Nernst model allows us to replace $D(C_{A+}/dx)_s$ by $(C_{Ab}^+ - C_{As}^+)/2$, thus

$$\therefore i/nF = -D\left(C_{A_b^+} - C_{A_s^+}\right)/\delta \qquad (2.32)$$

The equation help to develop the concept of the limiting current density, i_L the current density obtained when $C_{Ab}^+ - C_{As}^+$ is a maximum, i.e. $C_{As}^+ = 0$.

$$i_L = -DnFC_{Ab+}/\delta \qquad (2.33)$$

The maximum rate of the electrode reaction is defined by i_L. Once the current density reaches i_L, it is independent of potential, and the Butler-Volmer equation has broken down completely, as can be seen in Figure 2.13.

The most appropriate value of δ varies from roughly 10^{-4} m in stagnant aqueous electrolytes, to about 10^{-6} m with efficient stirring. It must be stressed that equations (2.32) and (2.33) are the result of some over-simplification, and that in many practical situations they provide an inadequate description of diffusion currents.

2.4 THERMODYNAMIC CONSIDERATIONS (Nicol, 1979a)

As a result of the work of Pourbaix who developed a simplified form of depicting the thermodynamic characteristics of aqueous systems (with particularly corrosion in mind), it is possible to assimilate a large amount of thermodynamic data in a relatively simple graphical form. In these "Pourbaix" diagrams (also known as E_H - pH diagrams), the plotted variables are pH and electrochemical potential. Other

variables such as metal ion or complexing ion concentration, temperature and pressure can be introduced as contour lines to provide a third dimension.

The Pourbaix diagram of the Zn - H_20 system will be discussed here. Under standard conditions, with only pH and E (the potential on the normal hydrogen (H) electrode scale) as variables, there are only 5 lines on the diagram (Figure 2.14). The chemical reactions represented by these lines are -

$$Zn^{++} + H_2O \Rightarrow ZnO + 2H^+ \quad (2.34)$$

$$\underline{ZnO} + H_2O \Rightarrow ZnO_2^{=} + 2H^+ \quad (2.35)$$

$$Zn^{++} + 2e \Rightarrow Zn^o \quad (2.36)$$

$$\underline{ZnO} + 2H^+ + 2e \Rightarrow Zn^o + H_2O \quad (2.37)$$

$$ZnO_2^{=} + 4H^+ + 2e \Rightarrow Zn^o + 2H_2O \quad (2.38)$$

The equilibria of equations (2.34) and (2.35) can be expressed in terms of pH as follows:

$$K_1 = [H+]^2/[Zn^{++}];\ pH_1 = -1/2 \log K_1 - 1/2 \log [Zn^{++}] \quad (2.34a)$$

$$K_2 = [H+]^2/[ZnO_2^{=}];\ pH_2 = -1/2 \log K_2 - 1/2 \log [ZnO_2^{=}] \quad (2.35a)$$

In the case of equations (2.36) to (2.38), the equilibrium is more appropriately written in terms of electrode potential, i.e.:

$$E_3 = E^\circ_3 + (2.3RT/2F) \log [Zn^{++}] \quad (2.36a)$$

$$E_4 = E_4^\circ - (2.3RT/F)pH \quad (2.37a)$$

$$E_5 = E_5^\circ - (2.3RT/F)(2pH) + (2.3RT/2F) \log [ZnO_2^{=}] \quad (2.38a)$$

n in which activity has been approximated by concentration.

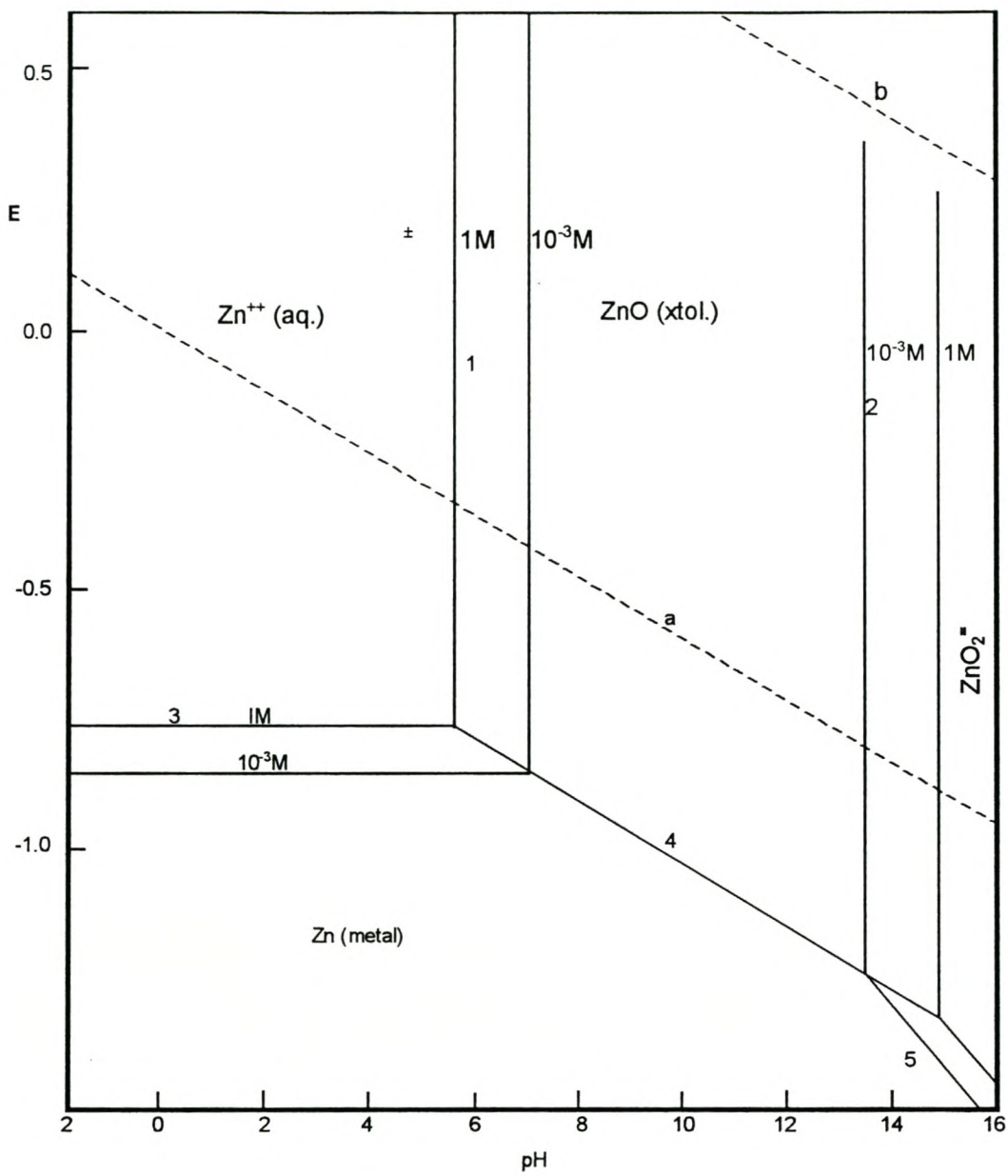

Figure 2.14: Zinc water phase diagram (Pourbaix, 1966).

Under standard conditions T = 298°K and (Zn^{++}) or $(ZnO_2^{=})$ = 1. These equations become -

pH_1	=	$-1/2 \log K_1$	= 5.48	(2.34b)
pH_2	=	$-1/2 \log K_2$	= 14.89	(2.35b)
E_3	=	$E°_3$	= -0.763	(2.36b)
E_4	=	$E°_4 - 0.0591$ pH	= -0.0439 – 0.0591pH	(2.37b)
E_5	=	$E°_5 - 0.1182$ pH	= 0.441 - 0.1182pH	(2.38b)

Thus, lines (1) and (2) on Figure 2.14 are vertical and are located at the pH values defined by equations (2.34b) and (2.35b), respectively. Line (3) is horizontal and is defined by equation (2.36b). Lines (4) and (5), have negative slopes and are defined by equations (2.37b) and (2.38b), respectively.

Note that equations (2.34b) to (2.38b) define the slope and intercept values of the lines, but do not indicate the extent of the lines. For example, line (3) extends only to pH of 5.48, where it intersects line (1). It cannot extend further because Zn^{++}, being hydrolyzed, will not maintain standard conditions at higher pH values. Note that equations (2.31) to (2.35) permit computation of slopes and intercepts for non-standard conditions.

In general, the Pourbaix diagram gives us the following information about the zinc water system:

- Above lines (3), (4) and (5), metallic zinc is unstable and should corrode or oxidize.
- At pH values less than defined by line (1) or greater than defined by line (2), zinc-oxide should dissolve as Zn in acid solutions or $ZnO_2^{=}$ in alkali solutions.
- Below lines (3), (4) and (5), metallic zinc is stable and would plate out of solution or reduce from ZnO. Electrowinning of zinc takes place below line (1), while the negative terminal of the experimental zinc-air storage battery operates at the junction of lines 2, 4 and 5 on this diagram.

Note that there are two additional dotted lines on the diagram. These correspond to the reactions -

$$\text{(a)} \quad 2H^{+} + 2e = H_2\,(g) \qquad (2.39)$$

and

$$\text{(b)} \quad O_2(g) + 4H^{+} + 4e = 2H_2O \qquad (2.40)$$

These lines are useful in predicting whether a species is stable with respect to oxidation by oxygen or to dissolution with the evolution of hydrogen. Thus, since line 3 lies below line (a), zinc metal is thermodynamically unstable in aqueous solutions with respect to the evolution of hydrogen. It must be noted, however, that thermodynamic instability is no guarantee that the reactions will proceed at rates appreciable enough to make them easily observable. For example, the well-known

corrosion resistance of galvanized iron is due to the protection offered by the ZnO layer (line 4). Any line on any Pourbaix diagram can be expressed by the general equation:

$$aA + bB \pm mH^+ + ne \Leftrightarrow cC + dD \qquad (2.41)$$

Here, A represents an oxidized and C, the reduced species of an element whose diagram concerns us. B and D represent auxiliary species such as complexing agents, precipitating agents, auxiliary species, or water. Hydroxyl ions are never permitted, because they can always be replaced by water and hydrogen ions to represent the same reactions, noting the pH is defined in terms of hydrogen ions. The electrode potential for equation (2.41) can be written as -

$$E = E^\circ \pm (2.3RT/F\ (m/n))\ pH - (2.3RT/nF) \log (a^c_C\ a^d_D / a^a_A\ a^b_B) \qquad (2.42)$$

Under standard conditions, the last term disappears because all relevant activities are unity. In any case, pure solids have unity activities, as have gases when present at 1 atm. On the diagram, the slope is always proportional to (- m/n). Thus, when m is zero, the line is horizontal, while when n is zero, the line is vertical. If the hydrogen ions are placed on the right hand side of the equation, the slope is positive.

2.5 METAL DEPOSITION

The cathodic deposition of a hydrated metal ion, $M(H_2O)_n^{2+}$, onto a metal electrode M, can be considered as occurring in several steps, the most important of which for this discussion are:

- Charge transfer to the hydrated metal ion in the double-layer with the formation of a neutral or partially charged "ad-atom" or "ad-ion" which is adsorbed within the inner-Helmholtz plane. This ad-atom or ad-ion may still be partially hydrated.
- Migration of the ad-atom by surface diffusion to a growth site (such as an edge or kink) at which further coordination with respect to other metal atoms in the lattice occurs with further loss of hydration molecules.
- Growth of the crystal lattice by successive transfer and diffusion steps.

The essential difference between an aqueous metal ion and a metal ion in a lattice is that the co-ordination sphere of the former is composed of water molecules, while

that of the latter is composed of other metal ions, i.e. metal - H_2O bonds have to be broken and replaced by metal-metal bonds. Several aspects of these will be discussed in more detail below.

2.5.1 Charge Transfer

The exchange current density of metal/metal-ion electrodes varies between wide limits depending on the nature of the metal-ion and its state in solution. For simple ions, the following table (Table 2.2) gives some idea of the range of reversibility of metal electrodes.

TABLE 2.2: Subdivision of Metals according to their Exchange Currents in Aqueous Solution.

Current Density (Amp/cm^2)		
10 to 10^{-3}	**10^{-3} to 10^{-8}**	**10^{-8} to 10^{-15}**
Lead	Copper	Iron
Tin	Zinc	Cobalt
Mercury	Manganese	Nickel
Thallium	Bismuth	Chromium
Cadmium	Antimony	Platinum Group
Silver		
Gold		

It has been theoretically postulated that the loss of hydrated water molecules is one of the main causes for the over-potential accompanying the cathodic reduction of cations in aqueous solutions, at least for small multiply-charged aqua-ions. For the reduction of a number of bivalent cations there is experimental evidence that the kinetically important step in the electro-deposition reaction is the loss of a water molecule from the hydration sphere of the ion. This is supported by the following correlation between the exchange current density (i_0) and the rate constant (k) for the substitution of water in the inner co-ordination sphere of the ions.

Replacement of water molecules by other molecules or anions in the co-ordination sphere can either accelerate or inhibit charge transfer. These effects are complex combinations of thermodynamic and kinetic origin and no simple picture has yet emerged which can be used to reliably predict variations in i_0 with solution conditions.

2.5.2 Electrocrystallization

Experimental observations of the structure and growth of electrodeposits can be summarized as follows:

- Electro-deposits are, with few exceptions, crystalline and the crystal structures normally correspond to those of the bulk metal.
- The size of the individual crystals constituting a deposit depends on the particular metal and the conditions of electro-deposition (solution composition, temperature, current density, pH, etc.).
- The shapes of the crystallites are determined by the mode of growth of these deposits.
- Unless special measures are adopted (such as the use of leveling agents), the surface topography indicates growth roughening.

These observations can, in general, be explained by the answers to the following two main fundamental aspects of electro-crystallization, i.e.

- What are the factors governing the lateral and outward growth of the crystals?
- What are the factors governing the nucleation of new crystallites?

The most important is the over-potential. It is not difficult to understand that the formation of nuclei on a crystal plane will be dependent on the surface concentration of ad-atoms which is, of course, dependent on the over-potential (or current density) since the rate of ad-atom formation (charge-transfer) increases with increasing over-potential. Thus, fine-grained (large number of small crystallites) deposits will be formed in preference to coarse-grained deposits at high over potentials. This is generally observed and in the extreme case where the current density is close to the limiting current density metal powders are formed. The use of complex metal ions which require high over-potentials for deposition such as $Ag(CN)_2$ also tends to promote the formation of dense fine-grained deposits. Finally, growth can be inhibited and nucleation therefore induced by the addition of various leveling or brightening agents, which adsorb preferentially on the crystal defects, which are the growth sites.

What about the shape of the crystallites, i.e. lateral versus outward growth? It should be apparent that outward growth of a perfect crystal face is dependent on the

nucleation of a new two-dimensional layer on the surface. On the other hand, lateral growth can generally always occur by growth at kink and edge sites formed in each layer, and would therefore be preferred. However, few crystals are perfect and the inevitable presence of screw dislocations in the crystal produces a mechanism by which lateral growth at the step produces a new edge and continual growth by rotation of this perpetuating edge normal to the surface is possible. Growth normal to the surface is often accelerated by other effects as well. Thus, if the height of the crystal is sufficiently large and/or its "radius of curvature" sufficiently small, the electrical field will be concentrated at the tip with a resultant increase in deposition rate in this region. It is obvious that those metals, which exhibit high exchange current densities, i.e. large changes in rate for relatively small variations in over-potential, will be most susceptible to this phenomenon. Thus, the metals in the left-hand column of Table 2.2 are known to form long needle-like or dendritic deposits while those on the right form smooth, dense deposits. This effect is the main contribution to the so-called "micro-throwing power" of particular baths.

If the outward growth of a needle or dendrite becomes sufficient (in the region of a millimeter), it can penetrate the diffusion layer at the surface and enhanced mass transport to the tip of the protrusion is possible. This further increases the rate of growth with the result that, once initiated, these tips can grow extremely rapidly often with disastrous results to a metal deposition process. This latter effect is the basis for the use of various smoothing agents in these processes. Thus, if the concentration of the additive is low enough, the enhanced mass transport to the dendrite tip should result in increased adsorption and growth inhibition in this area as opposed to valleys in the surface into which transport of the additive is difficult. This results in a general smoothing of the deposit.

2.6 REACTOR DESIGN (Pickett, 1979)

In many electrochemical processes mass transport control of the important cell reactions is a common occurrence. In such cases, the fundamental parameters describing the reactor performance are:

- the average mass transfer coefficient (K_{av}),
- the active electrode area to reactor volume ratio (A/V), and
- their product (K_{av} A/V).

The average mass transport coefficient can be determined using the diffusion limited current technique. This involves measuring the potential independent limiting current plateau, for a well behaved convective-diffusion controlled reaction by applying the following equation:

$$I_L = n\,F\,A\,K_{av}\,C_b \qquad (2.43)$$

where:

n = the number of electrons per molecule oxidized or reduced

A = the active electrode area

C_b = the bulk reaction concentration

This phenomenon of limiting current density could be due to the formation of a non-conducting passive film or to the decrease in the metal ion concentration at the electrode surface due to high surface reaction rates. The latter is also known as "concentration polarisation" and is due to the limiting transfer rate of the reacting ion species.

The rate at which an electrochemical reaction can occur will depend on the rate at which a reagent can reach the electrode or a product removed from it. From basic consideration the mass transfer coefficient K_L can be defined as -

where $C = K_{av} = CQ^{0,7}$ (2.44)

or $$K_L = \frac{D_A}{\delta} \qquad (2.45)$$

where D_A is the molecular diffusitivity of A and δ the thickness of the diffusion layer. Most correlations are expressed in terms of dimensionless groups. In mass transfer the Sherwood number is defined as -

$$Sh = \frac{K_L\,L}{D_A} \qquad (2.46)$$

Where L is some characteristic length dimension (e.g. electrode height or distance along the electrodes). This should be clearly defined for the correlation that is to be used to determine K_{av}. The mathematical form of the correlation will depend on the geometrical flow conditions and reactions that are occurring in the cell. The majority of

correlations are obtained by fitting experimental data to what may appear to be an arbitrary set of parameters.

2.6.1 Gas evolving at electrodes (Bryson, 1995)

In electro-winning processes such as zinc, hydrogen gas is simultaneously produced at the cathode. The nucleation, growth and detachment of these hydrogen bubbles considerably enhance the transfer of metal ions to the electrode surface. The process is similar to that of nucleate boiling in heat transfer and Stephan and Vogt (1979) have used this analogy to derive the semi-empirical relation.

$$Sh = 0.93\ Re^{0.5}\ Sc^{0.487} \qquad (2.47)$$

where $Sh = K_{av} L/D_A$

$Re = V_{G/A}\ d_A\ \delta/Au$

$Sc = u/\ \delta\ d_A$

d_A = diameter of bubble at break-off from electrode

$V_{G/A}$ = volume of gas produced per unit area of electrode per unit time.

The value of the break-off diameter is a function of many factors such as the type of gas, electrolyte composition and temperature, current density, electrode surface condition and the presence of surface-active agents. The value for d cannot be currently predicted from fundamental considerations, but a value of 50μm for metals in aqueous solutions is satisfactory for design purposes, provided that the surfaces are facing upwards or vertical.

The gas evolution at the anode must also be considered. In most electro-winning processes, a gas (usually oxygen) is evolved at an inert electrode. This oxygen not only enhances mass transfer at the anode, but also creates a convection flow of electrolyte causing mixing between the electrodes. This enhances any natural convection concentration gradients. The effect can be correlated by the following relation:

$$Sh = (Sh)_{nc} + 3.088\ Re^{0.77}\ Sc^{0.25} \left(\frac{L}{n}\right)^{0.336} \qquad (2.48)$$

Where $(Sh)_{nc}$ is the Sherwood number for natural convection as given by equation (2.46).

2.6.2 Natural Convection

Natural convection takes place due to density gradients in fluids. This may occur due to differences in temperature or concentration. Concentration differences may occur on the cathode side when the rate of deposition exceeds the supply of ions from the electrolyte. Since the density of the electrolyte is higher than the solvent in the electrolyte, a circulation pattern is set up. If the resulting flow of the electrolyte is in the laminar regime then the momentum and mass balances can be solved [Hohanta, 1977] to give the following:

$$Sh = 0.67\ Ra^{0.25} \qquad (2.49)$$

and the Rayleigh Number, Ra, is defined as:

$$R_a = \frac{L^3\, g\, p\, (p_\infty - p_\delta)}{\mu\, D_A\, p_\infty} \qquad (2.50)$$

Where:

L = height of electrode [m]

p = density [g/cm^3]

μ = viscosity [centipoise]

g = gravity constant [ms^2], and

D_A are evaluated at the arithmetic average concentration of the various components.

The fluid densities p_δ and p_∞ are the densities of the solution at the electrode interface and in the bulk of the solution, respectively.

In the case of electro-winning from an electrolyte, where the reactor volume is small compared to the electrolyte volume, and forced circulation takes place through the reactor, a combination of these processes occur, namely:

Sh = Natural convection (2.49) + gas evolution at the cathode (2.48) + gas evolution at the inert anode (2.47) + forced circulation.

In terms of the Sherwood number:

$$Sh = 0.67\, R_a^{0.25} + (0.67\, R_a)^{0.25} + 3.008\, Re^{0.77}\, Sc^{0.2}\, x \qquad (2.51)$$

$$\left(\frac{L}{H}\right)^{0.366} + 0.93 Re^{0.5}\, Sc^{0.487} + forced\ circulation$$

Equations (2.47) and (2.48) are two models of the same phenomena, where only the set of parameters to which the models can be fitted differ. This difference is allowed as each set of parameters has its own advantages and merits. This allows one to simplify the equations to give the semi-empirical equation, with the assumption that the breakaway diameter of the oxygen and the hydrogen are the same, i.e.

$$Sh = 0.67\ Ra^{0.25} + 2\,(0.93\ Re^{0.5}\ Sc^{0.487}) + forced\ circulation \qquad (2.52)$$

This equation can be simplified to -

$$Sh = 0.67\ Ra^{0.25} + x\ Re^{y}\ Sc^{z} \qquad (2.53)$$

if the + forced circulation term assumption does not hold.

Equation (2.44) presents K_{av} as a function of the volumetric flow rate. Thus, this equation allows one to determine the value of K_{av} once the limiting current density is obtained experimentally. This value of K_{av} encompasses the volumetric flow rate and can simplify equation (2.53) to the following -

$$Sh = 0.67\ Ra^{0.25} + x\ Re^{y}\ Sc^{2} + CQ^{0.7} \qquad (2.54)$$

This equation is equal to -

$$Sh = 0.67\ Ra^{0.25} + 1.9\ Re^{0.5}\ Sc^{0.487} + CQ^{0.7} \qquad (2.54a)$$

if the value of d is the same at both the cathode and the anode.

This leaves a universal equation for electrochemical reactors, which describe a system in term of its Sherwood number, Rayleigh number and volumetric flow rate. More important though is the mass transport coefficient, which can be analysed in terms of the different factors that determine it. Factors like density, concentration, flow rate and others, which are all independent measurable quantities.

Substitution delivers:

$$Sh = 0.67 \left(\frac{L^3 g p (p_\infty - p_\delta)}{\mu D_A p_\infty} \right)^{0.25}$$

$$+ 1.9 \left(\frac{V_G d p}{A \mu} \right)^{0.5} \bullet \left(\frac{\mu}{p D_A} \right)^{0.487} + CQ^{0.7} \qquad (2.54b)$$

In this way a set of parameters can be established to achieve a constant mass transport coefficient. The mass transport coefficient can in this way serve as the controlling parameter in an automated process.

TABLE 2.3: Dimensionless groups applicable to convective mass transfer at an electrode.

Name	*Usual Form*	*Alternative Form*
Sherwood number	$Sh_{av} = K_{av} d_e / D$ (a)	$Sh_x = K_x x/D$ (b) $Sh_L = K_{av} L/D$ (c) $Sh_l = K_x d_e /D$ (d)

(a) d_e = Reactor equivalent diameter, as the characteristic length.

(b) Local mass transfer rate at some distance x along an electrode.

(c) Overall rate over the length, L, of an electrode.

(d) Local mass transfer rate with the reactor equivalent diameter at a specific point on an electrode.

K_{av} = average mass transfer coefficient

L = electrode length

Equations (a) and (c) only differ by the ratio d_e:L which is constant for a given reactor, the choice is made on the basis of mathematical convenience.

D = the ionic diffusivity

2.6.3 The minimum voltage requirement for electrolysis (Pickett, 1979)

If only one reaction occurs at each electrode during an electrochemical process the process will be represented by the following stoichiometric equation:

$$V_A A + V_B B \rightarrow V_C C + V_D D \qquad (2.55)$$

Where V_A, V_B, V_C, and V_D are the stoichiometric coefficients for the species A, B, C and D. Consider the case where the operation proceeds at a constant temperature and pressure with no material input or output from the reactor. We recognise that the reaction (2.55) is an un-natural process at the temperature and pressure of the reactor without an applied voltage. This unnatural state is represented by the positive sign of the free energy change of the reaction Δ G:

$$\Delta G = V_C \mu_C + V_D \mu_D - V_A \mu_A - V_B \mu_B \qquad (2.56)$$

where μ_A to μ_D are the chemical potentials of the species, respectively.

The purpose of electrolysis is to increase the free energies of A and B, thus to reverse the sign of ΔG. With a certain voltage applied, the applied voltage is given by -

$$V = \varnothing_+ - \varnothing_- \qquad (2.57)$$

where $\varnothing_+$ and $\varnothing_-$ are the electrode potentials of the positive and negative terminals of the power supply. The voltage can be identified with three potential differences inside the reactor. Two of these potential differences occur at the electrode/solution interfaces and the other is across the solution and is associated with the resistance to ion transfer.

V is decreased until the current ceases, the solution potential decrease disappears but the two interfacial potential differences remain although they decrease in magnitude. At zero current, the voltage applied keeps the system at equilibrium-state. This voltage is the minimum electrolysing voltage.

To determine the minimum electrolysing voltage for a given system, we rewrite the stoichiometric equation to take into account the electronic charges so that -

$$Ze_c + V_A A + V_B B \rightarrow Ze_a + V_C C + V_D D \qquad (2.58)$$

when e_c and e_a represent an electron "consumed" and "produced" at the cathode and anode, respectively.

At equilibrium, the free energy of the system is at a minimum and under this condition -

$$Z \mu_{e_c} + V_A \mu_A + V_B \mu_B = Z \mu_{e_a} + V_C \mu_C + V_D \mu_d \qquad (2.59)$$

where: μ_{ec} and μ_{ea} represents the chemical potential of the respective electrons, and

μ = electro-chemical potential per gram equivalent of electron

Substituting (2.56) into (2.59) and rearranging gives the following -

$$Z(\mu_{e_c} - \mu_{e_a}) = \Delta G \qquad (2.60)$$

At equilibrium the chemical potential of an electron in an electrode is equal to the chemical potential of an electron in the adjacent power supply terminal, thus -

$$\mu_{e_c} = \mu_{e^-} \qquad (2.61)$$

$$and \ \mu_{e_a} = \mu_{e^+} \qquad (2.61a)$$

The difference between the chemical potentials of the electrons in the two terminals is equal to the difference in the reversible work needed to bring a measure of infinity to each terminal. This difference can be expressed by -

$$\mu_{e^-} - \mu_{e^+} = -F(\varnothing_- - \varnothing_+) \qquad (2.62)$$

(electron potential of 1 mole electrons)

Where the negative sign in the right hand side is due to the single negative charge on an electron, the potential difference thereby conforming to its usual electrostatic definition.

Making the requisite substitutions of equation (2.61) and (2.61a) into equation (2.60) we obtain -

$$\Delta G = zF(\varnothing_+ - \varnothing_-) \qquad (2.63)$$

Designating the minimum electrolysing voltage by V_{min}, it immediately follows that -

$$\Delta G = zF\,v_{min} \qquad (2.64)$$

Δ G = Gibbs free energy change of chemical reaction.

Equation (2.64) enables the minimum electrolysing voltage for a system to be calculated from free energy data.

2.6.4 The basic design for a plug flow reactor (Pickett, 1979)

Consider the operation of a generalised plug flow reactor shown in Figure 2.15. A volumetric flow rate, N, of electrolyte solution enters this reactor with reactant concentration, C_{av1}, and leaves with reactant concentration C_{av2}. For convenience, the principal exit of the reactor is straight and corresponds to the x- co-ordinate over a length, L, from x = 0 to x = L. The cross sectional area normal to the flow, S, is constant and the electrode area per unit length of reactor is also constant and equal to 0.

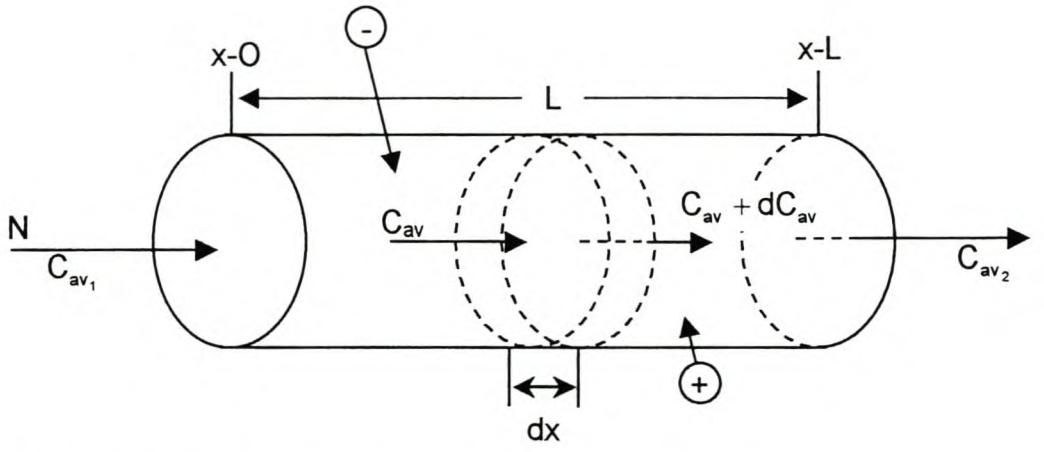

Figure 2.15: Material balances over a generalised plug flow reactor

If the total current passing through the reactor is I, and the reaction is a z electron process per reactant molecule, then the overall material balance is -

$$N\left(C_{av_1} - C_{av_2}\right) = \frac{I}{zF} \qquad (2.65)$$

A second material balance can be written for a small element of reactor, length = dx, situated at a distance x from the entrance. Assuming that the concentrations entering and leaving the element are C_{av} and $C_{av} + dC_{av}$, respectively, then we can write –

$$\left\{NC_{av} - D_s\left(\frac{dC_{av}}{dx}\right)x\right\} - \left\{N\left(C_{av} + dC_{av}\right) - D_s\left(\frac{dC_{av}}{dx}\right)x\right\}$$

$$= \frac{I_x \sigma}{zF} dx \qquad (2.66)$$

where i_x is the current density over the elemental area, σdx, and is taken to be constant over it. The first term in each bracket in equation (2.66) represents the input/output of reactant due to flow, and the second term's average input/output by diffusion. Simplification of equation (2.66) gives -

$$\frac{-NdC_{av}}{dx} + D_s \frac{d^2C_{av}}{dx^2} = \frac{i_x \sigma}{zF} \qquad (2.67)$$

where the right hand term account for reactant depletion due to electrolysis.

If the longitudinal diffusion and the dispersion are ignored, and the mean concentration obeys the first order differential equation, then -

$$\frac{dC_{av}}{dz} = \frac{i_x \sigma}{zFN} \qquad (2.68)$$

which is the basic design equation for a plug flow reaction.

Integration of equation (2.68) over the reactor will give equation (2.65) with -

$$I = \sigma \int_O^L i_x \, dx = \sigma L \, i_{av} \qquad (2.69)$$

where i_{av} is the average current density over the whole reactor. Equation (2.68) can easily be adapted to any type of plug flow reactor. Figure 2.16 shows a parallel plate reactor with a cross-sectional area equal to BS and a electrode area per unit length of B(=σ). Since U_{av} BS = N , where U_{av} is the average velocity of the electrolyte solution, then substitution in equation (2.68) gives -

$$\frac{dC_{av}}{dx} = \frac{-i_x}{z F U_{av} S} \qquad (2.70a)$$

In designing of reactors, we seek integral forms of equation (2.66), for the two types of electrode processes, namely the fast mass-transfer controlled reaction and the slow, activation controlled reaction.

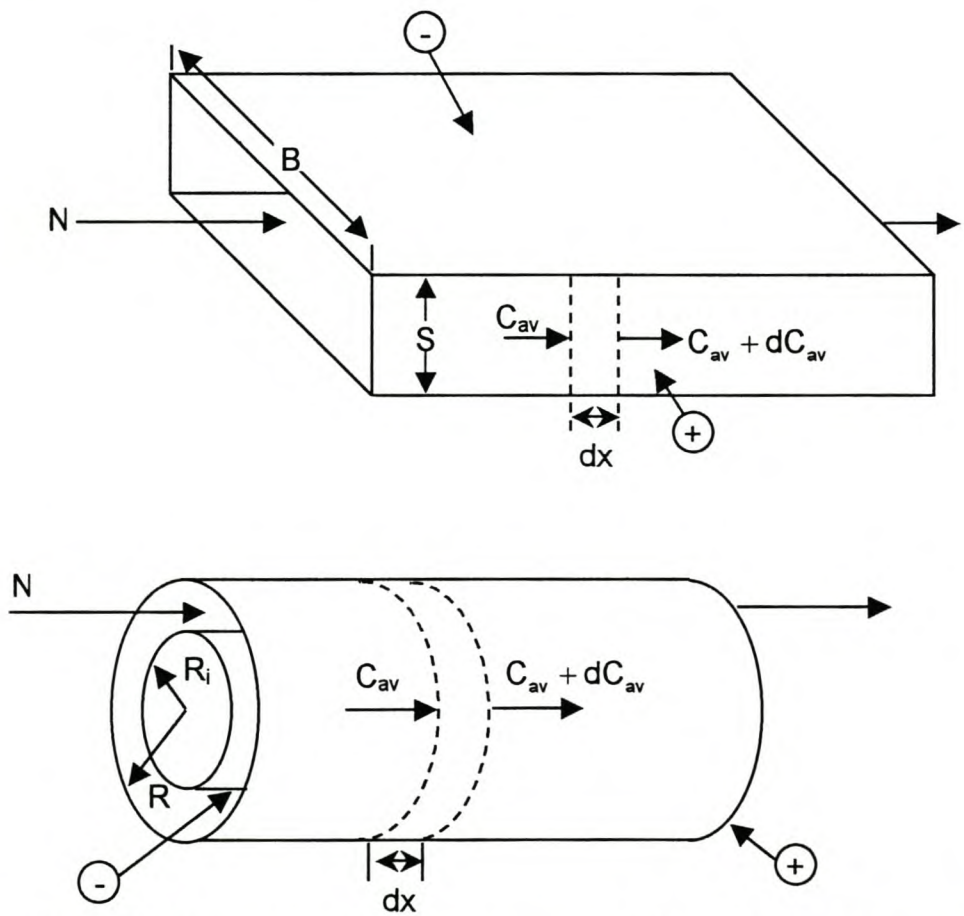

Figure 2.16: Material balances over plug flow reactors (a) Parallel plate reactor, and (b) Concentric cylinder reactor.

2.6.5 The minimum electrode area for a fast electrochemical reaction

For a fast electrochemical reaction, the local current density can be written in terms of a local mass transfer coefficient, K_x, using the following:

$$i_x = z F K_x (C_{av} - C_s) \qquad (2.70)$$

where C_{av} and C_s are the local bulk and surface concentrations of reactant, respectively. The use of the local value of the mass transfer coefficient indicates that any positional dependence is entirely arbitrary. Equation (2.70) can be used to eliminate i_x from equation (2.68) so that -

$$\frac{dC_{av}}{dx} = \frac{-\sigma K_x}{N} (C_{av} - C_s) \qquad (2.71)$$

which is the basic design equation for a plug flow reactor with a fast electrochemical reaction.

For a given conversion of reactant, the minimum electrode area required will be if the reactor operates at a limiting current throughout (i.e. the surface concentration, C_s, is zero at all points). This is only possible if a second reaction occurs simultaneously over the electrode.

Taking the reactor length as L_{min}, then from equation (2.71) -

$$-N \int_{C_{av1}}^{C_{av2}} \frac{dC_{av}}{C_{av}} = \sigma \int_{o}^{L_{min}} K_x dx \qquad (2.72)$$

which after integration gives -

$$A_{min} = \sigma L_{min} = \frac{N}{K_{av}} ln \frac{C_{av1}}{C_{av2}} \qquad (2.73)$$

where K_{av} is the average mass transfer coefficient over the reactor. Equation (2.73) represents an idealised condition, since the over-potential will be infinite.

An interesting version of equation (2.73) can be obtained by eliminating the flow rate, N, using equation (2.65).

$$\frac{I}{zF} = \frac{K_{av}\ A_{min}\ (C_{av_1} - C_{av_2})}{ln\ \frac{C_{av_1}}{C_{av_2}}} = K_{av}\ A_{min}\ C\ log\ mean \qquad (2.74)$$

Other useful forms of equation (2.73) and (2.74) are available. The concentration C_{av}, which will be obtained over part of the reactor up to a length of x, under ideal limiting conditions can be obtained from equation (2.73) or by a further integration of equation (2.71), i.e. -

$$C_{av} = C_{av_1}\ exp\left[\frac{-K_{av_x}\sigma x}{N}\right] \qquad (2.75)$$

where K_{avx} is the average mass transfer coefficient over the length x. The fractional conversion of reactant, which is achieved over the entire reactor is:

$$f_e = \frac{C_{av_1} - C_{av_2}}{C_{av_1}} = 1 - exp\left[\frac{K_{av}\ A_{min}}{N}\right] \qquad (2.76)$$

and the total current can be written in terms of the inlet concentration by combining equations (2.73) and (2.65) to give –

$$I = zFNC_{av_1}\left\{1 - exp\left[\frac{-K_{av}A_{min}}{N}\right]\right\} \qquad (2.77)$$

2.6.6 Non-limiting current operation for a fast reaction (Pickett, 1979)

The basic design equation for a plug flow reactor with a fast reaction has been given in the previous section, i.e. -

$$\frac{dC_{av}}{dx} = \frac{-\sigma K_x}{N}(C_{av} - C_s) \qquad (2.71)$$

If the reactor is not at a limiting current then C_s will be non-zero along at least part of the electrode length. However, a known variation of C_s with position exists in the case of a constant mass flux at the electrode surface. Both K and C_{av} - C_s are constant over the reactor for this condition, so that the evaluation of (2.65) is particularly simple. Thus

replacing K_x by K and integrating over a reactor of length L, we obtain the electrode area, A, in the form -

$$A = \sigma L$$

$$= \frac{N(C_{av_1} - C_{av_2})}{K(C_{av} - C_s)} \qquad (2.78)$$

The application of equation (2.78) requires that the reactor can be operated so that C_{av} - C_s remains constant along the reactor and dC_s/dx is constant.

An exact design procedure requires that equation (2.71) can be solved for any specific surface concentration distribution.

The method, which has to be adapted, is known as the "superposition method". It relies on the fact that the convective mass transfer equation, which gives rise to relationships for the mass transfer coefficient, is a linear differential equation and that the sum of all the solutions to it is also a solution. A good account of the procedure has been given by Kayj [1968].

The technique was adapted by Parrish and Newman, Newman, and Hansy and Newman (Pickett, 1979) to establish sub-limiting current distributions in various electrochemical reactors. In many situations, when the mass transfer coefficient is spatially independent, the superposition method becomes quite straightforward.

2.6.7 The fast reaction in a parallel plate reactor with short electrodes

2.6.7.1 Laminar flow

For laminar flow in a parallel plate reactor with short electrodes of length, L, the hydrodynamic and mass transfer entrance effects are ignored and the average mass transfer coefficient is calculated with –

$$\frac{K_{av} d_e}{o} = 1.85\left\{Re.Sc.\frac{d_e}{L}\right\} \qquad (2.79)$$

The average current density is given by -

$$i_{av} = zF(C_b - C_s)\, Sh_{av} \bullet \frac{D}{d_e} \qquad (2.80)$$

The equations apply only for mass transfer in a parallel plate reactor in an electro-refining process (metal deposition/metal dissolution) and when the reactor has infinitely wide electrodes and a long hydrodynamic entrance length.

If we substitute for K_{av} , from (2.79) into equation (2.75) we obtain an expression for the outlet concentration under limiting current conditions -

$$C_{av_2} = C_{av_1} \exp\left\{ \frac{-1.85\ \sigma\ D\ R_e^{\frac{1}{3}}\ Sc^{\frac{1}{3}}}{N} \left(\frac{L}{d_e} \right)^{\frac{1}{3}} \right\} \qquad (2.81)$$

The small change in concentration through the reactor provides evidence for the use of the exact method to a high degree of accuracy.

Two distinctions can be made between this situation, and long electrodes. Here the concentration profile is only developing along the electrode and the bulk of the solution will have an almost uniform composition. Consequently, Laplace's equation will be obeyed to a very close approximation for most of the reactor.

The primary current distribution is nearly uniform for all practical parallel plate reactors. The voltage balance for sublimating current operation of the above reactor becomes rudimentary under these conditions. Since the reactant concentration remains effectively constant, then the constant current density can be expressed as -

$$i = z F\ C_{av_1}\ \gamma_x\ K_x \qquad (2.82)$$

The local mass transfer coefficient associated with (2.78) is -

$$K_x = \frac{1.24\ D}{d_e}\ Re^{\frac{1}{3}} \bullet Sc^{\frac{1}{3}} \bullet \left(\frac{d_e}{x} \right)^{\frac{1}{3}} \qquad (2.83)$$

The variation of d_x along the electrode immediately follows from equation (2.82) and (2.83). The maximum value evidently occurs where x = L and using equation (2.79) gives the following expression for γ_{max} :

$$\gamma_{max} = \frac{1.5\ i}{z F\ C_{av_1}\ K_{av}} \qquad (2.84)$$

The voltage balance V is calculated directly from various values of γ_{max}, noting that the limiting value of unity gives an infinite voltage.

The total current is obtained from -

$$I = iBL \qquad (2.85)$$

2.6.7.2 Turbulent flow

When the flow is turbulent two equations can be used to describe the reactor. For combined hydrodynamic and mass transfer entrance regions (for $L \leq d_e$), the following equation can be used:

$$\frac{K_{av}\, d_e}{D} = 0.145\, Re^{\frac{2}{3}}\, Sc^{\frac{1}{3}} \left(\frac{d_e}{L}\right)^{\frac{1}{4}} \qquad (2.86)$$

and for the remainder of the electrode the following equation holds, i.e. -

$$\frac{K\, d_e}{D} = 0.023\, Re^{0.8}\, Sc^{\frac{1}{3}} \qquad (2.87)$$

The outlet concentration, which can be achieved under ideal limiting conditions in a reactor with ($L > 7.5\, d_e$), is obtained by successive applications of equation (2.81) to the above equations.

$$C_{av_2} = C_{av_1} \cdot \exp\left\{-\frac{\sigma}{N}\left[0.657\, D\, Re^{\frac{2}{3}}\, Sc^{\frac{1}{3}} + 0.023\, D\, Re^{0.8}\, Sc^{\frac{1}{3}}\left(\frac{L}{d_e} - 0.75\right)\right]\right\} \qquad (2.88)$$

Proceed using the voltage balance; the local coefficient at the front end of the electrode can be derived as follows -

$$\frac{K_x\, d_e}{D} = 0.109\, Re^{\frac{2}{3}}\, Sc^{\frac{1}{3}} \left(\frac{d_e}{x}\right)^{\frac{1}{4}} \qquad (2.89)$$

Thus, γ_{max}, evaluated at $x = 7.5 d_e$, is related to the current density by a similar expression to equation (2.83) -

$$\gamma_{max} = \frac{i}{0.75\, z\, F\, C_{av_1}\, K_{av}} \qquad (2.90)$$

The voltage balance is set up again from equation (2.81) for a single compartment reactor -

$$V = V_{min} + a_a + b_a \ln \{z K F \gamma C_{av}\} +$$

$$[\, a_c - b_c \ln \{z F K \gamma C_{av}\} - C_c \ln (1 - \gamma)\,] + \frac{z F K \gamma C_{av} S}{K} \qquad (2.91)$$

or for a two compartment reactor -

$$V = V_{min} + a_a + b_a \ln i + \left[a_c + b_c \ln i + c_c \ln \frac{C_{av}}{C_s} \right]$$

$$+ i \left(\frac{Sc}{K_e} + \frac{5_a}{K_a} + \frac{5_d}{K_d} \right) \qquad (2.92)$$

using equation (2.92) to calculate I.

There is no need for further corrections since the mass transfer coefficient and consequently, γ, becomes constant for $L/d_e > 7.5$.

Calculating the total current and outlet concentration as done for laminar flow completes the design.

This discussion completes the basic design criteria. It is now followed with a discussion on secondary effects that will change the values marginally. These effects include phenomena like gas evolution and re-circulation.

2.7 The Flow reactor with slow reactions at both electrodes

We now consider the design of flow reactors, when the reaction at both electrodes is slow, thus charged transfer controlled. Concentration gradients close to the electrode surfaces are small enough to be negligible and the current density will be substantially independent of the concentrations of the reactants. At high over potentials, the electrode kinetics will be described effectively by Tafel equations with the coefficient giving average values over the concentration ranges which supply to the process considered.

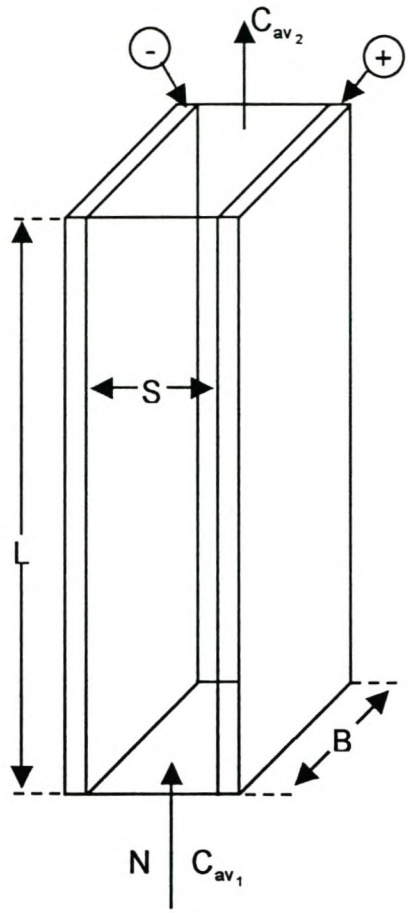

Figure 2.17: Parameters for a single compartment parallel plate reactor with slow reactions.

The analytical development will be made initially for the simple undivided parallel plate reactor in Figure 2.17.

The solution flowing into the reactor does so at a flow rate of N and the bulk concentration of the pertinent reactant have the usual terminal values C_{av1} and C_{av2}. The breadth of each electrode is B and the separation between the anode and cathode is equal to S.

The appropriate material balance is as usual:

$$N(C_{av_1} - C_{av_2}) = \frac{I}{zF} \qquad (2.65)$$

$$and \quad \frac{d\,C_{av}}{dx} = \frac{-i_x}{z\,F\,U_{av}\,S} \qquad (2.69a)$$

In this case the concentration changes that occur, both along and normal to the electrodes, are not very large and are not associated with a significant change in the

solution conductivity. The later is especially true if an excess of indifferent electrolyte is present.

Consequently, it is permissible to assume that the Laplace equation applies to the entire solution in the reactor.

As the local current deviation only depends on the magnitudes of local over potentials (through use of average Tafel coefficients), it is assumed that there are no potential drops in each electrode for the analysis to be very simple. The local current density over each electrode is then constant and the solution potential adjacent to each electrode is uniform. The solution drop V_{ohm}, obeys the one dimensional form of Laplace's equations so that -

$$i_x = -K\frac{d\varnothing}{dy} \equiv \frac{I}{BL} \qquad (2.93)$$

where L is the electrode length, and -

$$V_{ohm} = \frac{i_x S}{K} = \frac{I S}{B L K} \qquad (2.94)$$

The electrode over-potentials have constant values, i.e.

$$|n_c| = \left| a_c + b_c \ln\frac{I}{BL} \right| \qquad (2.95)$$

$$and \quad n_a = a_a + b_a \ln\frac{I}{BL}$$

The applied voltage is thus -

$$V = V_{min} + a_a + b_a \ln\left(\frac{I}{BL}\right) + \left| a_c + b_c \ln\left(\frac{I}{BL}\right)\right| + \frac{I S}{K B L} \qquad (2.96)$$

If required, equation (2.65) can be used to eliminate the total current from (2.96) and a relationship obtained between the applied voltage and terminal concentrations.

Chapter 3

EXPERIMENTAL DETERMINATION OF THE HARDWARE CONFIGURATION

3.1 Introduction

When facing the task of developing a plating reactor one is overwhelmed with all the possibilities of methods available. Not only, are there a whole range of possible plating liquids, but also a whole range of hardware configurations possible. One is therefore forced to do a detail preliminary study of the most likely methods and extract from them a few possible solutions and verify their suitability by laboratory scale experiments.

The coating of the zinc electrode with a polymer-layer was investigated. A successful method was established for using polyvinyl acetate (PVA) as a coating. Although the performance of some other coatings were superior, PVA proved to be the most affordable coating; however, the processes are more involved and the raw materials more expensive. A polymer coating on the zinc electrode retards oxidation of the zinc due to moisture. One of the problems in secondary (re-chargeable) AgZn batteries is the change in shape of the zinc electrodes during their cycle life. This problem is greatly reduced when a polymer coating covers the electrode.

The acid based zinc-plating bath options are described in detail in the Canning Handbook. Acid zinc plating solutions are recommended for plating high carbon steels, cast, wrought and forged iron components. These baths are usually based on zinc sulphate or chloride, and contains a portion of other salts and colloids necessary for production of smooth fine-grained electrodeposits. This method did not suit our requirements.

The alkaline-based Zinc plating bath options are also described in detail in the Canning Handbook (1982). The cyanide zinc solutions offer advantages where tolerance for contamination is required and where only a minimum control is available. These baths generally use sodium hydroxide as dilutant for the low cyanide zinc salts. Due to the strict environmental requirements, even the low cyanide zinc plating solutions could not be considered an option.

To adapt to the secondary battery application where re-plating of the zinc is executed in effect with each charging cycle, it was decided to use potassium hydroxide as the solute in the plating baths. This has the advantage that lessons learned from the plating technique can directly be applied to improve the secondary batteries. It had the added advantage that the effluent treatment could be of a simple nature. Though it is common practice to amalgamate the zinc with mercury, no mercury containing additives was added to the bath. The polymer coating provides for mechanical stability of the negative electrodes in the cells. The chemistry involved in the potassium hydroxide bath was well researched by various people. Dirkse et al (1954) and Dirkse (1954) did a detailed study on the nature of the Zinc ion in strong alkaline solutions. The results indicate that in the concentration range from 1-7M potassium hydroxide, all the zinc is in the form of a zincate ion, $Zn(OH)_4^{2-}$. The generalized reaction between the H_2O, KOH and the ZnO may be written as:

$$ZnO + 2KOH + H_2O \rightarrow Zn(OH)_4^{2-} + 2K^+ \qquad (3.1)$$

This reaction may be considered as taking place in stages:

$$ZnO + H_2O \longrightarrow Zn(OH)_2(aq) \qquad (3.2)$$

This is the general dissolving action of the solute. The second reaction taking place may be written as:

$$Zn(OH)_2(aq) + 2KOH \longrightarrow Zn(OH)_4^{2-} + 2K^+ \qquad (3.3)$$

This is the general dissolving action for the plating fluid.

Jackovitz and Langer (1968) refer to the presence of both $Zn(OH)_3^-$ and $Zn(OH)_4^{2-}$ in solutions that are strongly alkaline. As the solution becomes more alkaline, most of the dissolved zincate is in the form $Zn(OH)_4^{2-}$. Their spectroscopic investigation of the ZnO-KOH- H_2O system combining infrared and Raman determinations, established the zincate species to have tetrahedral symmetry in agreement with the tetra-co-ordinate species proposed by Dirkse (1954). These zinc compounds are colourless because the zinc ion contains no unpaired electrons. One of the noteworthy characteristics of the solubility of ZnO in KOH solutions is its independence of temperature, from -3 to 56 °C. This indicates that the enthalpy

change which accompanies the dissolution of ZnO in KOH is zero or very close to it. Plating takes place when a voltage is applied across the electrodes. The positive electrodes are two parallel Ni plates and the negative electrode consists of the Cu substrate onto which the Zn is plated. The plating process forces the Zn compound from a lower energy level in equilibrium to a higher state. The electrical current from the plating rectifier supplies the energy for this process. This process involves the movement of electrons that forms the current. The following generalized reaction occurs when an insoluble anode is used. Hydroxyl ions are derived from the dissociation of water:

$$2H_2O + 2e^- \Leftrightarrow 2OH^- + H_2 \qquad (3.4)$$

At the Anode (Positive), the reaction is:

$$4OH^- \Leftrightarrow 2H_2O + O_2 + 4e^- \qquad (3.5)$$

and the discharge of hydroxyl ions leads to the build up in hydrogen ions in solution, which becomes more acid (pH decrease). The net result is that two mol OH groups are converted to gas, for each mol of Zn plated. This leads to a gradual change in density due to:

- The decrease in OH content of the bath (lower pH value).
- A lower Zn content of the bath due to less solubility.

From these results is it obvious that to ensure constant plating conditions the Zn content and the OH content of the bath must be controlled.

Cathode reaction (Negative):

$$Zn(OH)_4^{2-} + 2e^- \Leftrightarrow Zn + 4(OH)^- \qquad (3.6)$$

To ensure total quality of the AgZn cells, it is of utmost importance that each negative electrode performs within a certain capacity range. The factors affecting this capacity are the effective zinc mass, the porosity of the zinc and the resistance of each electrode that is a function of the effectiveness of the binding between the zinc and the copper substrate. All these parameters are a function of the Zn content and the OH content of the bath.

To achieve this quality and reproducibility, various hardware configurations were tested and evaluated.

3.2 Plating Rectifier (Power supply)

Arouete et al (1969) reported on a plating method by means of a **Pulse Current source** in contrast with the traditional Direct Current method. In his method, a current pulse of 10 microseconds was applied with a no current state of 100 microseconds. This off time allows for the replenishment of the ions between the plating surface and the Outer-Helmholtz-Plane. A dense plating structure is achieved with the method. The method was verified on laboratory scale but could not be expanded to production scale due to fiscal constraints (production plating rectifier too expensive). The Bitrode programmable life cycle tester was used as a power supply during this experimental stage. This particular power supply was not suitable as a plating rectifier for production as it tends to overheat when misused as in these experiments. No verifications on the suitability for production in terms of the time-volume ratio were done. The method may have had the advantage that the rolling stage of the plated sheets could be simplified.

Traditionally plating is done with a **low voltage (6 – 12 V), high current (up to 2000 A)** plating rectifier. The advantage of such a low voltage is the safety associated with this operating condition. The plating environment is a wet messy area where leak voltages can easily develop. The low plating voltage minimises the risk of electrocuting the operators. The electrode configuration for this plating rectifier is graphically illustrated in Figure 3.1. The concept can be simplified to two parallel surfaces with a low voltage between them and the current evenly distributed over the whole surface area. The objects that are plated are usually suspended from the negative electrode by means of a hanger system with this technique. The positive electrode area is fixed. Control of the system is achieved by regulating the current density per unit area. The amount of material plated onto the suspended article cannot be controlled to the same extent with this system as in the chosen system. This is because the mass of the plated material depends on the amount of work done (quantity of Coulombs) on each object. This depends on the resistance between the buzz bars and the plated object, which can vary depending on the

effectiveness of the contact between the hanger and the buzz bars, and the contact between the hanger and object. A factor that complicated the plating further was the requirement that the plated object must be symmetrically placed in the electric field. This could not be achieved with a not-fixed hanger system. These factors lead to the non-uniform plating of the sheets and a large variation in plated mass. This concept was therefore rejected after a lot of experimental work.

3.3 High Current High Voltage

The requirement that each electrode must have the same mass enforced a serial plating system. The concept of the electrode configuration for this kind of plating system is graphically illustrated in Figure 3.2. This requires a deviation from the traditional plating rectifier concept of low voltage high amperage to a high voltage intermediate amperage rectifier. Such a rectifier was not readily available in commerce but was specially manufactured. A voltage limit of 48V for open wire applications is imposed by law. This restriction limited the number of plating baths in a serial connection to approximately eleven, if an average of a 4.2V voltage drop across each plating bath is assumed. After extensive laboratory scale experimental work, this concept was accepted as the most efficient system for this application. The final layout is discussed in Chapter 5.

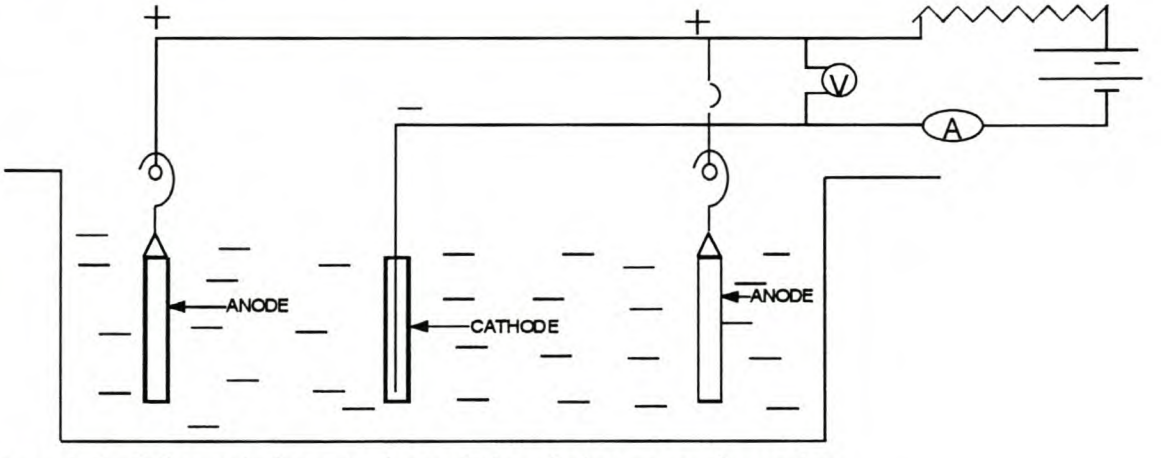

Figure 3.1: Schematic layout of a traditional plating configuration.

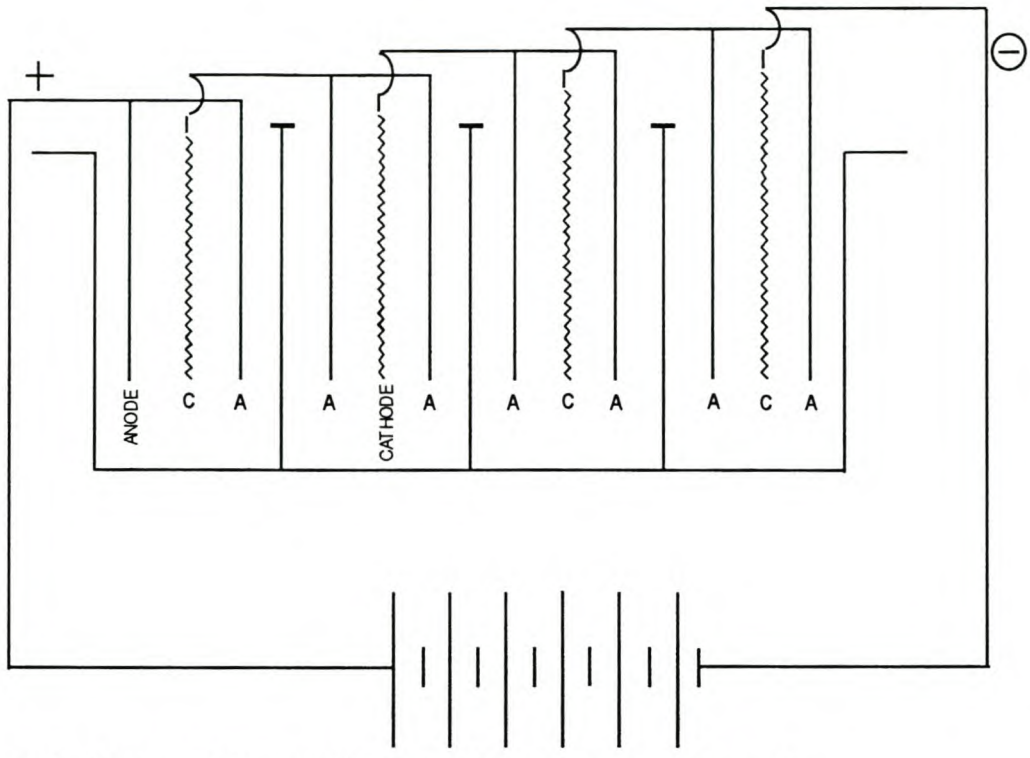

Figure 3.2: Schematic layout of a high voltage plating configuration

3.4 Plating Tanks

A variety of possible plating tanks are available. Historically, metal-plating tanks with a non-reactive lining like rubber are used - the biggest advantage being the strength of the tanks, and that they can be designed in any form and size. Depending on the design, they can carry any volume of liquid and are very rigid, and therefore unsusceptible to leaks. The disadvantages are that a thorough cleaning process is needed before it can be used, as well as the cost of the tanks. PVC tanks were used for all the experimental work due to the small size needed, the low cost involved, and their speed of manufacturing. They were unfortunately very susceptible to heat variations and often start leaking. The final choice of the type of tank depends on the size and the configuration of plating baths. The deciding factor for final design of the plating bath was the circulation configuration. This allows for small plating baths with one big reservoir tank. The design lends itself to the use of Polyethylene (PE) as construction material. This PE is more stable to heat changes and is resistant to alkaline attacks.

3.5 Electrodes

The aim of the electrode configuration is to expose the object that must be plated to a uniform electrical field. This is to ensure an even deposition of Zn over the whole plated area. The size of the electrodes was determined by the size of the electrodes required, the plating current density, and the maximum voltage permissible across the plating bath, and the heat generated at the specific current. The heat generated depends on the internal resistance of the plating fluid. Various sizes of electrodes were tested experimentally and the final design size extrapolated from this data. Two possibilities were considered as counter electrodes for the copper sheets onto which the plating was done. The first consideration was the use of Zn counter electrodes. Solid high purity Zn bars were used with this configuration as counter electrodes, the same as what would be encountered in a traditional plating setup. The problem encountered with this configuration was the availability of the high purity Zn counter electrodes, the amount of debris created by dissolving the electrode, and the shape change due to the dissolving of the electrode. The preferential dissolution of the electrode around its contacts with the buzz bars caused problems with the conduction of the electrical current. This manifested itself in an uneven plating distribution of the Zn caused by the non-uniform electrical field. The problem was solved by means of high purity (99.96%) inert Ni counter electrodes.

3.6 Fluid Replenishment

The initial experiments were conducted without circulating the plating fluid. This caused two problems, namely a concentration gradient owing to density in the plating bath, and the quick depletion of the bath. The first manifested itself by a gradual increase in the thickness of the plated Zn towards the bottom half of the electrode. This phenomenon is very obvious in fresh baths (newly mixed plating liquid) and high plating mass. This problem was negligible at low plating mass, although it was partially solved with the introduction of air-agitation. The problem encountered with the air agitation was that it was very difficult, in fact almost impossible, to establish an even agitation across electrodes in the different baths. However, this agitation showed that more movement of the plating liquid than that caused by the gas generated during plating was desirable. Mechanical agitation

was attempted but an even flow across the plating surface could not be effectively achieved. The second problem was solved with the use of a replenishment tank. This is, in effect, a big reservoir tank of such volume that when the spent liquid is mixed into the tank the difference in concentration is negligible. The influence of the circulation speed on the plating behavior is discussed in detail in latter chapters. Two methods of circulation were tested experimentally, namely, a serial-flow and a parallel-flow configuration. The serial flow configuration is a series of a cascading baths, and needs only a small pump driving it. The concept of the bath configuration for this kind of flowing system is graphically illustrated in Figure 3.3. This system has the advantage that exactly the same flow speed is achieved through each bath and that only a small pump is needed. The disadvantage is that the liquid exchange tends to happen only at the top of the tanks. Such a system is also more expensive to manufacture and needs a very complicated buzz-bar system. The final decision was that of a parallel flowing bath system where the flow is regulated with an adjustable inlet-manifold. This system requires a big pump to achieve the desired flow rate. It is discussed in detail in chapter 4.

3.7 Gas Removal

A great volume of very hostile gasses is generated during plating. To be able to work near the plating plant, these gasses have to be removed. Two methods of gas extraction were tested experimentally, namely, Lip suction and the Fume cabinet concept. Although the lip suction method provides a very elegant way of removing the gasses, the efficiency was low. The concept of the removal of gas by Lip suction is graphically illustrated in Figure 3.4. An existing Fume cabinet extraction fan structure was finally adapted for gas extraction.

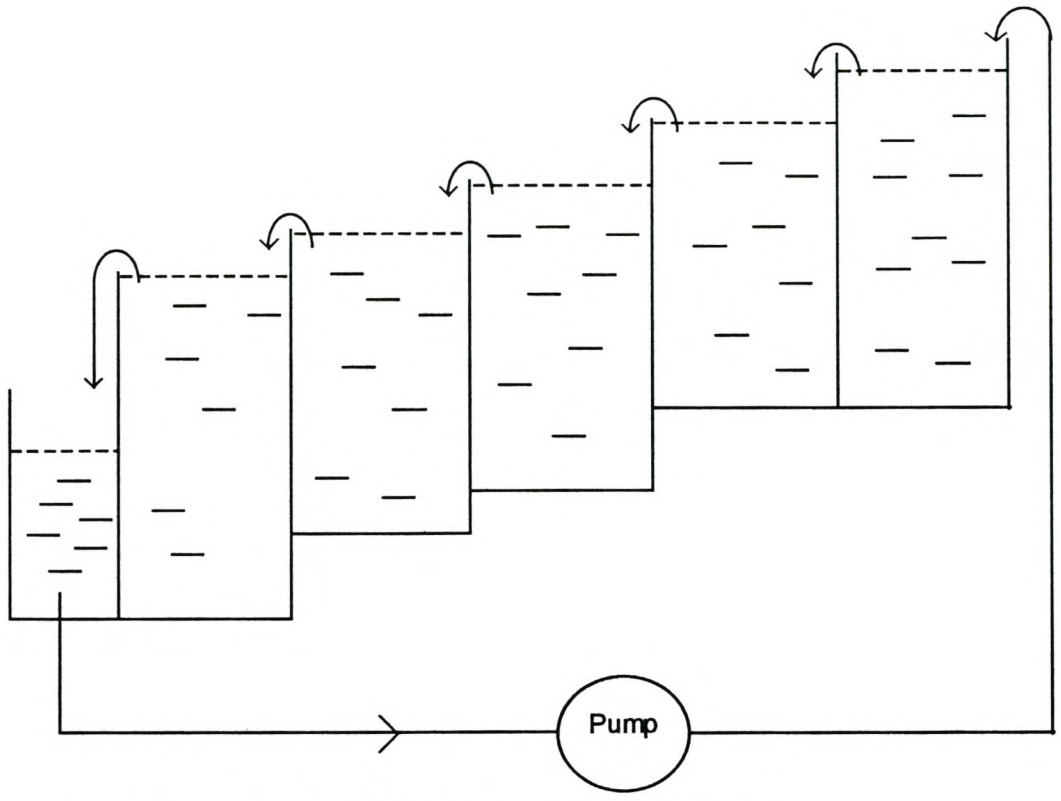

Figure 3.3: Schematic Layout of a cascading plating bath setup

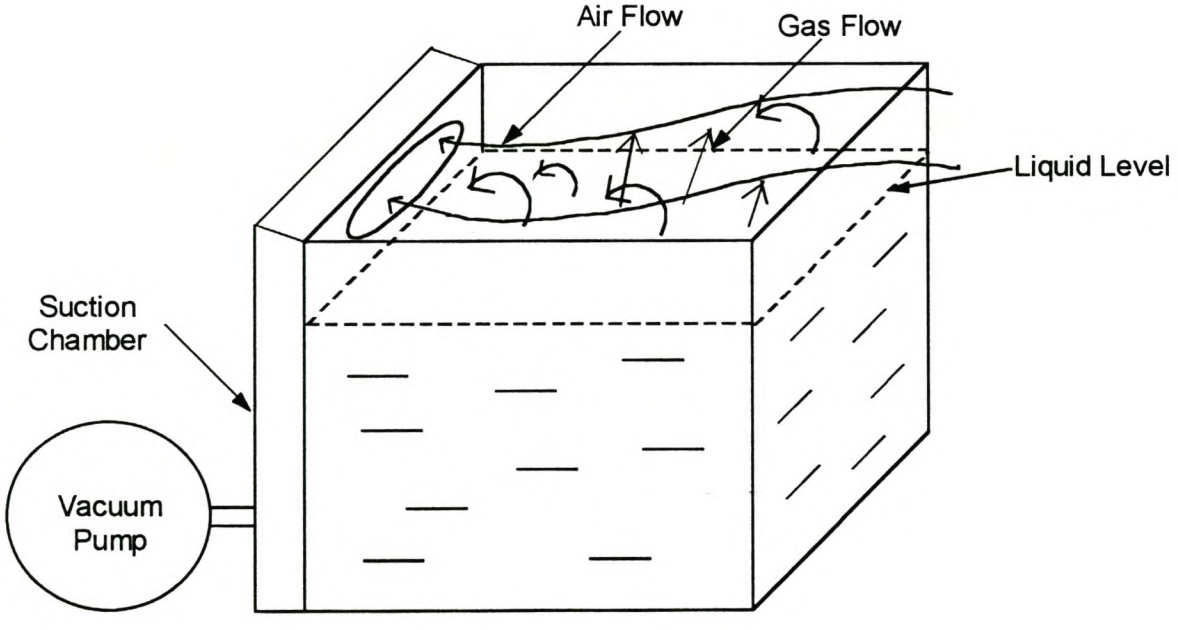

Figure 3.4: Schematic layout of a lip-suction gas removal system

Chapter 4

HARDWARE CONFIGURATION AND PRODUCTION PROCESSES

The research for this dissertation was executed on the pilot plant at Silvetech (Pty) Ltd in Stellenbosch. This pilot plant served as the main manufacturing plant after an ISO 9001 qualification was achieved. The operation consists of four main areas namely; the chemical pre-operational preparations, the actual plating operation, a post-plating operation and the electrode manufacturing operation.

4.1 Chemical Preparation

All the hardware was designed around the optimal performance of the plating solution. The plating solution consisted of a potassium hydroxide solution as basis in which zinc oxide was dissolved to form the plating fluid. The following method was used for the preparation of the plating fluid:

4.1.1 KOH Solution

A special stainless steel mixing tank with a cooling mantle was used for the mixing of the KOH crystals with de-ionised water. Cooling water was circulated through the cooling mantle to absorb the heat from the exothermic dissolving action. The tank was filled with approximately 40 litres of de-ionised water. This was followed by the slow addition of 25 kg of KOH crystals. A mechanical stirrer was used to keep the solution in suspension for at least four hours to homogenise the solution, which assisted in the dissolution of the crystals. The solution was cooled down to a temperature of 20 degrees Celsius. At this temperature a sample was taken and the density determined with the aid of a Hygrometer. If the density was not in the region of 1.380 ± 0.005 kg/m^3, the density of solution was adjusted until it fell within the specification.

4.1.2 Plating Solution

The plating-solution consists of the prepared KOH solution with ZnO added to it. Initially an excess of ZnO was added to the solution. The solution was stirred regularly in order to keep it saturated. This practice was abandoned because some ZnO precipitated from the solution in an insoluble form. In this way, one could not distinguish between the available and the insoluble ZnO. It was, therefore, decided

to keep the plating bath clean of all excess ZnO. The new method adopted was to dissolve adequate ZnO in the solution and monitor the dissolved Zn-ion concentration. This was done using a standard titration method. The saturated Zn concentration in a 1.38 g/l KOH solution was approximately 60 g/l. This value changes as the KOH solution ages. Standard values for the Zn-ion and OH-ion concentrations were set, i.e. 32-35 g/l Zn and 170-190 g/l OH, respectively.

4.1.3 Raw Materials

All the raw materials used in this process comply with strict quality standards for purity as well as physical requirements. A standard procedure for quality assurance, before acceptance, was adhered to.

4.2 Hardware

After initial experimental testwork a Parallel Flow Reactor (PFR) design was chosen. The hardware components were manufactured and the pilot plant assembled. All the plating experimental work was performed on this plant. The supporting infrastructure like the effluent-plant, the quality assurance equipment (both electrical and chemical), will not be discussed in this dissertation. Photographs of the pilot plant's main assemblies will be presented later in this chapter.

4.2.1 Plating Bath Wet Components

The plating bath (Figure 4.1) consists of the following components that are in direct contact with the plating fluid:

- plating compartments,
- reservoir tank,
- a circulation system,
- a filtration system, and
- electrode assembly.

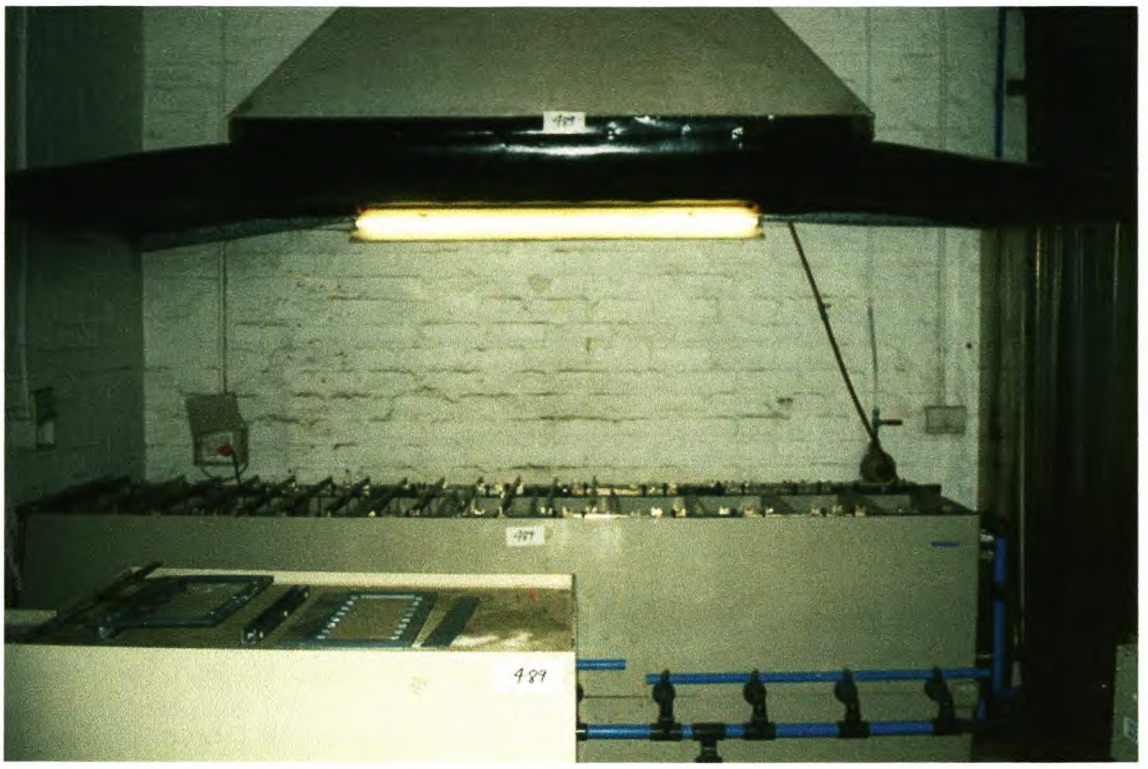

Figure 4.1: Side view of Plating Bath.

4.2.1.1 Plating Compartments

To ensure that the plating fluid in all the plating compartments is homogenous with the same characteristics, a parallel flow system was chosen. The plating bath consists of ten individual plating compartments. They are on top of a main reservoir tank. Each plating compartment's capacity is approximately 50 litres of plating fluid. The capacity of the main reservoir is approximately 1200 litres. This design ensures the minimum maintenance on the system as the volume of liquid is in such an excess that on normal usage of the system, overnight replenishment of chemicals is possible. A removable lid to prevent contamination and to ensure easy access covers the reservoir tank. The complete plating tank set-up is made from polypropylene to ensure minimum contamination and side reactions. Figure 4.2 shows the plating tanks, the (bottom) main reservoir and the manifold system.

Figure 4.2: Manifold System and side view of Plating Bath.

4.2.1.2 Circulation System

The plating fluid is circulated from the main reservoir through the plating compartments with the aid of a pumping system. The intake of the pump has a winded 20-micron polyethylene filter, which serves as a particle trap for the plating fluid to ensure that the plating liquid does not contain any suspended or solid particles. If necessary, this filter could be replaced with an activated carbon filter, which can remove elements such as chlorine. A flow divider is fitted on the flow-output side of the pump. Some of the plating fluid can be re-circulated back into the reservoir to maintain a specified flow rate. This recycle stream ensures that the liquid in the reservoir is kept in motion, thus homogenising the liquid. A flow meter is fitted before it enters into a manifold. Figure 4.3 shows the intake pump with the flow divider (set of valves) in the foreground.

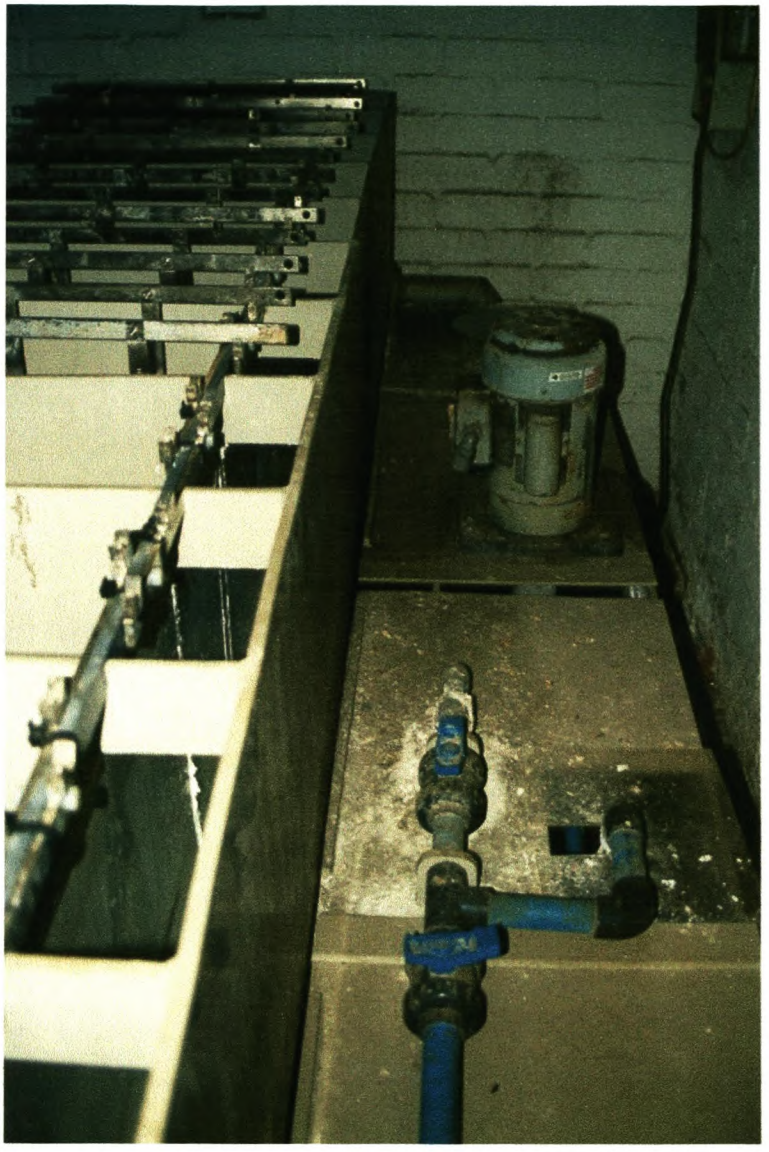

Figure 4.3: Pump System and Flow Divider.

Figure 4.4: The Flow Meter used.

The flow rate served as a filter condition indicator. The manifold system provided the plating fluid to each of the plating compartments (see Figure 4.2). Each compartment is fed via an adjustable valve on the manifold to ensure the equal distribution of plating fluid. The plating fluid overflow (from each plating compartment) is gravity fed back into the reservoir. This recycled plating liquid was filtered through a screen to remove solid particles from the liquid. This is, however, a course screen in order to filter the Zn lumps which formed on the exposed buzz bars.

Included into the manifold system is a set of valves which made it possible to dump liquid from the plating compartments, if needed. This was often necessary during washing and routine maintenance of the system. One of these valves also served as

a sampling point for the plating fluid. It was used when samples were taken for analysis.

4.2.1.3 Electrodes

In each plating compartment two high purity nickel (99.99%) anodes (counter electrodes) (Figure 4.5) were immersed into the plating fluid serving as the positive terminal.

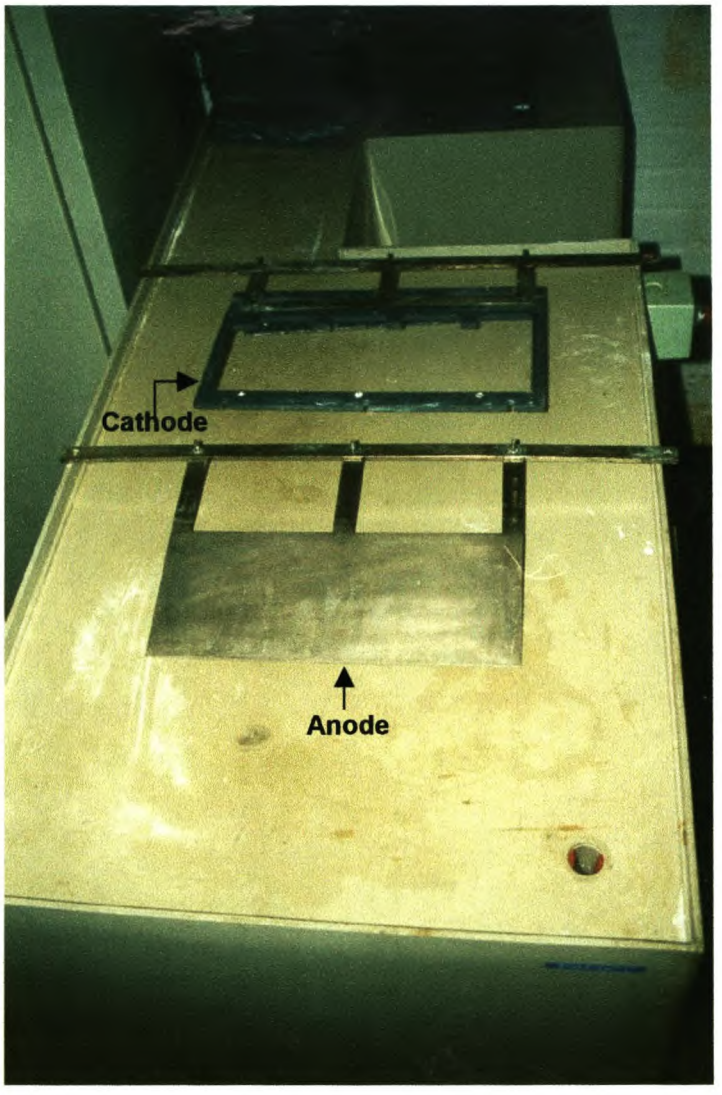

Figure 4.5: A Ni electrode, and the PVC masking of the cathode.

Sandwiched between these nickel anodes was a PVC masked plating electrode cartridge, serving as the cathode (negative terminal). This plating electrode cartridge used a foil of copper that served as the substrate for plating. The plating fluid served as conductor between the terminals. The separation between the cartridge and the counter electrodes were approximately 50 mm.

4.2.2 Gas-Extraction

Due to the nature of the reactions taking place during plating, excessive amounts of hydrogen and oxygen were produced. Concentrated volumes of these gases could cause an irritation to the respiratory system and should therefore be removed. This was accomplished with an extraction system, similar to a fume cabinet (see Figure 4.1). A galvanised hood fitted with mesh filters and a big extraction fan covered the complete plating compartment area. This ensured that the running of the plant could be performed with ease.

4.4 Infrastructure

Plating is a wet, messy process with hostile liquids. To accommodate this, a wet room is needed with specially treated floors and walls. A room was constructed with an inclining floor, and with draining channels to remove all spilled alkalis, acids and water. This effluent was channelled into an effluent waste tank. An effluent treatment plant was constructed for treatment of the effluent to ensure that the municipal bylaws on effluent water were met. To ensure operator safety, the floor was covered with an industrial grid in order to prevent possible slippage. Ample municipal water and de-ionised water taps were installed. Effective ventilation was ensured. The plating area was secured with a safety gate to prevent unauthorised access. All the equipment was equipped with emergency cut-off switches.

4.5 Electrical System

A standard DC plating-rectifier was used on the plant. The plating rectifier had the following characteristics:

- 200 ampere, 50 volt rating,
- Ampere-Hour meter,
- Independently adjustable Voltage and Amperage.

The voltage was kept below 48 volts in accordance with government safety regulations.

The plating rectifier was connected to the first and last plating compartment with copper buzz bars. All the copper buzz bars were coated with Ni to ensure that the copper did not react with the other chemicals present. The plating compartments between the first and last compartment were connected in series by means of short

bars ending in V-blocks (see Figure 4.6). The electrical circuit was only completed after two high purity Nickel (99.99%) counter electrodes were inserted in each plating compartment, serving as the anode (positive terminal). Sandwiched between the Ni counter electrodes was PVC masked plating electrode cartridge serving as the cathode (negative terminal). This plating electrode cartridge used a foil of copper that served as the substrate for plating. The plating fluid served as conductor between the terminals. The separation between the cartridge and the counter electrodes were approximately 50 mm.

Figure 4.6: Top view of electrodes in Plating Bath.

4.6 Procedures

Only a brief description of the procedures will be presented in this paper. Each procedure is covered in a detailed ISO 9000 standard document, which will not be discussed here.

4.6.1 Substrate Preparation

4.6.1.1 Blanking

The copper foil that was used as plating substrate is a high purity copper foil. This foil was hot rolled to a thickness of 0.06 mm. The copper was received as a coil of

± 250 kg. The first process was to verify the purity of the copper. Then the coil of foil was cut into sheets that fitted into the plating templates. These sheets were stacked in groups of 30. Depending on the application, these stacks were kept for further processing or sent for perforation. The sheets were perforated according to a predetermined pattern and then used. The purpose of these perforations was to reduce the weight and to increase the permeability of the electrode. The pattern used was a square arrangement with 2.1mm holes every 3.8 mm. Each of these sheets was then cut using a guillotine, to fit precisely into the plating template according to application. The sheets were then bundled into batches to be used at a later stage.

4.6.1.2 Degreasing

Each sheet was weighed and the mass and sheet number of each was recorded on the sheet with a metal engraver. This served as a quality control measure to ensure that the plated mass can be determined accurately after plating. Due to the flimsiness of the sheets, mechanical working on sheets (like drilling) can prove to be very difficult. Drilling fluids can be used and handling causes the deposit of fatty substances on the sheets. As a precaution to either eliminate or minimise contamination of the plating baths, these substances were removed with commercial alkaline degreaser. The cleaning of the sheets was done in an ultrasonic bath to ensure thorough cleaning in the shortest possible time. The ultrasonic waves also ensure that all lose particles, like burrs from the drilling, are removed.

4.6.1.3 De-scaling

De-scaling is the last chemical process the sheets undergo before plating. The de-scaling of the sheets in a mixture of hydrochloric and sulphuric acid serves two purposes, i.e. the process removes the oxidisation layers on the copper foil, and secondly the foils are scrubbed and slightly etched to ensure good bonding of the Zn onto the copper. This process is executed just before assembly into the plating templates. The process consists simply of dipping each sheet into the acid mixture for about 30 seconds until the correct copper colour was obtained. The sheet was then removed, rinsed with de-ionised water, and then assembled in the plating template.

4.6.2 Plating

All the actions under the plating header are wet processes that take place in the plating room. This is a continuous process in which time is a critical parameter. In order to make the description of the process easier, it is sub-divided into different stages.

4.6.2.1 Charge Plating Templates

The plating templates consist of three parts. They are:

- The electrical contact, which consists of the buzz bar and the nickel contact area that connects the copper substrate to the electrical circuit.
- The PVC templates, which form an integrated part with the electrical contacts. They consist of a bottom part that is permanently fixed to the electrical contact to form a unit, and the covering part. The template's shape is determined by the application of the Zn-electrodes that are manufactured. Each type of Zn-electrode has its own shape and size, depending on usage. Because a standard size of copper substrate is used, a different number of Zn-electrodes are manufactured with each type of template. The templates are designed in such a way that they stretch the copper foil so that it fits tight in the template (see Figure 4.7). They also have blanking areas, which cover the copper substrate to prevent plating onto selected areas. Conducting strips will be spot-welded onto these areas at a later stage. Alignment pins are situated on the PVC templates in order to ensure that the copper substrate is always in a similar position, and that the template sections are aligned.
- The templates are held together with PVC U-bars. They slide onto the sides of the templates ensuring tight closure and good electrical contact.
- For assembly, a freshly de-scaled copper substrate is taken and placed into position on the bottom part of the PVC template in such a way that the alignment pins protrudes through the alignment holes in the copper substrate. The top part of the PVC template is placed on top of the bottom part and pressed down to ensure that the substrate is stretched smoothly and evenly. The U-bars then slide onto all four sides securing the assembly. This charged template is placed into a plating bath. This process is repeated in all the plating baths.

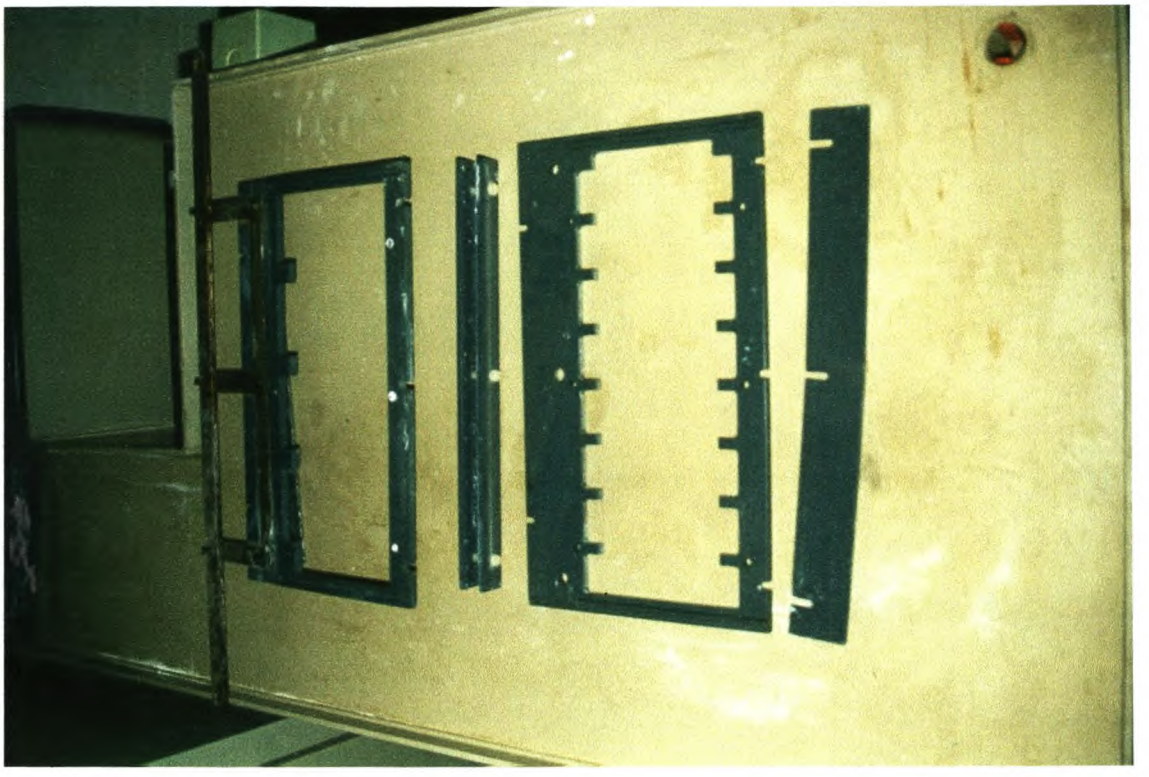

Figure 4.7: Assembly of anode.

4.6.2.2 Foundation Layer

A foundation layer of Zn is plated onto the copper substrate to ensure that the copper is covered totally by the zinc. This is performed at a low current density. This process ensures good bonding between the copper and the zinc. Before the operator can proceed with the plating, the required plating profile must be known. The process then commences in the following sequence:

- Connect the last plating template assembly with the negative terminal of the plating rectifier.
- Measure the density of the plating fluid and the temperature, and record it in the plating record.
- Reset the ampere-hour meter on the plating rectifier.
- Switch the plating rectifier to "ON".
- Adjust the voltage to maximum voltage and the current to 2 ampere.
- Start the stopwatch.
- Verify that there is gas generation on both counter electrodes in each plating bath.

4.6.2.3 Mossy Deposit

The crystal structure achieved during the plating depends on the current density. If the current density is kept at the limit-current density a specific structure can be achieved. This crystal structure is recognisable, and deviations are noticeable. Inspection is done when the plated sheets are removed from the plating baths. To ensure the correct dendrite morphology, the current is set at the limiting current density. After 10 minutes of plating at 2 ampere, the current is set at the limiting current density amperage. The mass that plates onto the copper substrate depends on the time of plating. A time to ampere-hour relationship is established and the time of plating is set accordingly.

4.6.2.4 Discharge Plating Templates

The mossy zinc that is plated onto the copper substrate is a very spongy, soft, fragile substance. With the removal of the plating templates from the plating baths, care must be taken not to bump or scratch the surface structure as lumps of Zn can be removed from the plates. Time is allowed (about 45 seconds) for the drip drying of the Zn sponge after removal from the bath. The process is performed in the shortest period of time possible as the Zn starts to oxidise immediately after it is exposed to air and will re-dissolve in the plating fluid when left in the baths. The plated copper substrate is discharged from the plating templates by removing the U-bars and lifting it from the bottom part of the template.

4.6.2.5 Mechanical Compression

The zinc sponge on the copper substrate can have a thickness of up to 1cm on each side of the substrate. It is then rolled down to 0.5mm thickness in total with the aid of mechanical rollers. The rolling action work-hardens the zinc to a tough compacted structure with a high porosity (see Figure 4.8). This is usually a two-step process as too much strain on the zinc crystals can tear them from the substrate. The mechanical rollers are a set of hardened chrome-plated metal rollers that are fixed in a horizontal plane. The gaps between the rollers are set with a Feeler Gauge using a set of set-screws. A three-phase electrical motor turns the rollers. The zinc plated copper substrate is fed vertically into the rollers. The plating fluid pressed from the zinc sponge drops into a dripping tray. The rolling action is repeated a few times to

ensure proper compacting. After the rolling, the plated copper substrate is placed into de-ionised water for washing.

Figure 4.8: Roller used during compaction of electrodes.

4.6.2.6 Passivation

For a long shelf life of the Zn electrodes, it is of utmost importance that the residual KOH in the Zn structure should be removed as far as possible. The plated copper substrate is therefore placed into de-ionised water for 24 hours. During this period, the water is changed frequently until the pH reading of the washing water decreases to below a pH of 8. After 24 hours the copper substrate is removed and tested with a phenophtaline indicator for the pH. If it passes this test, it is then passivated in a 10% boric acid solution. If the pH is still too high, further washing takes place, until it passes the test. The plated copper substrates are then dried in a oven at 35 degrees Celsius. The plated copper substrates are then grouped into batches. Each foil is

weighed and the mass recorded. One plated copper substrate from each batch is destructively tested for mechanical stability and electrochemical capacity. The electrochemical capacity test is in effect a de-plating test where the energy to de-plate the electrode is measured at a specific current density. If it passes the acceptance criteria, the batch is accepted. The batch is then stored under dry conditions.

4.6.3 Electrode Manufacturing

Although all the following information is not directly important to this dissertation, it is given as background to the process.

4.6.3.1 Blanking

From each plated copper substrates a number of electrodes are blanked. The blanking tools fits onto a hydraulic press (Figure 4.9) where the blanking is done. Each type of electrode has its own set of blanking tools. The blanking tools are designed in such a way that the zinc on the plated copper substrates is not compacted during the blanking process.

4.6.3.2 Weighing of Electrodes

Each electrode contains an area that was blanked off from plating during the plating process. This area serves as the attachment area for a conduction strip. The next step is to clean this area thoroughly from all deposits to ensure that the copper-substrate is completely exposed. Each electrode is weighed to ensure that the correct amount of zinc is present.

4.6.3.3 Spot-welding of Electrodes

A high purity silver strip is attached onto each electrode. This is done by means of a spot-welding process. Each strip should receive at least three welds in order to ensure proper binding. The electrode is now enfolded in a nylon compound wig and stored until it is assembled into a battery.

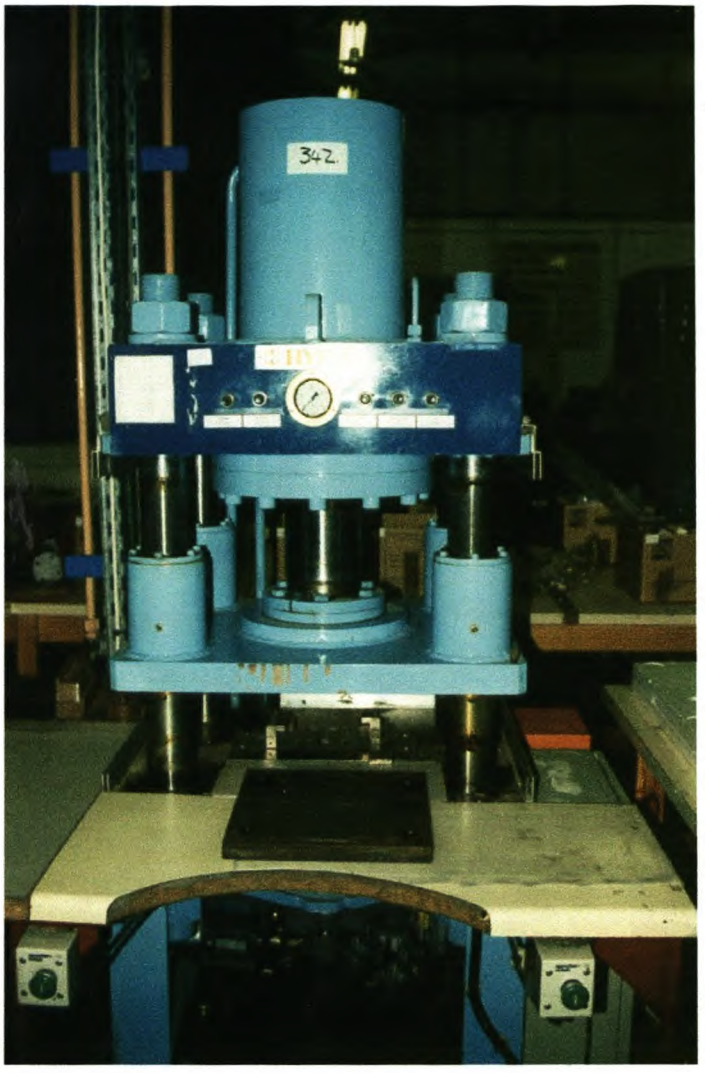

Figure 4.9: Hydraulic Press for blanking of electrodes.

4.7 Measurements

4.7.1 Electrical Measurements

A different power supply is used for experimental work on the plant to the plating rectifier used in production (as discussed in paragraph 3.5). A Bitrode 100 ampere, 40 volt power supply with 8 standard measurement channels capable of 8V (DC) each, and a reference DC voltage channel is used for experimental work. It can operate in either voltage limiting or current limiting mode. This power supply is fully programmable and records data in accessible ASCII files. For operation at low amperage, a similar 20 ampere, 25 V unit is available. Both these units can work in conjunction with the 200 ampere plating rectifier as data recording units. The voltage sensing leads connect with crocodile clamps onto the buzz bars when voltages are measured. An internal shunt measures the current.

As reference electrode a Hg/HgO couple is used. The Hg is poured on top of HgO in a lugging capillary with a platinum wire connecting the sensing leads. When freshly prepared, this capillary with the mercury compounds is filled with KOH and left for at least four hours, after which it can be used. In practice, this reference electrode is suspended with its spout next to the substrate and the sensing leads connected between the platinum wire and one of the working electrodes.

4.7.2 Chemical Measurements

4.7.2.1 Density

The density of the plating fluid is measured with commercial glass bulb hydrometers with a range of 1,350 to 1,400 kg/m^3. The fluid is mixed and a sample is drawn in a plastic beaker in order to measure the density. This is done to minimise the parallax faults. The hydrometers are rinsed down after each measurement.

4.7.2.2 Temperature

The temperature of each bath is measured with a calibrated electronic thermometer. Glass thermometers are not used due to fear of breakage and the resulting contamination.

4.7.2.3 Titration

A standard EDTA titration method is used. It can determine both the Zn-ion and the OH-ion concentration.

4.8 Summary

The hardware configuration and production process of the pilot plant to produce the negative electrodes of the AgZn battery were discussed in this chapter. All the various parameters applicable to this dissertation were investigated and optimised. In the following chapters the effects of physical parameters, chemical parameters, as well as the sensitivity analysis on the process will be discussed in detail.

Chapter 5

THE EFFECT OF PHYSICAL PARAMETERS

Chapter 5 and Chapter 6 cover the results of the investigation into the effect of controlling physical parameters on the plating process. The parameters are divided into a physical group (Chapter 5) and a chemical group (Chapter 6), although they are inter-related.

5.1 Relationship between density, concentration and temperature in the plating bath

The two variables that are the most convenient to determine are the density and the temperature of the plating liquid. Normally a hygrometer is calibrated at 20°C, and it is therefore necessary to establish a relationship between the density and the temperature of the solution, as the process temperature can vary between 15°C and 40°C. Secondly, one should be able to relate a specific density with a specific concentration. To achieve this, the following procedure was followed:

- Six plastic beakers were filled with 500ml KOH at a density of 1.38 kg/m^3.
- Pre-determined amounts of ZnO were added to the 500 ml KOH in the containers.
- The solutions were mixed until all the ZnO was dissolved.
- The solutions, as well as the hygrometer, were heated to the specified temperature in an incubator. The containers were sealed to prevent evaporation. A stabilisation period of minimum two hours at each temperature was applied.
- The density as well as the solution temperature were measured and recorded after the stabilisation period.

The results of this test work are presented in Table 5.1.

TABLE 5.1: The effect of density, concentration and temperature

Temp (°C)	Dens (kg/m³)	Temp (°C)	Dens (kg/m³)	Temp (°C)	Dens (kg/m³)	Temp (°C)	Dens (kg/m³)	Temp (°C)	Dens (kg/m³)	Temp (°C)	Dens (kg/m³)
ZnO	14g/l		28g/l		42g/l		56g/l		70g/l		82g/l
15.0	1.392	14.5	1.403	15.5	1.414	15.0	1.425	14.5	1.436	15.5	1.446
19.0	1.390	19.0	1.402	18.5	1.412	19.5	1.422	19.0	1.433	18.5	1.444
25.5	1.388	24.0	1.401	25.5	1.408	24.0	1.420	24.5	1.430	25.0	1.440
29.0	1.386	28.5	1.396	30.5	1.406	28.5	1.416	30.0	1.426	30.0	1.437
34.5	1.384	35.0	1.394	35.5	1.403	34.5	1.414	35.0	1.423	35.0	1.434

Various mathematical relationships can be deduced from this data.

To convert from density at t_1°C (at a temperature t_1) to density at 20°C (expressed in g/cm^3), the following formulas are applicable:

$$D_{20} = D_t(1-(20-t)\,\beta) \text{ - if t is less than 20°C and} \quad (5.1)$$

$$D_{20} = D_t(1+(t-20)\,\beta) \text{ - if t is more than 20°C} \quad (5.2)$$

β is the thermal expansion coefficient, which can be dependent on the concentration in solutions. β has to be determined experimentally.

In Figure 5.1, the relationship between temperature and density from the measured data is presented graphically. A linear regression analysis on each data set was performed.

The linear fits to the data sets are excellent (as $R^2 = 1$ is a perfect fit), the average R^2 value of the sets is 0.98. The relationship between density and temperature is clear from the graph. There is a decrease in density with an increase in temperature. It can be deduced from the graph, therefore, that the relationship between density and the temperature is similar for all the ZnO concentrations tested.

In Figure 5.2, the relationship between density and concentration from measured data is shown graphically. A linear regression analysis on each data set was executed. The linear fits to all the data sets are excellent; the average R^2 value is 0.99. The relationship between density and concentration is clear from the graph.

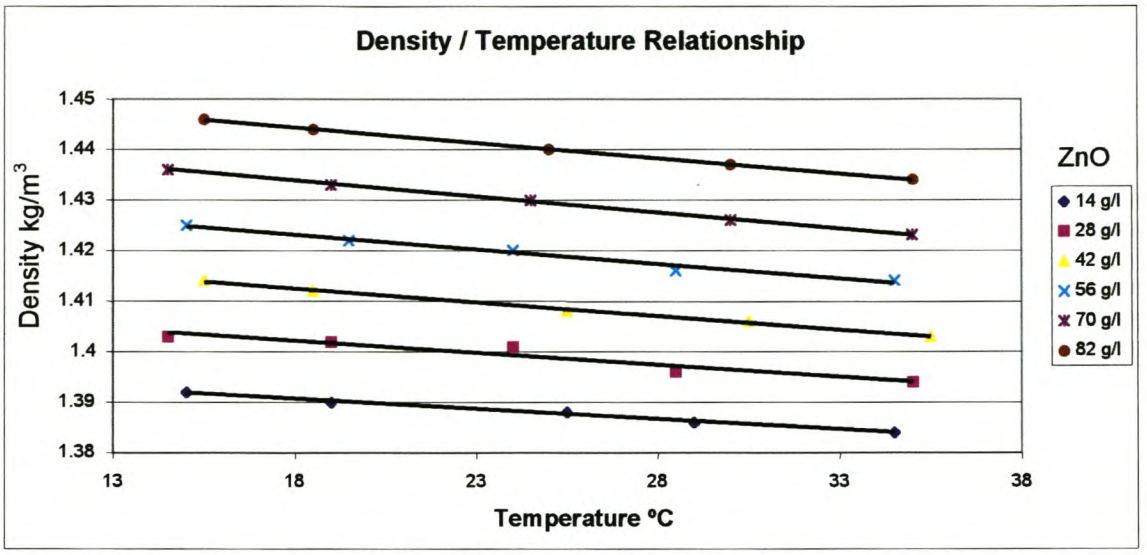

Figure 5.1: Graphical presentation of relationship between density and temperature

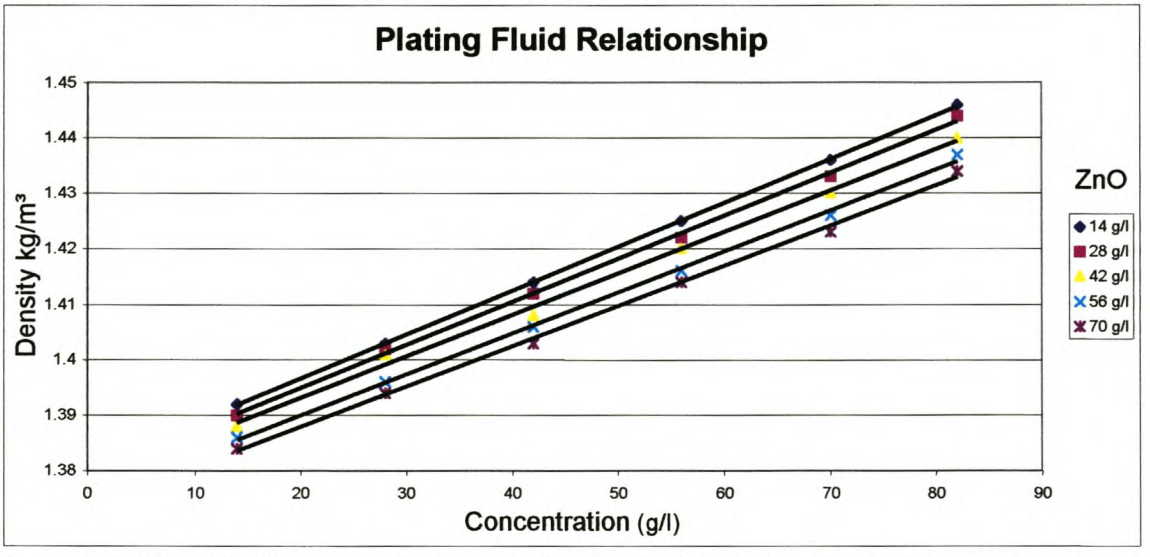

Figure 5.2: Graphical presentation of relationship between density and concentration

These two figures indicate that a set of linear equations can be used to describe the concentration as a function of density and temperature.

The set of values in table 5.1 can be arranged into a set of linear equations, which can be solved with the Gauss elimination method to give an equation. This equation can then be used to calculate the concentration if the density and temperatures are known.

The set of linear equations are presented in Table 5.2.

TABLE 5.2: Set of linear equations from Figures 5.1 and 5.2

Linear	Equations	Evaluation	
Value	**Linear Equation**	**Cal. Value**	**Error**
14 g/l	0.9528*T + 1.384*P + C	15.9415	-1.49
14 g/l	0.9816*T + 1.388*P + C	14.6622	-0.6622
14 g/l	1.0174*T + 1.392*P + C	12.347	1.653
28 g/l	0.9513*T + 1.394*P + C	26.5162	1.4838
28 g/l	0.9865*T + 1.401*P + C	30.794	-2.794
28 g/l	1.0191*T + 1.403*P + C	29.019	-1.019
42 g/l	0.9498*T + 1.403*P + C	41.376	0.620
42 g/l	1.0051*T + 1.412*P + C	41.7891	0.2109
42 g/l	1.0156*T + 1.414*P + C	41.2257	0.7743
56 g/l	0.9865*T + 1.420*P + C	55.9371	0.0629
56 g/l	1.0174*T + 1.425*P + C	55.8913	0.1087
56 g/l	0.9865*T + 1.420*P + C	55.1189	0.8811
70 g/l	0.9513*T + 1.423*P + C	70.1063	-0.1063
70 g/l	1.0034*T + 1.433*P + C	67.3255	2.6700
70g/l	1.0191*T + 1.436*P + C	69.476	0.5240
82 g/l	0.9513*T + 1.434*P + C	84.0584	-2.0584
82 g/l	0.9832*T + 1.440*P + C	81.8556	0.1444
82 g/l	1.0156*T + 1.446*P + C	83.0100	-1.0100

The solution to the matrix of equations is:

Variables		Values
C	=	-1610.4135
P	=	1320.9132
T	=	-212.25755

This simplifies to the linear equation:

Concentration = -212.258T + 1320.913P - 1610.414 (5.3)

Where P = the plating bath density, and

T = 293.2/(plating bath temperature + 273.2)

When the validity of the equation was tested at all the data points, a maximum error of 2.7940 g/l was encountered.

This culminated in a valid equation for the concentration as a function of the directly measurable parameters, density and temperature. This equation determines the concentration at any time from available measurements without the need for complicated analysis or time-consuming titration methods.

The data in Table 5.1 were also used for the determination of the linear expansion coefficient of the plating liquid. Equation 5.2 can be written as:

$$D_{2o} / D_T = \beta (t - 20) + 1 \qquad (5.4)$$

This is the equation for a straight line where β represents the slope of the line. In Figure 5.3, the relationship between D_{2o} / D_T and delta temperature (20±T) is graphically shown. A linear regression analysis on each data set was executed. The linear fits to all the data sets are excellent; the average R^2 value is 0.95. The slope from the graph gives a β value of 0.0004 for all concentrations.

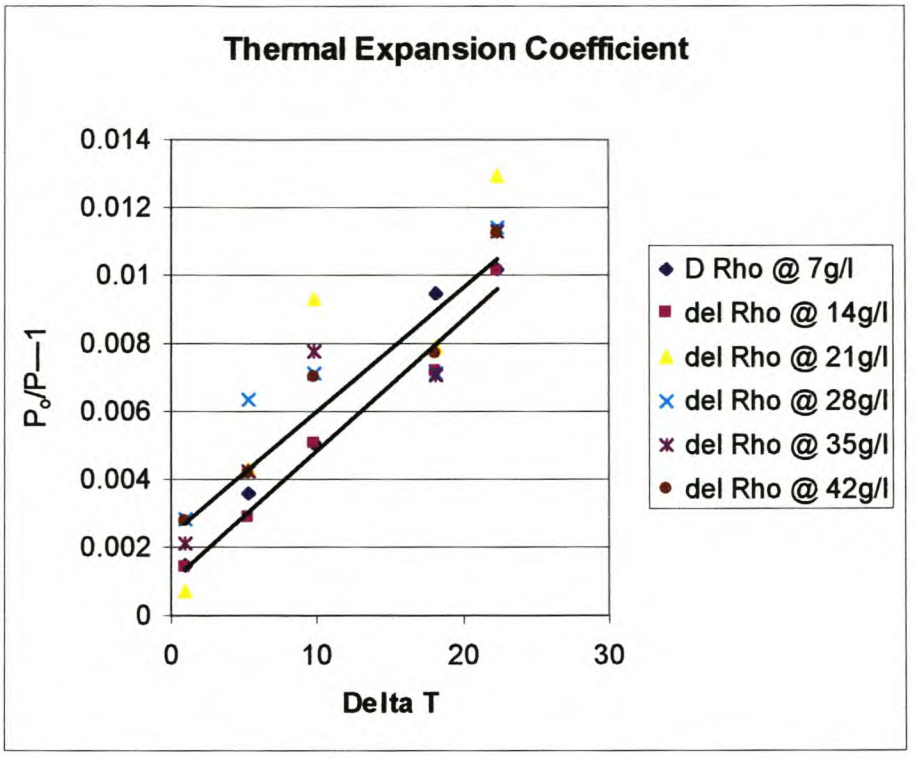

Figure 5.3: Determination of Thermal Expansion Coefficient

Because the solubility of zinc is independent to the temperature in the region –5 to 56 °C, the concentration of dissolved zinc is only a function of the hydroxyl concentration. The zincate concentration can, therefore, be determined from the density and temperature values as shown.

5.2 Effect of flow rate on the bath voltage

With the initial experimental work, the influence of the plating fluid flow rate on the behaviour of the system was investigated. The aim of this investigation was to find the optimum flow rate, i.e. the flow rate where the minimum power is consumed for the maximum throwing power (i.e. maximum plating efficiency).

A selection of five flow rates was possible with the hardware available. They varied from a static plating fluid that had no flow, to a flow rate of 1052 litres per hour through a single plating bath with a 48 litre capacity. Four baths with parallel electrolyte flow and serial electrical connections were used. The total flow was measured with a calibrated flow meter. The flow rate was controlled using a bypass/throttle valve. The flow rate through each bath was set using the throttle valves on the manifold system. The standard plating frames were used.

For this procedure the Bitrode 100 power supply was operated in voltage limiting mode. The total voltage was increased stepwise every 180 seconds by 240-millivolt. The current behaved independently until the maximum current of the power supply (100 ampere) was reached. The total voltage across, as well as the current through the baths, was monitored every 30 seconds. The measurements at the different flow rates were measured sequentially.

The standard plating procedure was followed as described in chapter 4.

The first observation from the data was that the minimum voltage required for the current to start flowing through the baths was approximately 3.12 V at a current of 30 mA. This converts to a minimum electrolyzing voltage of 0.78 V. These measurements were only performed when at static flow. From thereon, the lower boundary of voltage measurements was set at 5.24 V (total) across the set of baths.

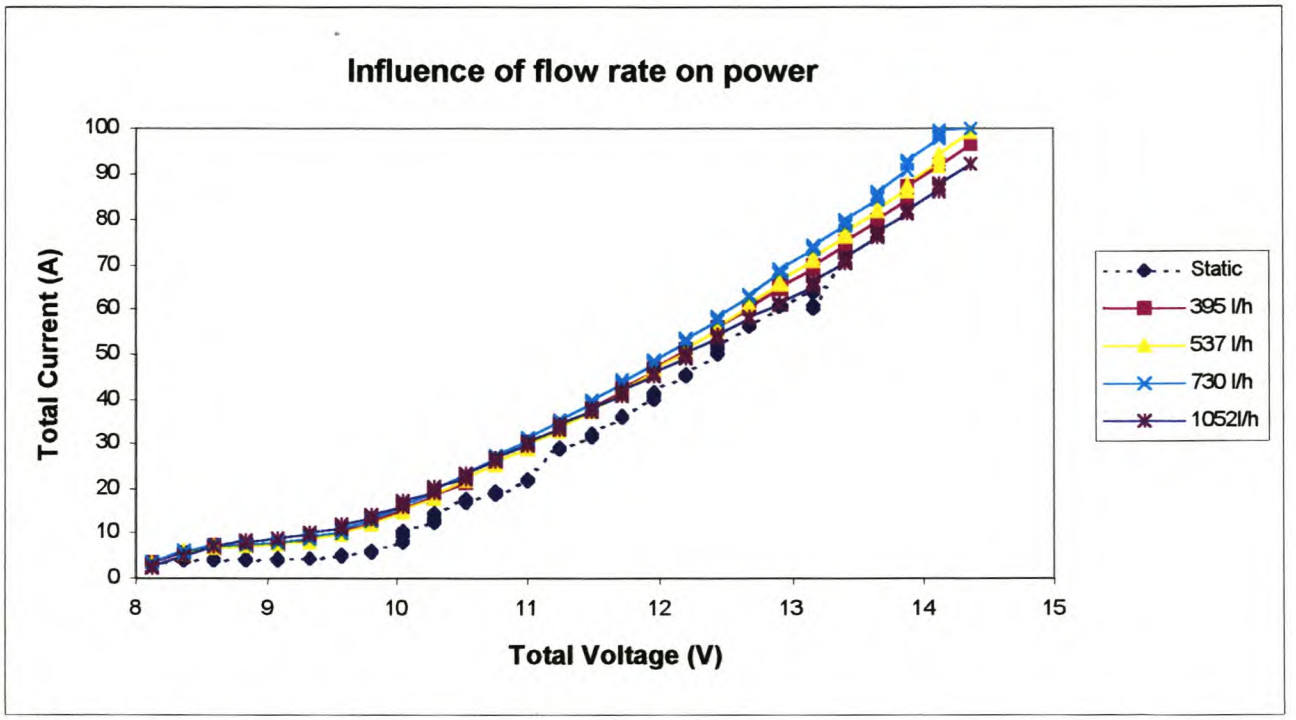

Figure 5.4: Influence of flow rate on power consumption

In Figure 5.4, the voltage-current relationship, as measured in this experiment, is shown graphically. The data is only shown from 8 V onwards as at this point the current rises above 2 A.

The following important observations can be made from Figure 5.4, i.e. three distinguishable areas are evident, namely:

- A relatively flat ampere/voltage slope from 8.36 V to 9.56 V, where a 1.2 V increase results in an average increase of 4.4 A.
- A relatively uniform ampere/voltage slope from 9.56 V to 10.76 V, where a 1.2 V increase results in an average increase of 15.5 A.
- An area from 10.76 V onwards, where the ampere/voltage slopes of the different flow rates is evident, and much higher than in the previous two areas above.

The different flow rates have a remarkable influence on the efficiency of the plating.

The efficiency rating (see Figure 5.5) in ascending order in terms of flow rate, is the following:

- 730 litre/hour
- 537 litre/hour
- 395 litre/hour
- 1052 litre/hour
- static

The results of a least squares fit onto the data are summarised in Table 5.3.

TABLE 5.3: Result of Least Square fit on Measured Data

Flow speed	Voltage Range	Amp. increase	Equation	R^2
730	9.56 to 10.76 V	16.22		
537	9.56 to 10.76 V	15.65		
395	9.56 to 10.76 V	15.43		
1052	9.56 to 10.76 V	14.89		
730	10.76 to 14.36 V	72.83	Y = 26.61X - 277	0.97
537	10.76 to 14.36 V	68.93	Y = 25.04X – 260	0.96
395	10.76 to 14.36 V	66.52	Y = 24.73X – 257	0.96
1052	10.76 to 14.36 V	61.83	Y = 21.13X – 211	0.98

The difference in the slopes and voltages at the high current values can be seen in Figure 5.5. This implies that a flow rate of 730 l/h is most efficient for plating in this bath. The fact that the higher flow rate is less efficient indicates that turbulent flow occurs.

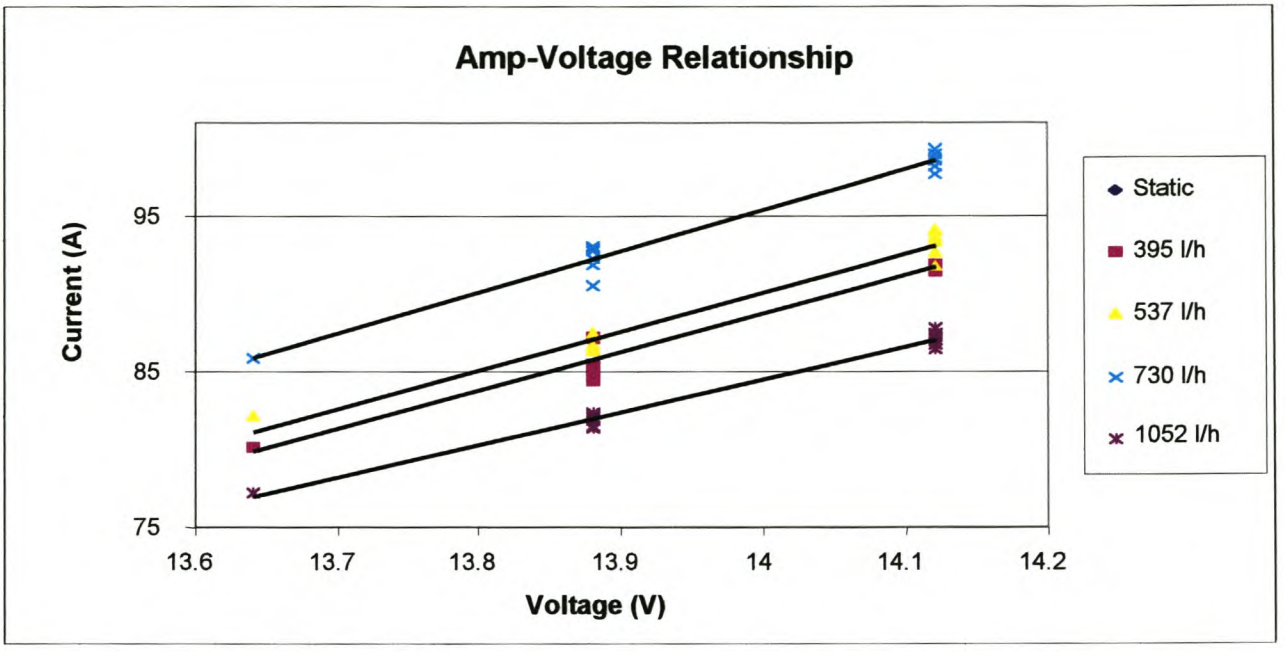

Figure 5.5: Relationship between Ampere and Voltage at a High Current Density

5.3 Relationship between plated-mass and ampere-hours spent

The plating records supply ample data for the determination of the relationship that exists between plated–mass and the ampere-hours needed for plating. Table **5.4** is an extract of the data of the plating records. The table shows the relationship between the mass and ampere-hours. It should be kept in mind that this value is only valid in the lower range of the limiting current density region. Excess plating current is inefficient and results in excess generation of gasses and undesired heating of the plating fluid.

TABLE 5.4: Plating Data

Batch	Amp-h	mass	G/Ah	Batch	Amp-h	mass	g/Ah	Batch	Amp-h	mass	g/Ah
18	59.50	64.50	1.08	68	50.00	56.40	1.13	106	51.50	58.00	1.13
19	59.00	60.00	1.02	69	51.00	58.60	1.15	107	51.20	58.50	1.14
20	58.20	63.90	1.10	70	52.00	58.80	1.13	108	51.30	57.30	1.12
21	58.20	63.80	1.10	71	54.00	57.20	1.06	109	51.00	57.60	1.13
22	59.00	63.40	1.07	72	50.00	58.50	1.17	110	51.40	57.40	1.12
24	52.30	56.60	1.08	73	50.00	56.80	1.14	111	51.60	57.60	1.12
25	52.40	55.60	1.06	74	52.00	57.60	1.11	112	51.80	58.70	1.13
26	49.90	55.60	1.11	75	53.00	58.60	1.11	113	52.00	57.90	1.11
27	47.80	52.70	1.10	76	54.50	59.50	1.09	114	51.20	58.90	1.15
28	48.30	53.70	1.11	77	55.00	60.70	1.10	115	51.40	58.20	1.13
31	55.50	60.80	1.10	78	50.00	55.90	1.12	116	51.60	58.00	1.12
32	55.90	60.80	1.09	79	51.10	57.60	1.13	117	51.80	59.90	1.16
33	55.40	60.50	1.09	80	52.00	60.10	1.16	118	51.20	58.10	1.13
34	55.40	59.00	1.06	81	52.40	60.90	1.16	119	51.40	57.80	1.12
41	49.70	57.00	1.15	82	53.20	61.50	1.16	120	51.60	57.70	1.12
42	52.60	59.00	1.12	84	50.00	60.00	1.20	121	51.80	58.10	1.12
43	52.00	58.20	1.12	85	51.00	62.30	1.22	122	52.00	57.40	1.10
44	52.70	58.00	1.10	86	52.00	59.90	1.15				
45	48.60	53.60	1.10	87	50.00	55.80	1.12	125	51.00	58.10	1.14
46	48.40	54.20	1.12	88	51.00	55.70	1.09	126	51.60	58.50	1.13
47	49.70	55.80	1.12	89	51.50	56.20	1.09	127	51.00	57.40	1.13
48	49.80	54.90	1.10	90	47.10	54.80	1.16				
49	48.70	54.00	1.11	91	48.00	53.10	1.11	128	51.80	56.20	1.08
50	51.10	57.20	1.12	92	49.20	52.80	1.07	130	51.40	57.90	1.13
51	53.20	58.50	1.10					131	51.80	58.80	1.14
52	51.30	56.80	1.11	94	51.50	58.70	1.14	132	52.00	57.20	1.10
53	51.40	52.70	1.03	95	52.90	59.90	1.13	133	52.10	57.40	1.10
54	50.90	53.30	1.05	96	53.50	59.70	1.12	134	51.80	56.30	1.09

Batch	Amp-h	mass	G/Ah	Batch	Amp-h	mass	g/Ah	Batch	Amp-h	mass	g/Ah
TABLE 5.4: Plating Data (Continued)											
55	53.00	54.60	1.03	97	53.00	59.10	1.12	135	51.80	58.50	1.13
56	52.90	54.80	1.04	98	53.50	60.10	1.12	136	52.00	58.70	1.13
57	50.90	54.40	1.07	99	54.00	60.70	1.12	137	52.50	59.30	1.13
58	55.00	56.50	1.03	100	54.10	60.70	1.12	138	52.20	58.30	1.12
59	52.10	53.60	1.03	101	54.20	60.50	1.12	139	51.80	58.80	1.14
60	52.00	57.50	1.11	102	52.20	59.00	1.13	140	51.80	58.80	1.14
61	53.00	58.80	1.11					141	52.00	58.90	1.13
63	50.00	55.10	1.10	102A	51.00	58.30	1.14	142	52.10	59.00	1.13
64	51.00	58.30	1.14	103	52.00	58.30	1.12	143	52.20	58.40	1.12
65	52.00	58.90	1.13	104	50.00	57.70	1.15	144	52.30	58.30	1.11
66	53.00	58.30	1.10	105	51.00	57.90	1.14	145	52.10	58.40	1.12
67	54.00	59.60	1.10					146	52.00	58.40	1.12
								147	52.10	58.80	1.13
								148	52.20	59.30	1.14

The mass ampere-hour relationship can be summarized as follows:

Average	:	1.11
Median	:	1.12
Std. Dev.	:	0.02
Count	:	117

Confidence: Level %	Error
95	.004
98	.005
99	.006

This means that for each ampere-hour plated, a mass of 1.11g $\pm$ 0.004 g is retrieved from the plating solution and one can be 95% sure that the plated mass will be in the region of 1.106 g to 1.114 g.

To plate a specific mass, the required mass can be divided by 1.11 to determine the ampere-hours needed for plating. The error in mass will be within the range of 0.004 times the required mass.

The associated zincate concentration of the batches in Table 5.4 is graphically presented in Figure 5.6. The zincate concentrations were calculated using equation 5.3.

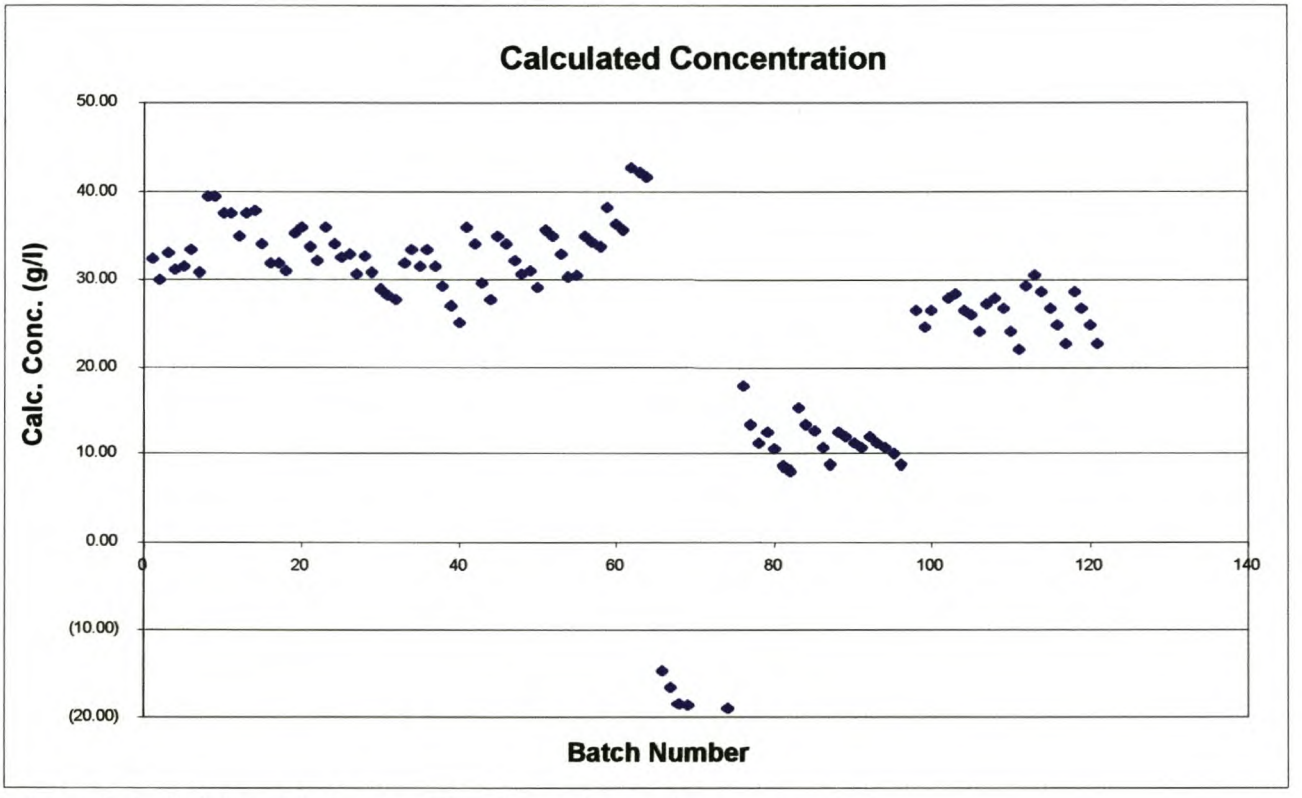

Figure 5.6: Relationship between Batch number and concentration

The following deductions can be made from Figure 5.6:

- The zincate concentration decreased gradually until batch 66, where after it took a sharp drop.
- The zincate concentration recovered partially after batch 76.
- The zincate concentration increased even more after batch 96.
- The zincate concentration showed a definite drop during each plating batch.
- The daily batch groupings can easily be identified by the associated drop in the zincate concentration.
- The zincate concentration recovered with the overnight replenishment period.

5.4 Summary

It can be seen from the plating build-history records and the batch acceptance records that the batches manufactured at the low zincate concentration were rejected due to brittleness. A higher zincate concentration was achieved by replacing one third of the plating liquid with KOH (1.38 density). This improved the quality of plates produced (less brittle). The problem was only solved once the plating current was raised to 148 amperes.

The above facts infer that the morphology is not only a function of the zincate concentration, but also of the total plating current density. When this result is compared to the data in Table 5.4, one can deduct that the plated-mass ampere-hours relationship is independent of the zincate concentration.

Chapter 6

THE EFFECT OF CHEMICAL PARAMETERS

6.1 The influence of the ion concentration on the plating behaviour

During a major plating batch run, the ion concentration decreases with time as the plating liquid gets older. The reactivity of the plating solution decreases, as the pH becomes less, causing a drop in the zincate concentration. As it is not possible to replace the plating liquid at regular intervals, the effect of this on measurable plating parameters must be known to compensate for this effect. To determine the effect of this phenomenon on the plating parameters the following experimental programme was conducted.

The tests were executed on the normal production equipment, as described in Chapter 4. Solutions with various Zn-ion concentrations were prepared in four 48-liter standard plating baths. The average Zn-ion concentrations during these tests were 78g/l, 88g/l, 95g/l and 105g/l, respectively. The plating fluid in the baths could not be circulated and the plating was done in the static solutions. The temperature and density of each bath was taken before plating commenced. The voltage versus time between the anode and cathode of each bath was recorded. The anode voltages relative to $Hg(\ell)/HgO(s)/OH^-$ (aq) reference electrodes were recorded. The amperage through the baths was recorded during each plating procedure. The plating rectifier and recording equipment used were those discussed in Chapter 4. The tests were executed at nine different plating current densities. The range covered is from a current of 30 ampere to 190 ampere (constant surface area). For each experiment the current was increased by 20 ampere. The duration of a plating run was 30 Ah, while the voltages were recorded at 30 second intervals.

Experiments were conducted during the intervals between long production runs. The reasons for this were two-fold; firstly a matter of availability of the equipment; and secondly, to determine the effect of deterioration on the behaviour of the system. A very noteworthy observation was made in this test series, i.e. in a parallel configuration with the anode sandwiched between two cathodes, it is not uncommon for the voltages across the electrodes to fluctuate between high and low. That is, the

voltage between the anode and cathode to the left may be high while that on the other side of the anode will be low at a specific time, while moments later it may become similar or even change from low to high. This process balanced out in the end as the mass distribution on the plated foil became even on both sides. The reason for this is random voltage change is apparently the condition of the buzz-bars and V-blocks coupled with the over-voltage of the plating fluid. This effect caused the voltage reading to be very noisy and uneven. In Figure 6.1 an example of the voltage behaviour at a current of 130 ampere is presented.

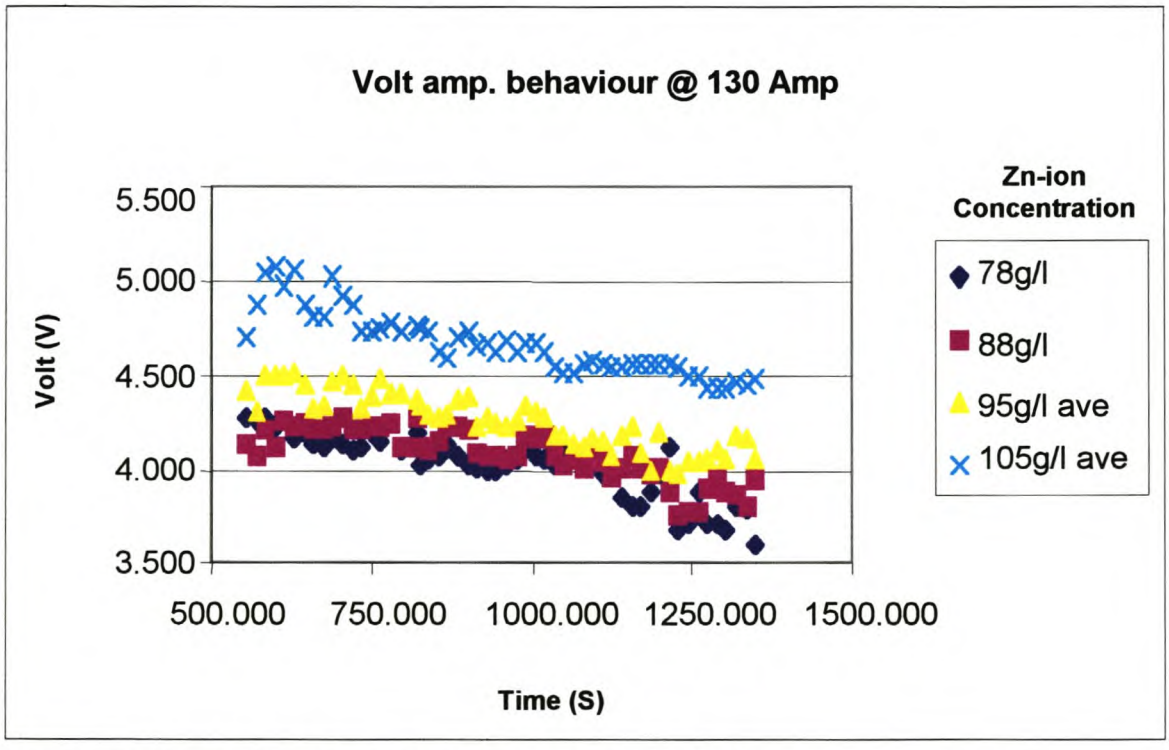

Figure 6.1: Voltage behaviour at a plating current of 130 A.

The following points can be deducted from Figure 6.1:

- A 10g/l concentration difference causes a voltage difference in the region of 200-mV.
- The higher ion concentrations are associated with higher voltages.
- The noise on the data can be as high as the difference in voltage between the neighbouring concentrations.

The uncertainty in the data, caused by the noise, prevented exact quantitative conclusions. The average voltages, at high currents, for all the plating baths are summarised in Table 6.1.

TABLE 6.1: Average Voltages of plating baths of different ion concentrations

Amp	*Amp dens*	*conc. 78g/l*	*conc. 88g/l*	*conc. 95g/l*	*conc. 105g/l*	*ref 78g/l*	*ref 88g/l*	*ref 95g/l*	*ref 105g/l*	*bath Ave*
20.00	0.015	2.523	2.399	2.419	2.384	0.831	0.895			2.431
30.00	0.022	2.677	2.751	2.948	2.827	1.056	0.952			2.801
50.00	0.037	3.042	2.964	3.043	3.104	1.458	1.380			3.038
70.00	0.051	3.296	3.296	3.287	4.210			1.628	1.921	3.522
90.00	0.066	3.858	4.050	3.507	4.017			1.735	2.016	3.858
110.0	0.080	4.525	4.267	4.507	4.495			2.239	2.176	4.449
130.0	0.095	4.321	4.054	4.268	4.764	2.073	2.212			4.352
150.0	0.110	4.481	4.430	4.542	4.482	2.104		2.571		4.484
170.0	0.124	4.339	4.245	4.326	4.899	2.432			2.508	4.452
190.0	0.139	4.591	4.587	4.728	4.993	2.523	2.450			4.725

The data of Table 6.1 is graphically presented in Figure 6.2. The following are conclusions, which can be deduced from Figure 6.2:

- Two areas in terms of slopes are distinguishable.
- The ampere range from 20 A to 110 A is associated with an elevated slope.
- The ampere range from 110 A to 190 A is constant (even slope).
- This behaviour is reflected in the reference voltage.

In Figure 6.3 and Figure 6.4 the data is split into two figures. Figure 6.3 represents the area where the Butler-Volmer equation is valid and the Tafel slope can be calculated. The Tafel slope value for this solution is 0.0211. Figure 6.4 represents the area of limiting current density. The slope value in the limiting current-density range is 0.0007. This slope is almost level, which implies that for currents above 110 A, there are almost no voltage increases for large current increases.

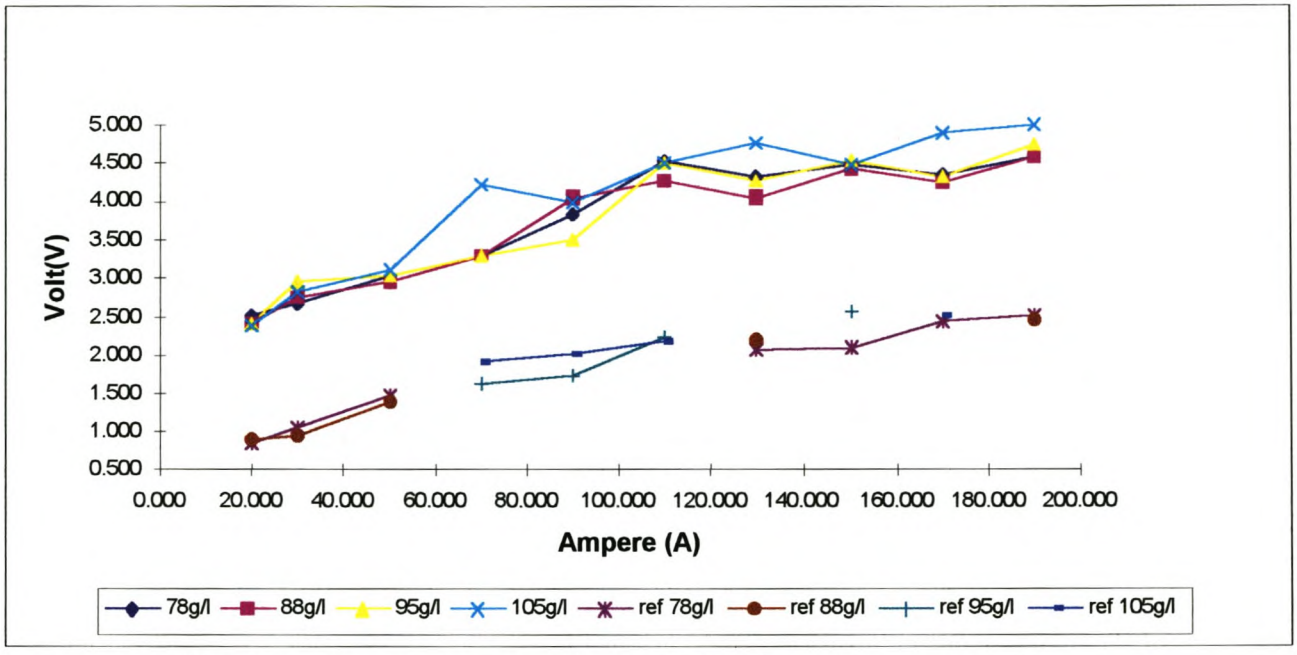

Figure 6.2: The Voltage versus Ampere behaviour at different ion concentrations

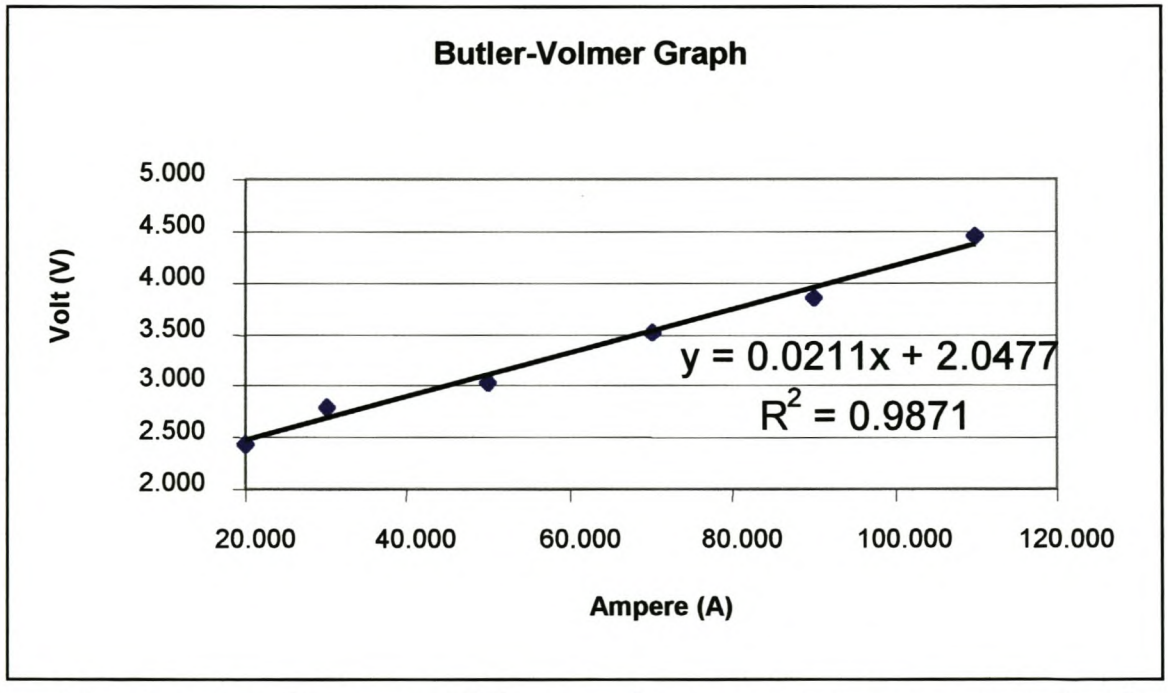

Figure 6.3: Average voltage-current behaviour of ion concentrations investigated, at low currents.

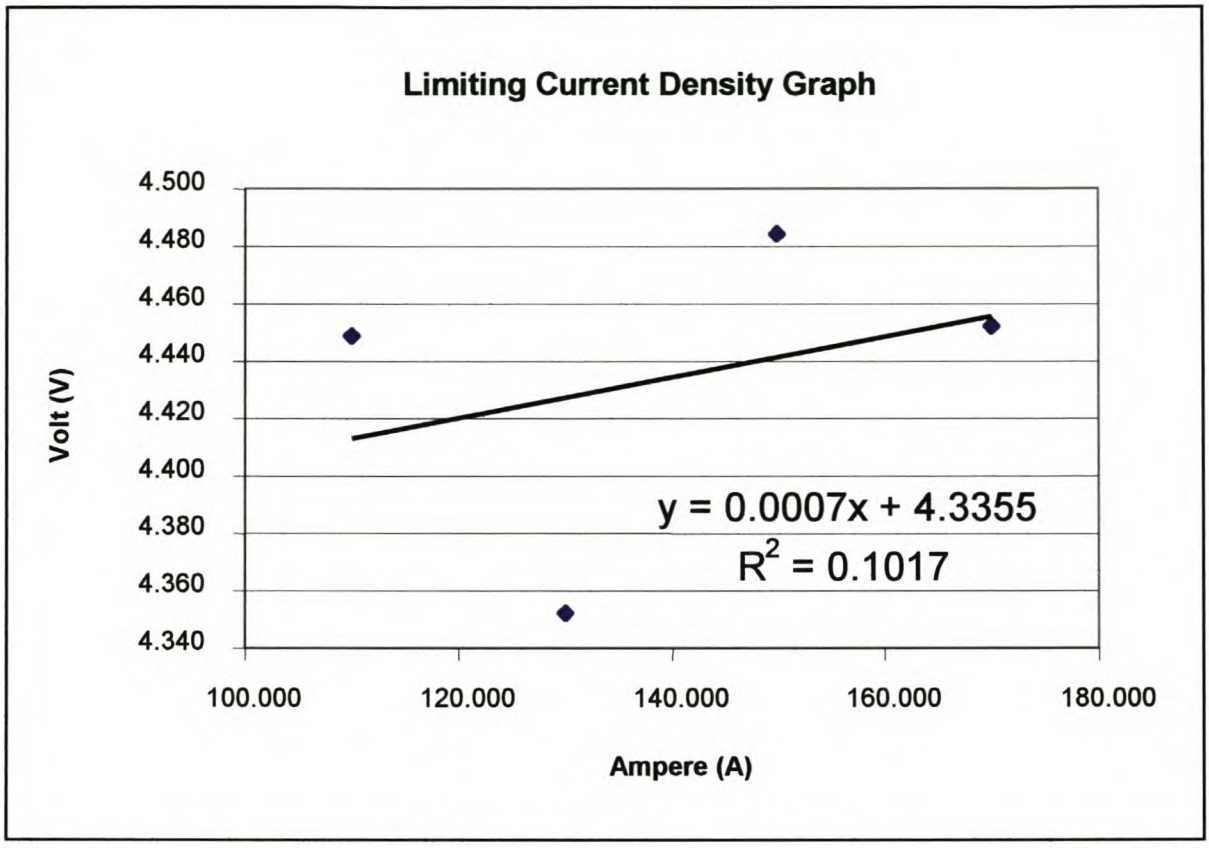

Figure 6.4: Average voltage-current behavior of ion concentrations investigated, at high currents.

6.2 The influence of the plating current on the crystallisation behaviour

It was evident from plating that was conducted, that the total plating current density had a major effect on the crystallization morphology. The functionality of the Zn electrodes is dominated by their crystal-morphology. To quantify this, several electrodes were manufactured at different plating-current densities and their physical and electrical properties evaluated. The electrical properties were determined by means of BITRODE LCN (life cycle network), and a test set-up (special jig) where the capacity, discharge, and voltage behaviour were determined against an inert electrode relative to an Hg(*l*)/HgO(s)/OH^- (aq) reference electrode.

6.2.1 Experimental Procedure

The tests were executed on the normal production equipment. The standard plating solution was used in four 48-litre standard plating baths. The zincate concentrations during the test were not exactly known but are calculated using equation 5.3. These values are much too low. The potassium hydroxide solution's density was not 1.38

kg/m^3 as the tests took place after a long series of production runs. This caused the pH value to decrease (OH^--concentration decrease). Although these zincate concentration values are not absolute values, they are useful as relative values to verify that the zincate concentration did not change during the course of the experiment.

The plating fluid in the baths was circulated at 400l/h during plating. The temperature and density of each bath were recorded before each plating. The voltage versus time between the anode and cathode of each bath was recorded. The anode voltages relative to Hg(ℓ)/HgO(s)/OH^- (aq) reference electrodes were recorded, where possible. The amperage through the baths was kept constant during plating. The plating rectifier and recording equipment used was the same as discussed in previous sections.

The tests were executed at eight plating current densities. The range covered is from a current of 10 ampere to 80 ampere. For each experiment, the current was increased by 10 ampere. The duration of plating was 30 Ah while the voltages were recorded at 30-second intervals.

The plating morphology was determined by means of a SEM (scanning electron microscopy) analysis.

6.2.2 Results

A summary of the plating criteria for the plated foil is given in the following table. The relative density before and after the plating is given.

TABLE 6.2: Summary of Plating Parameters

Batch No.	*Temp. (°C)*	*Dens. (kg/m^3)*	*Rel. Conc. (g/l)*	*Ampere (A)*
9	17.5	1.394	19	10
9	17.8	1.393	19	
10	17.9	1.392	18	20
10	17.9	1.392	18	
11	17.9	1.392	18	30
11	18	1.391	16	
12	17.9	1.392	18	40
12	17.9	1.391	16	

Batch No.	*Temp. (°C)*	*Dens. (kg/m³)*	*Rel. Conc. (g/l)*	*Ampere (A)*
13	17.9	1.393	19	50
13	18.5	1.394	20	
14	17.5	1.392	18	60
14	18	1.393	19	
15	17.5	1.394	20	70
15	18	1.392	17	
16	18	1.394	20	80
16	18.1	1.393	19	
17	17.9	1.394	20	10
17	18	1.393	19	

Zinc electrodes were manufactured from these plated sheets. Samples of electrodes were taken from each plating batch at the different current densities. Some of the electrodes were discharged in an attempt to find a difference in discharging behaviour in terms of voltage and capacity. No conclusive deductions were possible from these results as the voltages and the capacities differed only a small amount and no definite pattern was displayed. On the other samples, a SEM analysis was executed and photos were taken. The following procedure was followed while taking of the SEM photos. A SEM analysis was performed at two magnifications, namely a 500X and a 2500X magnification. A major portion of the time was spent on each sample in an effort to find a representative area of the zinc structure on the electrode before a photo was taken. The photos are, therefore, representative of the zinc morphology at the specific plating conditions. The SEM photographs are presented in Appendix 1.

It is clear from the SEM photographs that the crystallisation morphology is determined by the current density. In Appendix 1 the scanning electron microscope photographs (SEM) of the different morphologies are shown. The morphology varies randomly from amorphous zinc morphology (Figure I.1) to dendrite zinc morphology fern structures (Figure I.2). In between these two morphologies is a pallet-like Zn morphology (Figure I.3) that is associated with brittleness.

The SEM photos show that the mixture of morphologies is present at low current densities. Near the edges of the base Cu foil, dendrite morphology is dominant. At

the solid areas, the amorphous structure is dominant (Figure I.4). This infers that availability of zincate plays a major part in the plating morphology. From the morphology associated with the different amperages, it can be deduced that the morphology is rate dependent.

The randomly packed Zn morphology exhibits a black, non-reflective appearance when rolled down to electrodes. The thin homogenous cover of the Zn moss on the plated copper substrate also characterises this phase.

It is found that the crystal structure does not change with a different morphology. This investigation was conducted by means of X-ray analyses. The X-ray diffraction pattern of the two classes of morphology, namely the more amorphous and the dendrite, were determined. Both samples were pulverized and exposed to X-rays of various energies. A Phillips X-ray defractometer was used to measure the diffraction angles and the relative intensities at each angle. Both samples exhibited identical diffraction patterns in terms of the diffraction angles and the diffraction intensities. From these results can be deduced that the Zn crystallizes in the same crystal structure (cubic) independent of the morphology it exhibits.

It is very difficult to make qualitative measurements of the crystal morphology, as its field of view is minute in comparison with the overall size of an electrode. One must take the macro image of the electrode into consideration when interpreting the micro-scale SEM images. The SEM image interpretation must comply with the broader view observed on the electrode. The following observations are in ascending current density order:

- No dendrite morphology is discernible at a very low current density. The Zinc appears to be in an amorphous morphology (Figure I.1).
- Dendrite morphology becomes discernible (Figure I.5).
- Dendrite morphology becomes more fern-like in appearance. It changes from almost rectangular shape (like a fish finger) to a sharp fern-leaf shape (Figure I.6).
- Dendrite morphology increases in volumetric density. This means that there are more Zinc fern-leaves per unit volume (Figure I.2).

- Dendrite morphology becomes smaller in size in comparison with the lower current densities (Figure I.3 and Figure I.7).

The very low current density plating is, from experience, a solid coating that is almost indestructible. This current density is used to solidly attach the zinc to the copper substrate. This bonding can only be removed with heavy mechanical abrasion or chemicals. This is why a plating mask is used during production to shade certain areas from the plating activities. These areas serve as attachment areas for the conduction lugs.

At intermediate plating current densities, the morphology consists of almost rectangular shape fern leaves. This, from experience, is a brittle structure that is useless as an electrode. The plated zinc rubs off easily which makes it unreliable as an energy source.

The high current density plating delivers the optimum electrodes. The structure associated with this plating is a dense zinc dendrite fern morphology with high mechanical stability and optimum porosity when rolled down to the correct thickness (Figure I.8 and Figure I.9). The high current densities are defined as the limiting current density plateau. That is where an increase in plating current density through the plating bath only amounts to a small increase in voltage across the plating bath. Once the limiting current density plateau is reached, an increase in current will only lead to energy spent for heat generation. This is unnecessary as it causes heating of the buzz bars, V-blocks and plating fluid (Figure 6.4).

6.3 Summary

From the results presented in this chapter, it is evident that the effect of various chemical parameters are important in ensuring good plating conditions and optimum crystallisation morphologies on the electrode surfaces. The current plays an important part in the crystallisation structure of the plated Zn on the electrode surfaces. The control of the process is thus of utmost important to ensure an effective result.

Chapter 7

SENSITIVITY ANALYSIS

In the research that was done, the relationships between the controlling parameters were established for this specific reactor. The sensitivity of the reactor to the influence of a parameter change must still be summarized. Five controlling parameters were identified and the sensitivity of the process to each one of these will now be discussed.

7.1 Relationship between density, concentration and temperature

A mathematical relationship between these three parameters was established in paragraph **5.1**. This relationship is given by equation 5.3. With the analysis of the research results, it became clear that this relationship is only valid at a density of 1.38 kg/m^3. A graphical presentation of the effect of a change of this reference density is given in Figure 7.1. The data for this graph is shown in Table 7.1.

TABLE 7.1: Calculated concentration from density taken at 20 °C:

Density (kg/m^3)	Calculated Concentration (g/l)
1.36	-26.23
1.365	-19.62
1.370	-13.02
1.375	-6.42
1.380	0.19
1.385	6.79
1.390	13.40
1.395	20.00
1.400	26.61

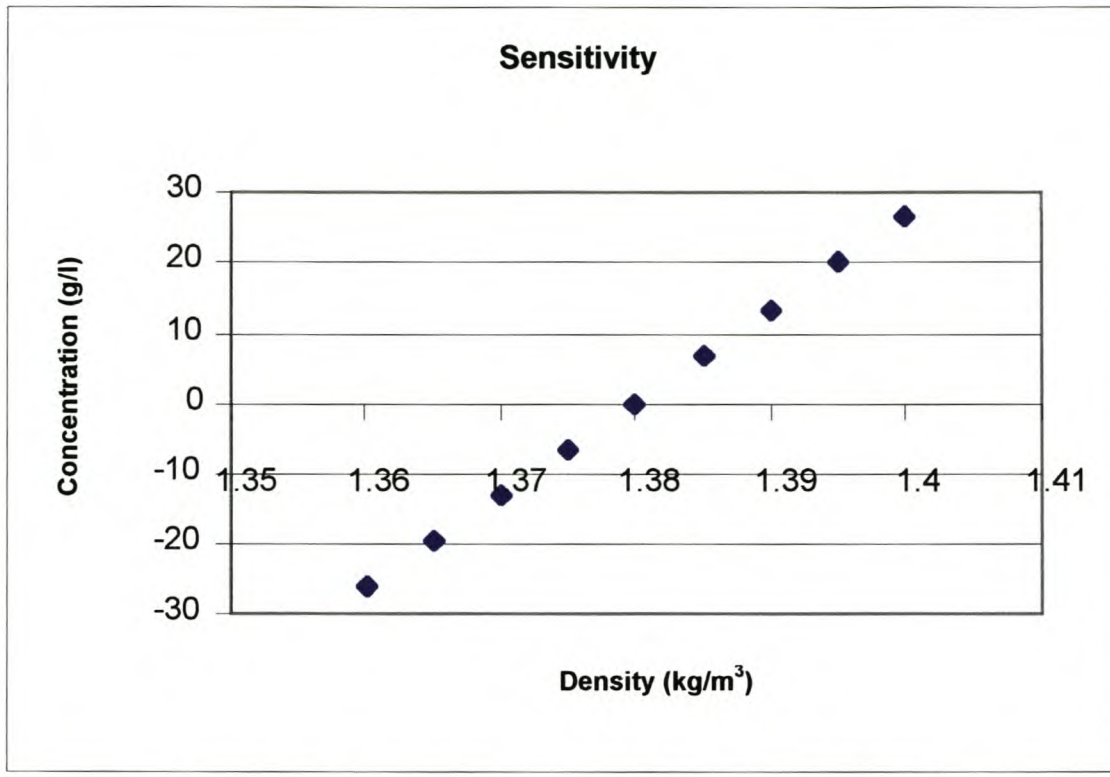

Figure 7.1: Calculated concentration as a function of the density taken at 20^0C

It is clear from this graph that the density of the plating fluid should be kept at a value close to 1.38 kg/m^3. This means, in terms of chemical composition, that the hydroxyl concentration (OH^-) should be controlled. This density value is achieved if 625g KOH is dissolved in 1 litre of water. KOH has a molecular mass of 56 g/mol, K a molecular mass of 39 g/mol, and OH^- a molecular mass of 17 g/mol. This implies a hydroxyl concentration of 189 g/l. This concentration was verified daily by means of a standard titration. If the hydroxyl concentration was too low, the amount of KOH needed for the correction was calculated, dissolved and added. If the need arises for plating at a lower hydroxyl concentration, it can be accommodated. A correction to the constant in equation 5.3 can be deducted from graph 7.1. It should be kept in mind that a lower hydroxyl concentration could imply a lower zincate concentration. This will cause a higher limiting current value. The system control is therefore very sensitive to the hydroxyl concentration and this should be monitored continuously.

7.2 Flow rate

The rate of circulation of the plating fluid is defined as the flow rate. The influence of the flow rate on the system behaviour is discussed in detail in paragraph 5.2. The results are summarized in Figure 5.5. The current voltage relationship changes

according to the flow rate. The advantage of circulation is, therefore, that it lowers the limiting current density potential. The purpose of circulating of the plating fluid is to replenish the zincate concentration. The continuous circulation of the plating fluid is the most time-efficient and productive method of replenishment. It has the added advantage that filtration and homogenising of the plating fluid can be done at the same time. The controlling electrical parameter during plating is the current and not the potential. Current control implies current density control as the system has a fixed cathode area. The system is, therefore, only insensitive to the flow rate if it is operated in the limiting current density region. The plating can even be operated with static plating solution in this region, as long as the hydroxyl concentration and zincate concentration are kept within the specified range.

7.3 Relationship between plated-mass and ampere-hours spent

The relationship between plated-mass and ampere-hours spent (as discussed in paragraph 5.3) is fixed for this reactor. This was proven during the plating of batch 19 to batch 148. The data from Table 5.3 is graphically presented in Figure 7.2.

When considering this graph, the following should be kept in mind:

- The mass is that of the plated sheets. The limited amount of zinc that is lost during the processing of these sheets varies.
- The zincate concentration varied dramatically during these plating processes. This is illustrated in Figure 5.6 where the relative zincate concentration did vary up to 60 g/l.
- The plated sheets are not the final product. The final product is electrodes which are accepted on a much stricter mass requirement.

It can therefore be said that the ampere-hour relationship is insensitive to zincate concentration variation. The plated mass is very sensitive to the ampere-hours spent. By illustration: Plating is usually done at 130 ampere, at which a current of 2.2 ampere-hours pass in one minute. This represents a plating rate of 2.2 g/min. It is, therefore, very easy to do excessive plating if the time is not closely monitored.

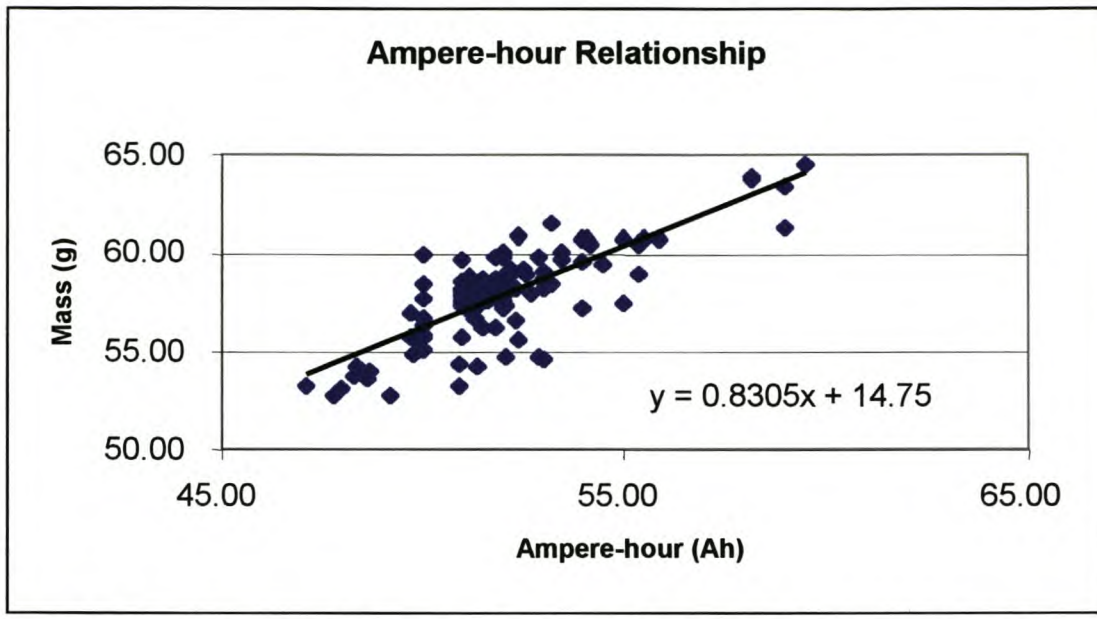

Figure 7.2: Plated mass as a function of the ampere-hours used during the plating

7.4 The influence of the ion concentration on the plating behaviour

This subject is discussed in detail in Chapter 6. It can be concluded from Figure 6.3 that the ion concentration has no major effect on the plating characteristics. The ion concentration has hardly any effect on the plating voltage or current. The ion concentration plays a major role in the Zinc morphology. The limiting current density area (see Figure 6.4) is associated with dendrite morphology plating (see Paragraph 6.2). From the data gathered during the research, no conclusive result could be made as to when the onset of the limiting current density area occurred. The plating process for the manufacture of electrodes is therefore sensitive to the ion concentration as far as the morphology is concerned. It should always be ensured that plating takes place in the limiting current density region.

7.5 Summary

It is evident from the sensitivity analysis that the system is very sensitive to the hydroxyl concentration, and that it should be monitored and controlled. The system is, however, insensitive to the flow rate if it is operated in the limiting current density region, as is the case with this system. The ampere-hour relationship is relatively insensitive to the zincate concentration changes.

The plating process is, however, very sensitive to the zinc-ion concentration. The morphology of the system depends very much on the zinc-ion concentration of the system.

Chapter 8

CONCLUSION

The research terminated successfully in the form of a production plant. The standard of the production plant, the control mechanisms, and production procedures are of such high quality, that they were certified by the SABS (South African Bureau Of Standards), meeting the ISO9001 standards. The goals set for this project were met successfully. The following milestones were achieved:

- The design of the plating reactor ensures that all cathodes in the reactor are exposed to exactly the same current density. This was achieved by the in series configuration of electrical layout. The parallel plating liquid circulation configuration of the plating baths ensure that all baths experience the same ion concentration replenishment tempo. This ensures that the ion concentration is the same in each bath. Replenishment of the plating liquid comes from a big reservoir. The use of a reservoir dampens the effect of temperature changes and ion concentration changes. These design characteristics ensure that each plated foil has the same mass, even during long production runs.
- The influence of the plating liquid circulation rate on the plating behaviour of the system is discussed in paragraph 5.2. A flow rate of 730 l/h was identified as the most efficient flow rate in terms of power consumption, i.e. the lowest voltage at the highest current. The voltage gain, achieved by the circulation, enabled the use of eleven plating baths instead of nine, which still complies with industry regulations. This made the whole process more productive. It further implies that the plating liquid in each bath is replaced about 14 times per hour, or every 4 minutes. This also means that all the plating fluid is filtered twice per hour, which ensures that the plating liquid is clear and free of unwanted particles that can deteriorate the product quality.
- An equation for the relationship between ion concentration, density and temperature was established. The result of this research led to the deduction of equation 5.3. This equation can be adapted for different densities of the

KOH solution that forms the basis of the plating fluid, and also allows for the fast and efficient determination of the ion concentrations in the plating liquid. This allows for efficient process control.

- A relationship between the plated mass and the ampere-hours spent was established. This relationship was amazingly linear, and the ion concentration had no significant effect on the relationship. It was found that one ampere-hour resulted in 1.1g of plated mass. Variations in the ion concentration only led to a different plating morphology.
- It was established from this research that the optimum electrode in terms of mechanical stability and chemical reactivity was linked to a specific plating morphology. This morphology is not dependent on the crystal structure. It was found that the crystal structure of the plated zinc is fixed under all the plating conditions. The zinc morphology identified as the most suitable for electrodes is that which occurs if plating is done at the limiting current density. The limiting current density is sensitive to the ion concentration in the plating fluid. A suitable set of parameters, for optimum manufacturing conditions and electrode characteristics, was identified. Several hundred plating batch runs verified this setting.
- The plating morphology for the optimum electrode was clearly identified. Although the characteristics of the morphology could not be measured, they were clearly identifiable. The correct morphology is associated with densely packed but finely grained fern structured zinc. This structure has a shiny appearance on visual inspection and has a very smooth and solid feeling to it. When exposed to abrasion, it proves to be mechanically very stable. The fern leaf structure is clearly identifiable even at very low magnification (20X – 100X).

Chapter 9

REFERENCES

1. Arouete, S., Blurton, K.F., and Oswin, H.G., Controller Current Deposition of Zinc from Alkaline Solution, Journal of Electrochemical Science, pp 166 – 169 (1969).
2. Bird, R.B., Steward, W.E., Lightfoot, E.N., Transport Phenomena, Wiley, New York (1960).
3. Bryson, A.W., Mass Transport at electrode surfaces, Electrometallurgy: Fundamentals, Applications, Plant Practice, School of Process and Materials Engineering, University of the Witwatersrand (October 1995).
4. Canning, W., Canning Handbook, Publisher E & F.N. Spon Ltd, 11 New Fetter Lane, London, EX4P 4EE (1982).
5. Dirkse, T.P., The nature of the zinc-containing ion in strongly alkaline solutions, Journal of the Electrochemical Society, Vol 101, pp 328-331 (1954).
6. Dirkse, T.P., Postmus, C. and Van den Bosch, R., A study of Alkaline Solutions of Zinc Oxide, Journal of the American Chemical Society, Vol 76, notes pp 6022 – 6024 (1954).
7. Hitchman, M.L., Millington, J.P., Walsh, F.C., Ralph, T.R., The design and performance of filter press reactors for clean and efficient electrosynthesis under mass transport controlled conditions, IChemE Symposium Series No 127.
8. Hohanta, S. Fahidy, T.Z., The effect of anodic bubble formation on cathodic mass transfer under natural convection conditions, J. Appl. Electrochem, vol 7, pp 235 – 238 (1977).
9. Homsy, R.V. Newman, J., J. Electrochem. Soc. 121, page 1448 (1974).
10. Jackovitz, J.F., Langer, A., A Spectroscopic investigation of the Zinc-Hydroxyl System, Journal of Electrochemical Society, pp 30 – 35 (1968).
11. Kayj, W.M., Convective Heat and Mass Transfer, McGraw-Hill, New York, pp 133-142 (1968).
12. Newman, J., J. Electrochem. Soc. 113, page 1235 (1966).

13. Nicol, M.J., An Introduction to the Basic Concepts of Electrochemistry, Parts 1 and 2, School of Pure and Applied Electrochemistry, 23 pages (1979a).

14. Nicol, M.J., Application of electrochemical principles to problems in the Metallurgical Industry, School of Pure and Applied Electrochemistry, 27 pages (1979b).

15. Orchard, S.W., Quantitive Electrode Kinetics, School of Pure and Applied Electrochemistry, 22 pages (1979).

16. Parrish, W.R., Newman, J., J. Electrochem. Soc. 116, page 169 (1969).

17. Parrish, W.R., Newman, J., J. Electrochem. Soc. 117, page 43 (1970).

18. Pickett, D.J., Electrochemical Reactor Design, 2nd Ed., Elserivier, Amsterdam (1979).

19. Pourbaix, M., Atlas of electrochemical equilibria in aqueous solutions, Pergamon Press, Oxford, London, First English Edition (1966).

20. Selman, J.R., Tutorial Lectures in Electrochemical Engineering and Technology, Alkire R.C. and Beck T. (Eds.), AIChE Symp. Series No. 204, vol 77, page 88 (1981).

21. Stephan, K., Vogt H., A Model for correlating mass transfer data at gas evolving electrodes, Electrochemia Acta, vol 24, pp 11-18 (1979).

22. Walsh, F.C., A First Course in Electrochemical Engineering, The Electrochemical Consultancy Romsey (1991).

APPENDIX 1

SCANNING ELECTRON MICROSCOPE PHOTOGRAPHS

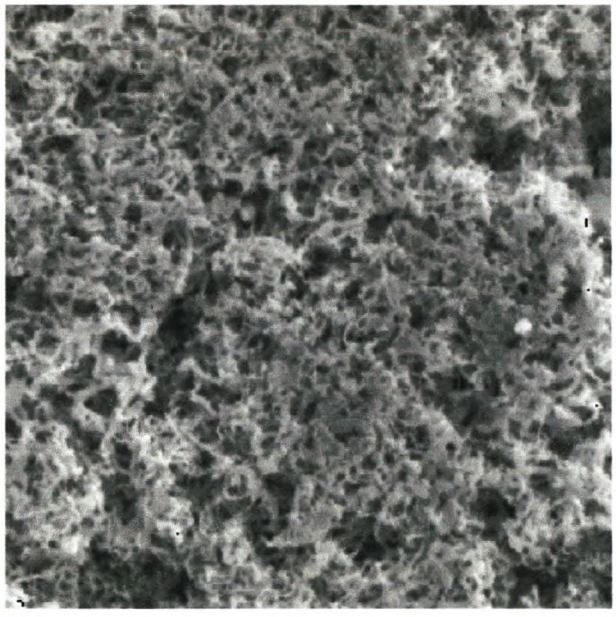

Figure 1.1: Zinc morphology at a plating current of 10 A, the SEM image at 2500 X magnification

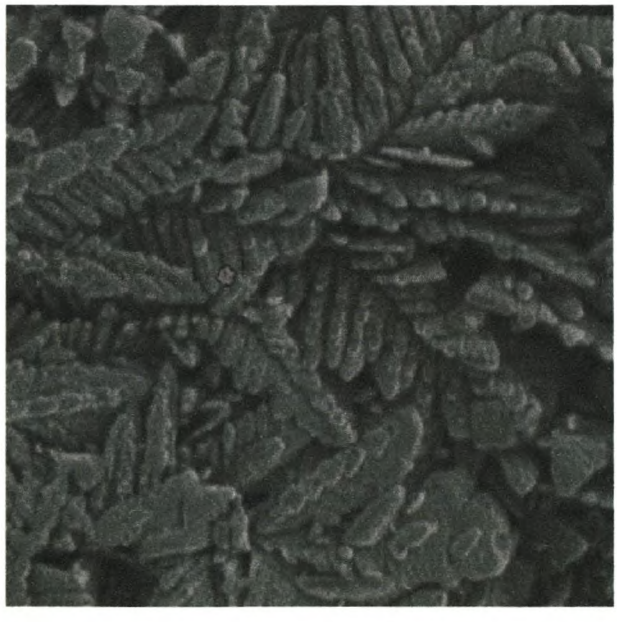

Figure 1.2: Zinc morphology at a plating current of 60 A, the SEM image at 500 X magnification

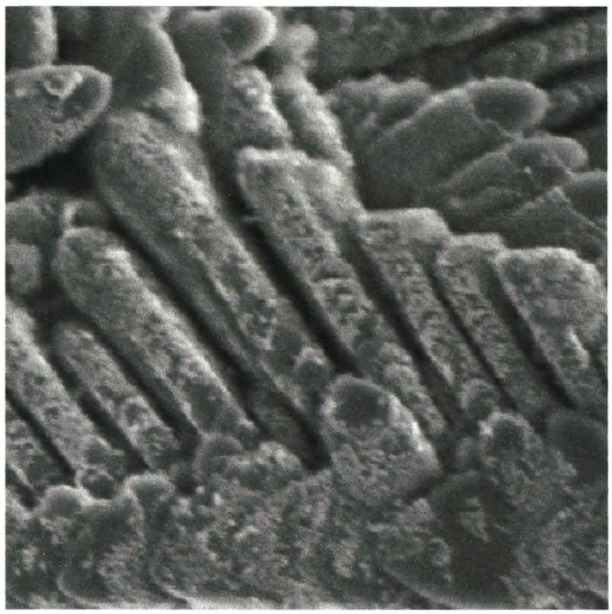

Figure 1.3: Zinc morphology at a plating current of 40 A, the SEM image at 2500 X magnification

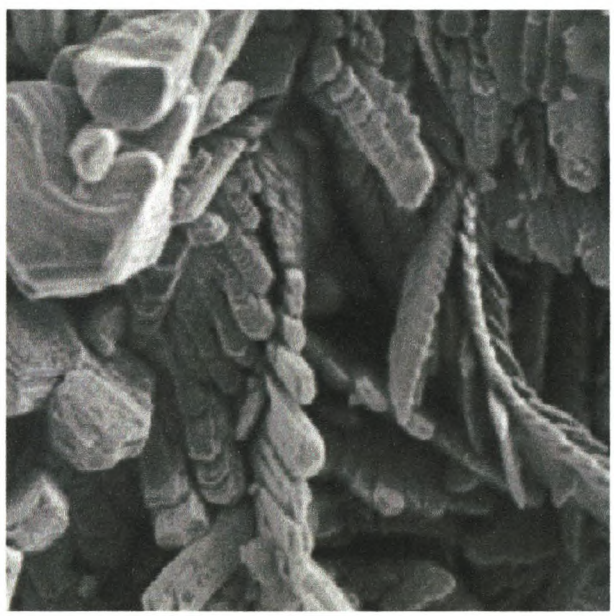

Figure 1.4: Zinc morphology at a plating current of 30 A, the SEM image at 500 X magnification

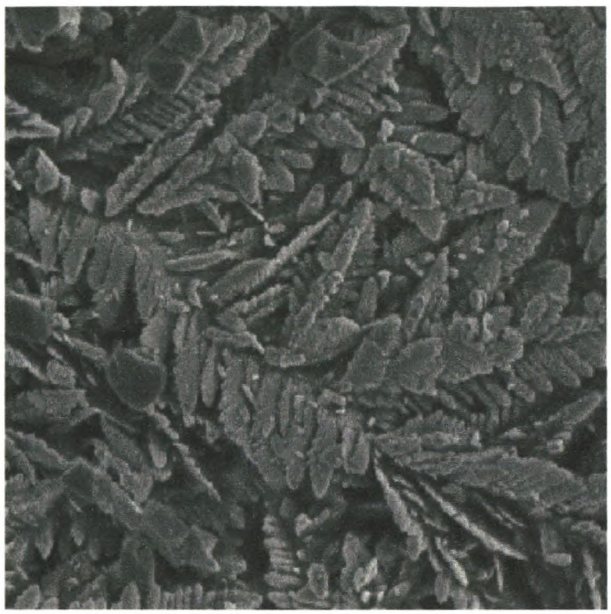

Figure 1.5: Zinc morphology at a plating current of 50 A, the SEM image at 500 X magnification

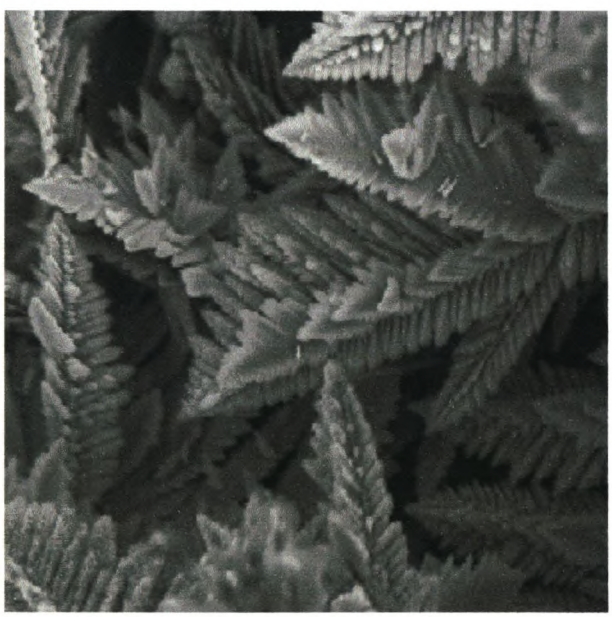

Figure 1.6: Zinc morphology at a plating current of 40 A, the SEM image at 2500 X magnification

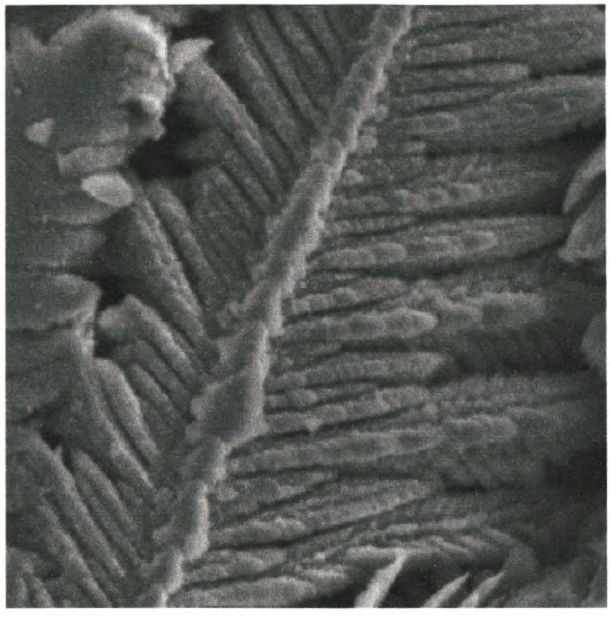

Figure 1.7: Zinc morphology at a plating current of 80 A, the SEM image at 2500 X magnification

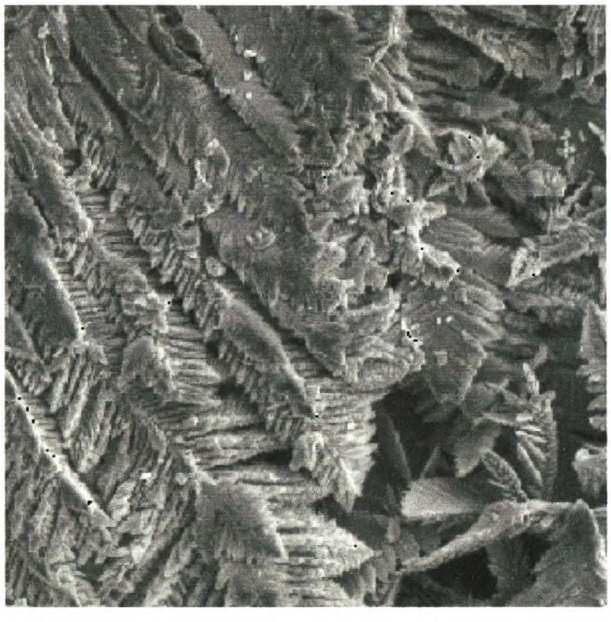

Figure 1.8: Zinc morphology at a plating current of 80 A, the SEM image at 500 X magnification

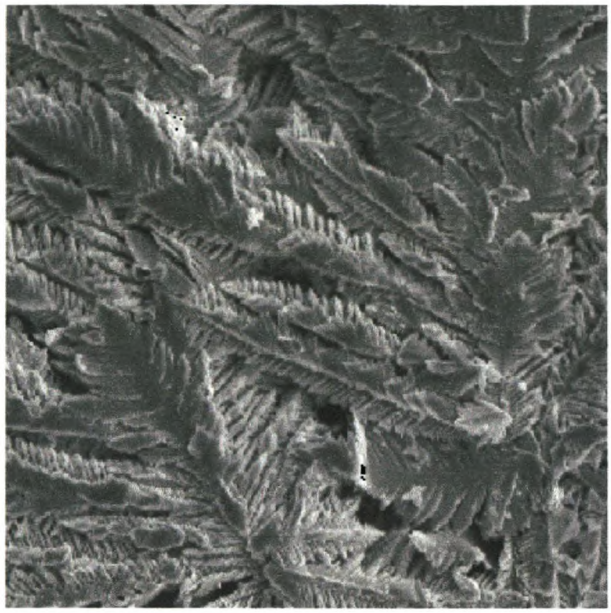

Figure 1.9: Zinc morphology at a plating current of 80 A, the SEM image at 500 X magnification

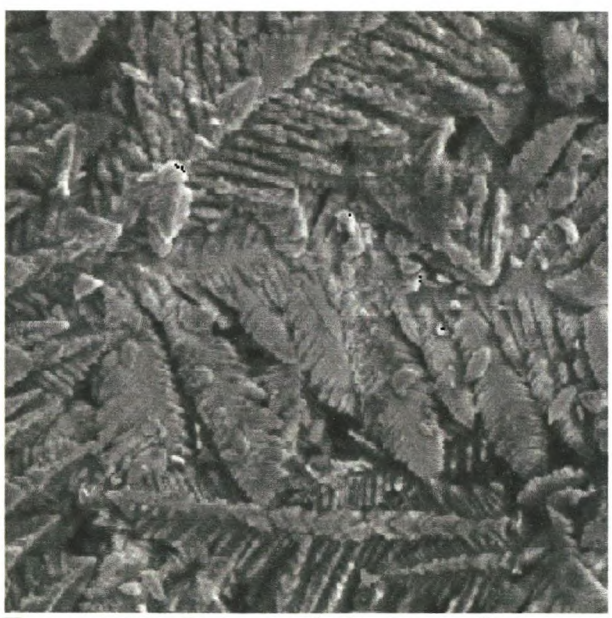

Figure 1.10: Zinc morphology at a plating current of 70 A, the SEM image at 500 X magnification

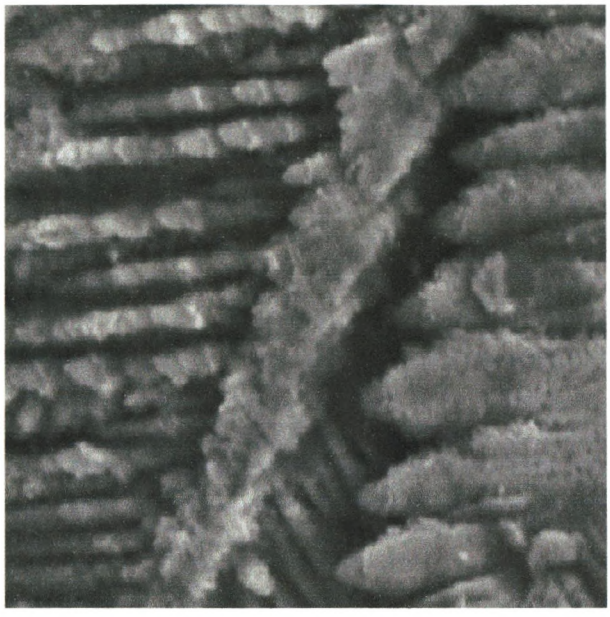

Figure 1.11: Zinc morphology at a plating current of 70 A, the SEM image at 2500 X magnification

The following series of photographs are not discussed in the text but are presented in this Appendix as information only. The series consists of a group of SEM photographs are taken of randomly selected zinc electrodes, and a randomly selected production battery. These electrodes were manufactured at a current of 130 ampere. The highly porous fern-like zinc morphology is very prominent at every magnification. This ensures an optimum reaction area for the electrodes.

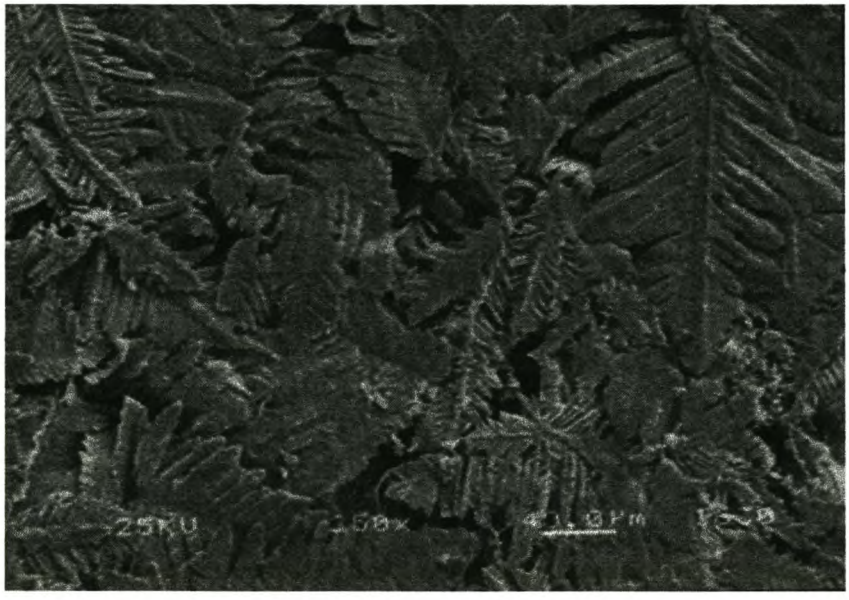

Figure 1.12: The fern-like zinc morphology clearly visible at a magnification of 250X.

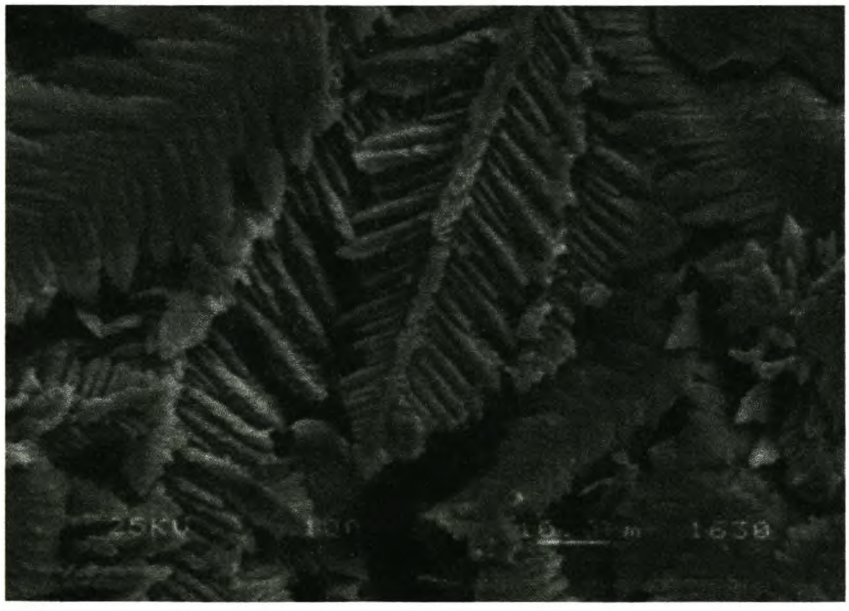

Figure 1.13: The fern like zinc morphology clearly visible at a magnification of 1000X.

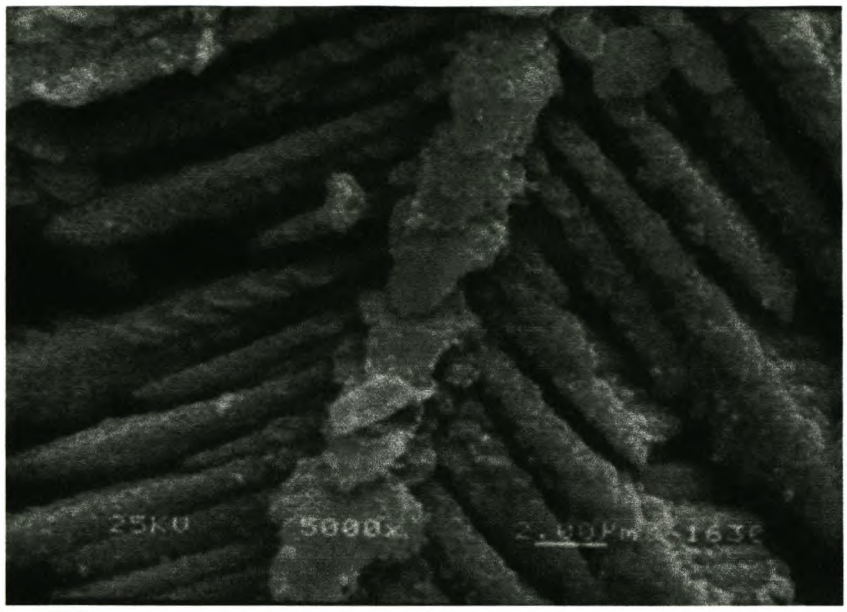

Figure 1.14: The fern like zinc morphology clearly visible at a magnification of 5000X.

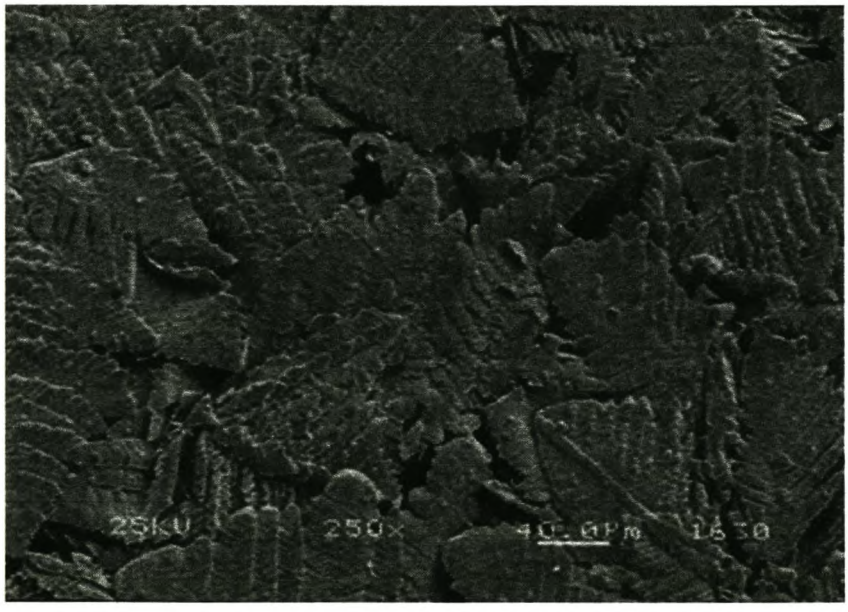

Figure 1.15: The fern-like zinc morphology clearly visible at a magnification of 250X. In this photograph the effect of the rolling of the zinc morphology is clearly visible. The surface is smoothed by the ironing effect of the rollers. Underneath the surface, the zinc morphology is unchanged.

Figure 1.16: The fern-like zinc morphology clearly visible at a magnification of 1000X. In this photograph the effect of the rolling of the zinc morphology is clearly visible. The surface is smoothed by the ironing effect of the rolls. Underneath the surface, the zinc morphology is unchanged.

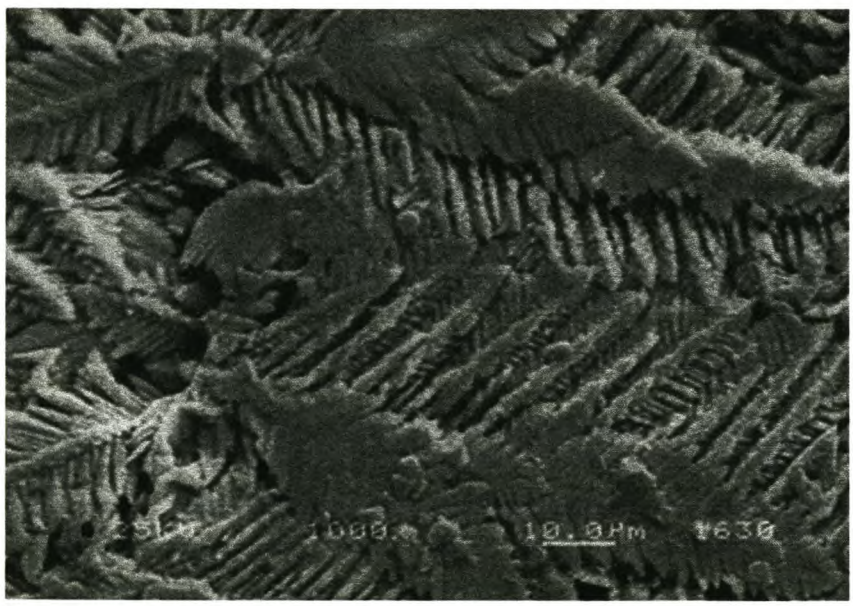

Figure 1.17: The fern-like zinc morphology clearly visible at a magnification of 1000X from another area. The effect of the rolling of the zinc morphology is not as prominent in this photograph as in the previous photograph.

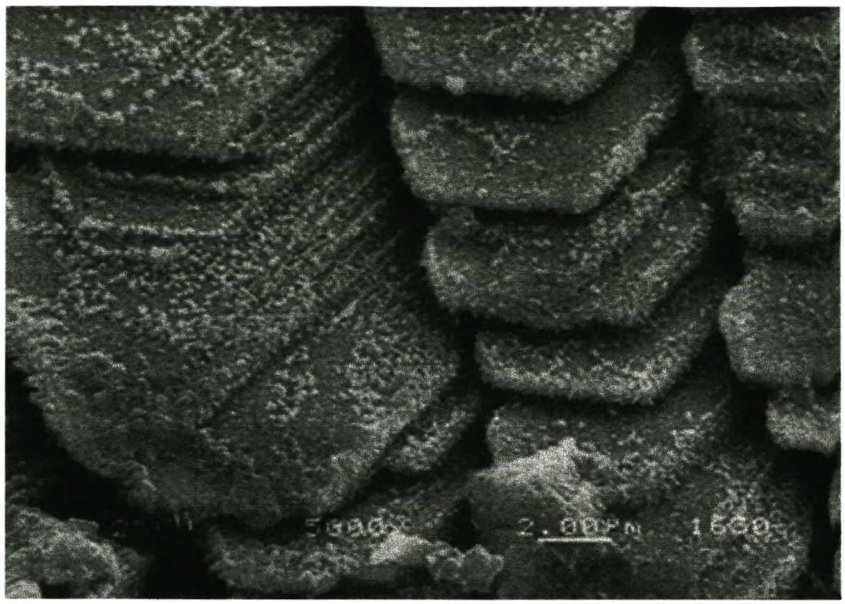

Figure 1.18: The fern-like zinc morphology at a magnification of 5000X from a heavy rolled area. The high porosity of this area is clearly visible and is not destroyed by rolling but only diminished.